IMPURITY INDUCED FAR-INFRARED ABSORPTION IN KBr AND KCl

IMPURITY INDUCED FAR-INFRARED ABSORPTION IN KBr AND KCl

by

ROGER WILLIAM WARD, B.Sc.

A Thesis

Submitted to the Faculty of Graduate Studies

in Partial Fulfilment of the Requirements

for the Degree

Doctor of Philosophy

McMaster University

October 1971

DOCTOR OF PHILOSOPHY (1971) McMASTER UNIVERSITY
(Physics) Hamilton, Ontario.

TITLE: Impurity Induced Far-Infrared ABsorption in KBr and KCl

AUTHOR: Roger William Ward, B.Sc. (University of London, England)

SUPERVISOR: Dr. T. Timusk

NUMBER OF PAGES: ix, 112

SCOPE AND CONTENTS:

High resolution measurements of the far-infrared absorption spectra due to a number of substitutional impurities in KBr and KCl are presented. Several Van Hove singularities of the phonon spectrum of the host lattice are directly observed and found to shift to higher frequencies as the impurity concentration is increased. The first direct experimental evidence for the change of shape or metamorphism of singularities is also presented. The experimental spectra are compared with numerical calculations based on the ordinary shell model for the defect together with phonon data obtained from inelastic neutron scattering experiments. Agreement between experiment and calculation is generally good when impurity resonant modes are absent.

ACKNOWLEDGEMENTS

I would like to thank my supervisor, Dr. T. Timusk, for his guidance and help throughout the course of this work. I would also like to thank Dr. R. W. MacPherson for help with the computer programs, Dr. R.G.V. Hancock for assistance with the chemical analysis and John Neimanis for his help in improving the data acquisition electronics.

Dr. Rolfe supplied the O_2^- doped samples for this investigation, and Dr. M. A. Buchanan grew the Sm^{++} and Eu^{++} doped crystals.

This research was partially funded by the Defence Research Board of Canada and by the National Research Council of Canada to whom I am also grateful for the award of a scholarship.

Finally, I thank Mrs. H. M. Kennelly for typing the final draft of the manuscript.

TABLE OF CONTENTS

		Page
CHAPTER I	INTRODUCTION	1
CHAPTER II	EXPERIMENTAL	5
	A. EQUIPMENT AND TECHNIQUE	5
	General Introduction	5
	Interferometer and Sample Chamber	7
	Detector	12
	Electronics	13
	Procedure of a Run	15
	B. SAMPLE PREPARATION	17
CHAPTER III	THEORY	20
	A. UNPERTURBED LATTICE	21
	The Shell Model	23
	B. PERTURBED LATTICE	25
	C. FAR-INFRARED INDUCED ABSORPTION	29
CHAPTER IV	RESULTS AND DISCUSSION OF KBr IMPURITY SPECTRA	34
	A. GENERAL REMARKS	34
	B. SPECIFIC ABSORPTION SPECTRA	40
	1. Sodium	40
	2. Lithium	49
	3. Thallium	56
	4. Samarium	58

		Page
	5. Chlorine	63
	6. Fluorine	68
	7. Hydroxide	70
	8. Oxygen	73
CHAPTER V	RESULTS AND DISCUSSION OF KCl IMPURITY SPECTRA	77
	A. GENERAL REMARKS	77
	B. SPECIFIC ABSORPTION SPECTRA	79
	1. Chlorine Isotope	79
	2. Sodium	82
	3. Lithium	87
	4. Samarium	90
	5. Europium	90
	6. Fluorine	92
	7. Bromine	95
	8. Iodine	98
	9. Oxygen	100
CHAPTER VI	CONCLUSION	104
BIBLIOGRAPHY		107

LIST OF FIGURES

Figure	Description	Page
1.	Schematic representation of the FS-720 far-infrared Michelson interferometer	8
2.	Sample and detector chamber	11
3.	Block diagram of electronics	14
4.	Sample interferograms	16
5.	Defect molecule	27
6.	Induced far-infrared absorption due to Na^+ ions in KBr. Concentration effect.	35
7.	Induced far-infrared absorption due to Na^+ ions in KBr	41
8.	The frequency of singularity A vs Na^+ concentration in KBr	43
9.	The frequency of singularity B vs Na^+ concentration in KBr	44
10.	The frequency of singularity C vs Na^+ concentration in KBr	45
11.	Unperturbed phonon density of states for KBr	48
12.	Induced far-infrared absorption due to Li^+ ions in KBr	52
13.	The frequency of singularity A vs Li^+ concentration in KBr	53
14.	The frequency of singularity B vs Li^+ concentration in KBr	54
15.	Induced far-infrared absorption due to Tl^+ ions in KBr	57
16.	Calculated far-infrared absorption due to Tl^+ ions in KBr with zero force constant changes	59
17.	Induced far-infrared absorption due to Sm^{++} ions in KBr	60

Figure	Description	Page
18.	The frequencies of singularities A and B vs Sm^{++} concentration in KBr	62
19.	Induced far-infrared absorption due to Cl^- ions in KBr	64
20.	High concentration, far-infrared absorption spectra of KBr:Cl^-	66
21.	Metamorphism of Van Hove Singularities	67
22.	Induced far-infrared absorption due to F^- ions in KBr	69
23.	Induced far-infrared absorption due to OH^- ions in KBr	72
24.	Induced far-infrared absorption due to O_2^- ions in KBr	74
25.	Unperturbed phonon density of states for KCl	78
26.	Induced far-infrared absorption due to the stable isotopes Cl^{35} and Cl^{37} in KCl	80
27.	Induced far-infrared absorption due to Na^+ ions in KCl.	84
28.	The frequency of the saddle point singularity at (0.52,0.52,0) vs Na^+ concentration in KCl	86
29.	Induced far-infrared absorption due to Li^+ ions in KCl	89
30.	Induced far-infrared absorption due to Sm^{++} ions in KCl	91
31.	Induced far-infrared absorption due to Eu^{++} ions in KCl	93
32.	Induced far-infrared absorption due to F^- ions in KCl	94
33.	Induced far-infrared absorption due to Br^- ions in KCl	96

Figure	Description	Page
34.	Induced far-infrared absorption due to I^- ions in KCl	99
35.	Induced far-infrared absorption due to O_2^- ions in KCl	101

LIST OF TABLES

Table	Description	Page
1.	Positions of singularities in KBr	37
2.	Force constant changes in KBr	76
3.	Positions of singularities in KCl	83
4.	Force constant changes in KCl	103

CHAPTER I

INTRODUCTION

The introduction of an impurity atom into a crystal can significantly alter the normal modes of vibration of the atoms in the crystal (Lifschitz 1944, Montroll and Potts 1955, Dawber and Elliott 1963a,b, Maradudin 1963, Takeno 1967, and Benedek and Nardelli 1967,1968). Localized modes of vibration can occur when the impurity and its surroundings vibrate at a frequency outside the band of normal modes of the perfect host crystal. In this case the vibrational amplitudes of the atoms decay exponentially with increasing distance from the defect. Resonant modes whose frequencies lie within the normal phonon frequencies of the host crystal may also occur. Interaction between the oscillating impurity atom and crystal phonons of the same frequency will cause a damping in time of the oscillation, the degree of daming will depend largely on the density of phonon states in the vicinity of the resonance.

In addition to local modes and resonances that occur, impurities destroy the translational symmetry of a crystal and cause previous symmetry forbidden vibrational transitions to become allowed in the doped crystal. This was originally shown to be the case by Lax and Burstein (1955) who made

early calculations of the impurity induced infrared absorption in diamond. Subsequent calculations by Dawber and Elliott (1963a), and in particular calculations of the optical absorption by vibrations of defects in silicon (Dawber and Elliott 1963b), have shown that impurities could in principle be used as probes of the vibrational spectra of pure crystals.

Since 1960, when Schäfer first discovered a local mode of H^- in several alkali halides, there has accumulated a wealth of experimental data on defect lattice dynamics. Notable among these have been measurements of thermal conductivity, side bands accompanying electronic transitions, infrared absorption, and quite recently with the advent of laser techniques, Raman scattering. In particular impurities in the potassium halides have been studied through thermal conductivity (Baumann and Pohl, 1967), specific heat (Karlsson 1970) and Raman scattering (Harley et al. 1969,1971), but the most extensive study of lattice resonant modes has been made using far-infrared spectroscopy. In a series of papers, Sievers group at Cornell, has reported results of far-infrared experiments on impurity resonant modes, including isotope shifts (Kirby et al. 1967), stress effects (Nolt and Sievers, 1968), temperature effects (Alexander et al. 1969), electric field effects (Nolt and Sievers, 1966, Clayman et al. 1971) and off-centre and dipolar impurities (Kirby et al. 1970).

Most of the earlier infrared work on impurity systems has dealt exclusively with lattice resonant modes, however since the advancement of far-infrared interferometric techniques at higher frequencies, especially the development of high-sensitivity low-noise detectors it has become possible to study the fine structure associated with defect induced, single phonon absorption. It should then be possible to correlate this structure with features of the host lattice density of phonon states (Timusk and Ward, 1969). Early attempts by Klein and Macdonald (1968) and Macdonald et. al. (1968) working on doped NaCl were made but a lack of instrumental resolution hampered the earlier work.

It was thus decided to study the structure of the far-infrared induced absorption in KBr and KCl, using a large number of different substitutional impurities. In this manner one is able to differentiate impurity gap modes and resonant modes from the host lattice absorption. It should then be possible, with sufficient resolution, to observe and identify discontinuities in the absorption that correspond to Van Hove singularities of the host lattice. In this way one can make high resolution optical measurements of certain phonon frequencies.

Such unambiguous identification of lattice singularities requires, in addition to high resolution spectra, a

detailed model of the defect and lattice. In this work we have used the extended defect relaxation model of Woll et al. (1968), which is based on the unperturbed phonon data derived from the shell model for KBr (Woods et al. 1963) and KCl (Copley et al. 1969). This defect model was developed originally by Gethins et al. (1967) to account for the vibronic side band of the high frequency local mode absorption of H^- ions in KBr and KI. It has also been used successfully to calculate the far-infrared absorption due to H^- in KBr and KI (Woll et al. 1968) and the vibronic side band of fluorescent Sm^{++} in KBr and KCl (Buchanan and Woll, 1969). Similar calculations of the present type have been performed by Benedek and Nardelli, (1967) and by Patnaik and Mahanty (1967) for the case of Li and Ag impurities in KBr. MacPherson and Timusk (1970a, 1970b) have recently extended the model to account for the shell effects of the valence electrons of the impurity atom.

Chapter II of this thesis discusses the experimental technique and sample preparation. The background theory and calculation of the far-infrared absorption is the subject of Chapter III. Chapters IV and V compare the calculated results with experimental measurements for KBr and KCl respectively. The conclusions drawn from this investigation are discussed in the final chapter.

CHAPTER II

EXPERIMENTAL

A. EQUIPMENT AND TECHNIQUE

General Introduction

The far-infrared region of the spectrum, (10-200 cm^{-1}) has always presented difficulties to experimenters for two main reasons. Firstly, no really intense source of radiation has been found for this region. The mercury arc source, first used by Rubens and Wood (1911),is still in general use today. Until recently the second and related difficulty associated with measurements in the far-infrared was the lack of high sensitivity detectors. In the last decade however, with the advent of interferrometric techniques and liquid helium cooled bolometers, more efficient use has been made of the available energy.

A detailed account of the theory and advantages of Fourier spectroscopy will not be presented here. These have been discussed in great length by many authors, (Strong and Vanasse 1959; Jacquinot 1960; Connes 1961; Richards 1964; Bosomworth and Gush 1965). However, an outline of the basic principles as described by Richards (1964) will serve to illustrate the technique. The interference pattern or interferogram $I(\Delta)$ produced by a Michelson interferometer for

monochromatic radiation of frequency ν (in cm^{-1}) is of the form

$$I(\Delta) = S_o(1 + \cos 2\pi\nu\Delta) \ , \qquad \text{(II-1)}$$

where Δ is the path difference and S_o is proportional to the illumination of either one of the two beams producing the interference pattern. If we now consider an arbitrary spectral illumination $S(\nu)$ our equation becomes

$$\begin{aligned} I(\Delta) &= \int_o^\infty S(\nu)\,[1 + \cos 2\pi\nu\Delta]\,d\nu \\ &= \tfrac{1}{2} I(o) + \int_o^\infty S(\nu)\cos 2\pi\nu\Delta\, d\nu \end{aligned} \qquad \text{(II-2)}$$

where $I(o)$ is the intensity at zero path difference. Taking the Fourier transform of the even function $I(\Delta)$ gives us the desired spectrum

$$S(\nu) = 4 \int_o^\infty [I(\Delta) - \tfrac{1}{2} I(o)]\cos 2\pi\nu\Delta\, d\Delta \qquad \text{(II-3)}$$

in terms of the measured quantity $I(\Delta)$.

In practice the interferograms are recorded and sampled at equally spaced intervals Δx between the zero path position and some finite path difference D so that equation (3) is approximated by a finite sum

$$S(\nu_1) = \sum_{\Delta=0}^{\Delta=D} [I(\Delta) - \tfrac{1}{2} I(o)]\cos(2\pi\nu_1\Delta)\,\Delta x \qquad \text{(II-4)}$$

where $\Delta = n\Delta x$ and $n = 0, 1, 2, 3 \ldots D/\Delta x$. The spectrum is then computed from equation (4) by digital computer.

Interferometer and Sample Chamber

The interferometer used in this work was a commercial Michelson, type FS-720, manufactured by the Research and Industrial Instruments Company. A maximum path difference of ± 10 cm limits the theoretical resolution to 0.1 cm^{-1}. A diagram of the optics involved is given in Fig. (1). Light from the source, a Philips BA15D high pressure mercury arc lamp with a fused quartz envelope, is reflected by the off-axis paraboidal mirror M1. The parallel beam is then divided by the Mylar* beam splitter and passes to the moving plane mirror M2 and the fixed plane mirror M3. Mirrors M4 and M5 are used to condense the recombined beam and focus it into the 3/4" I.D. of a polished brass cone. The cone is connected to a 0.43" I.D. brass light pipe (Ohlmann et al. 1958) which leads to a helium cryostat. The mirror M2 is mounted upon a movable carriage and can be moved at constant speed by a motor-driven lapped piston and cylinder system. This provides a variable path difference between the two beams.

A Moiré fringe system is used to sample the interferogram at equal intervals of path difference. The system consists

*Polyethylene terephthalate, registered trade name El Du Pont de Nemours and Co.

Figure 1

Schematic representation of the FS-720 far-infrared Michelson interferometer. The arrows indicate the light path from the source to the exit light pipe.

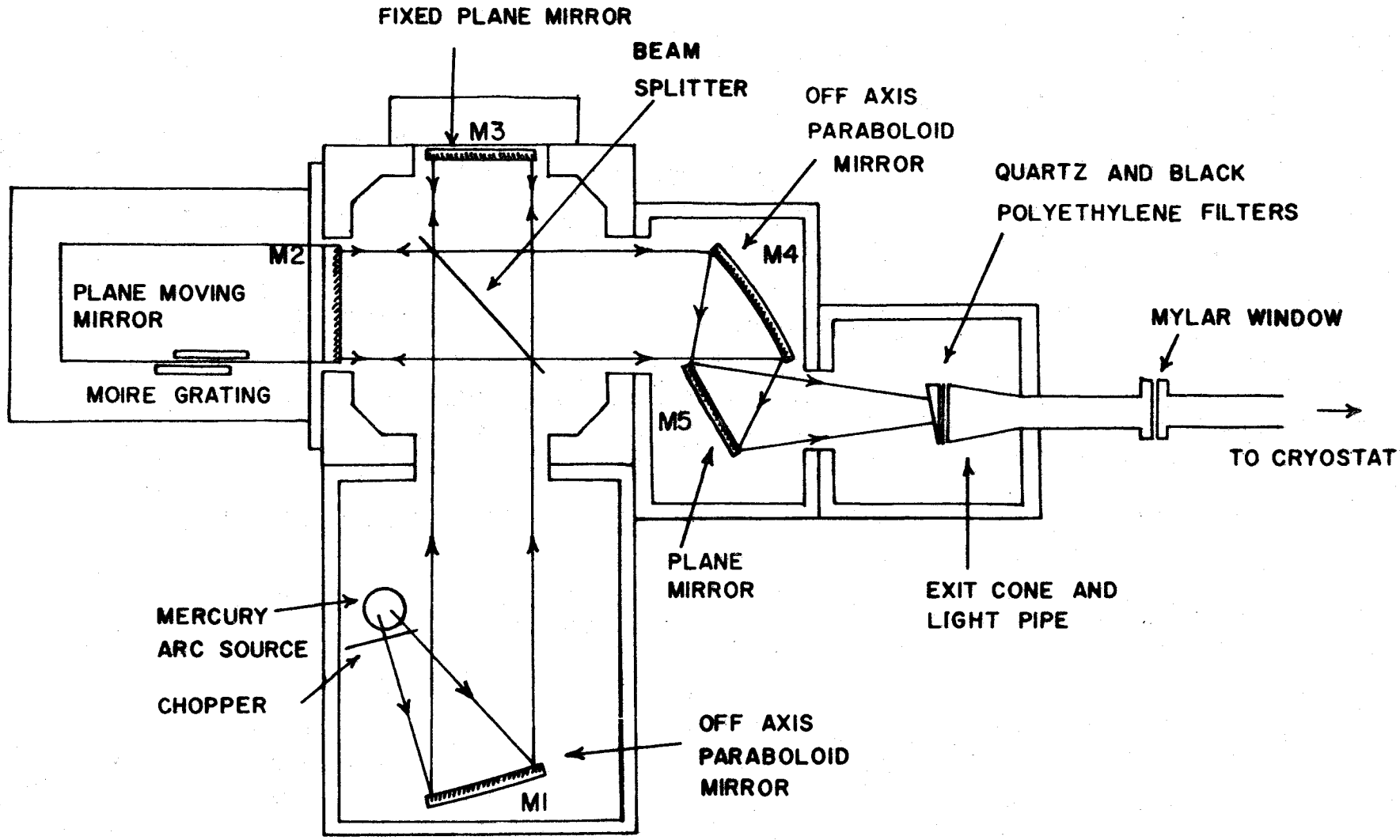
FIXED PLANE MIRROR
BEAM
SPLITTER
M3
OFF AXIS
PARABOLOID
MIRROR
QUARTZ AND BLACK
POLYETHYLENE FILTERS
M2
M4
PLANE MOVING
MIRROR
MYLAR WINDOW
MOIRE GRATING
M5
TO CRYOSTAT
PLANE
MIRROR
EXIT CONE AND
LIGHT PIPE
MERCURY
ARC SOURCE
CHOPPER
OFF AXIS
PARABOLOID
MIRROR
M1

of two identical transmission gratings. One is mounted on the carriage and moves with the mirror M2. The second grating is mounted on the fixed base of the interferometer. The two gratings are spaced approximately 50 microns apart. A small lamp and lens system produces a collimated beam of light which passes through the parallel ruled gratings and falls on a photo diode. Parallel movement between the gratings causes a near sinusoidal variation in the intensity of the transmitted light. The photodiode output is then amplified and fed to a Schmitt trigger circuit, which produces a single voltage pulse each time the moving grating is advanced by one grating spacing. In the FS-720 the rulings on the gratings are 4 microns apart, allowing a sampling path difference interval of 8 microns. This corresponds to a maximum unambiguously observable frequency of 625 cm^{-1}.

The interferometer is enclosed within a vacuum tank to eliminate water vapour from the light path and is isolated from the sample chamber and detector vacuum by a thin Mylar window and polyethylene spacer. The spacer is used to electrically isolate the interferometer and detector circuits and decrease ground loop problems. The interferometer is evacuated by a 100 litre/min. rotary pump. During a run a pressure of about 20 microns of Hg is maintained by a Varian 941-6001 Vac Sorb pump. The Vac Sorb pump works on the adsorption principle, and since it has no moving parts it is

ideally sutied for evacuating the interferometer tank which is very sensitive to mechanical vibrations.

Radiation is transmitted to the sample chamber via a reflector of highly polished brass set at 45° to the incident beam. The light then passes down a 25" section of 1/2" diameter brass light pipe into the sample and detector chamber. Inside the cryostat, the light pipe is machined to 0.01" thickness to reduce heat conduction into the liquid helium. Fig. (2) shows a cross-sectional view of the sample and detector chamber.

The whole assembly is mounted inside a conventional glass helium dewar. The sample chamber is maintained under a vacuum of 10^{-5} torr. The main feature of the chamber is the externally rotatable sample holder which can support eight 1/4"×1/4"×1/4" samples simultaneously. Thus different samples can be rotated into the light beam during the course of a run. The rotatable wheel is held in position with spring loaded ball bearings, which are arranged in such a manner as to enable a sample crystal to be accurately aligned over the light pipe exit.

A copper braid thermally anchors the sample wheel to the outside wall. The sample wheel also contains one junction of a gold + 0.02 at.% iron vs chromel thermocouple (Rosenbaum 1968) which is used to measure the temperature of the samples. The junction was glued onto a KBr crystal mounted

Figure 2

Cross-sectional view of the sample and detector chamber. The drawing is approximately full size. Indium "O" ring seals are used to insure a vacuum tight chamber. The arrows indicate the light path. The copper braid connecting the sample wheel to the side of the chamber is not shown in the diagram.

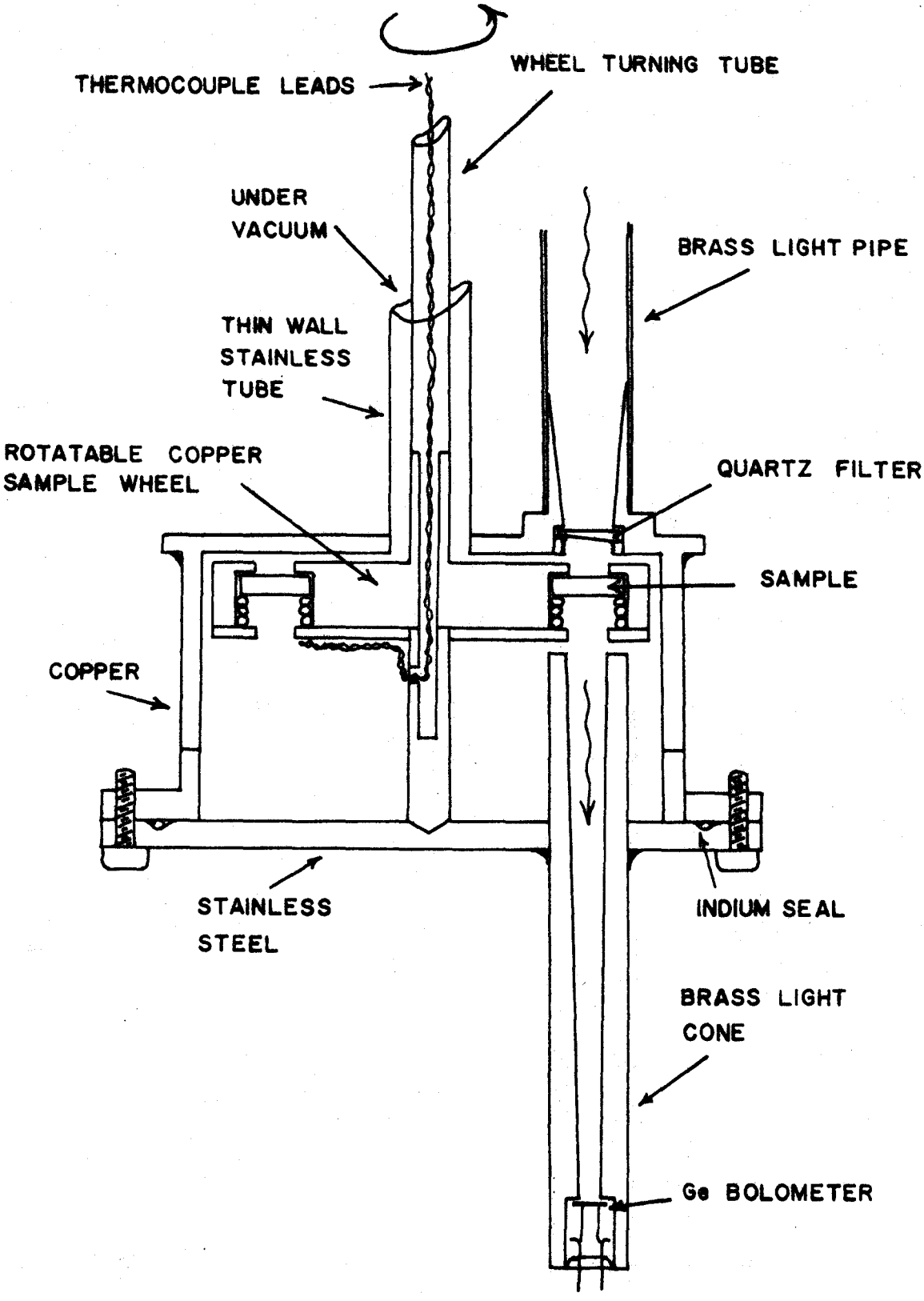
THERMOCOUPLE LEADS
WHEEL TURNING TUBE
UNDER VACUUM
BRASS LIGHT PIPE
THIN WALL STAINLESS TUBE
ROTATABLE COPPER SAMPLE WHEEL
QUARTZ FILTER
SAMPLE
COPPER
STAINLESS STEEL
INDIUM SEAL
BRASS LIGHT CONE
Ge BOLOMETER

in one of the holders with G.E. 7031 varnish. Sample temperatures were usually 11°K.

Room temperature radiation is prevented from reaching the samples and detector by a composite single crystal quartz and black polyethylene filter, mounted at the top of the light pipe. Another thin plate of single crystal quartz is used as a cold filter just above the sample. Both of the filters used were wedge-shaped to prevent interference fringes being formed from their parallel sides. Immediately below the sample is a 4" long brass light cone (Williamson 1952) which matches the light pipe diameter to the detector diameter.

Detector

As was mentioned at the beginning of this chapter, the low intensity source necessitates the use of very sensitive detectors. The detectors used throughout these experiments were Low type (Low 1961) gallium doped single crystal germanium bolometers developed in our laboratory by A. J. Tumber (1968).

The incident far-infrared radiation produces a temperature change which causes a rapid variation in the resistivity of the germanium. From a room temperature resistance of about 8 ohms, the germanium elements usually increase to about 400 k ohms at 4.2°K. A complete recipe for cutting and etching the germanium is given by Tumber (1968). The

finished elements are typically 0.12" diameter discs approximately 0.006" thick. A standard T.O.-5 type transistor header is used to mount the element inside the bottom of the detector cone. Contact to the header is made with 0.005" diameter gold wires soldered with pure indium* to the germanium disc. The combined thermal time constant of the bolometer and leads was typically 6 ms. at 4.2°K.

The operation of the bolometer is as follows. A small constant bias current of between 0 and 15 μA is provided by mercury batteries in series with a one meg-ohm wire wound precision load resistor. The resistor is mounted inside the helium cryostat close to the bolometer. Because of the variation in temperature of the bolometer due to the incident chopped radiation, a corresponding periodic variation in resistance and thus voltage is induced across the element. This voltage signal is then amplified and fed into a phase sensitive detector system which is described in the next section.

Electronics

A block diagram of the electronics is shown in Fig. (3). Radiation from the mercury arc source is modulated by a chopper at a frequency of usually 21 Hz. The bolometer signal is amplified by a Brookdeal 450 low noise preamp and then synchronously

*Indium Corporation of America.

Figure 3

Block diagram of the data acquisition electronics. The punched paper tape is converted to cards and the spectrum calculated by a CDC 6400 digital computer.

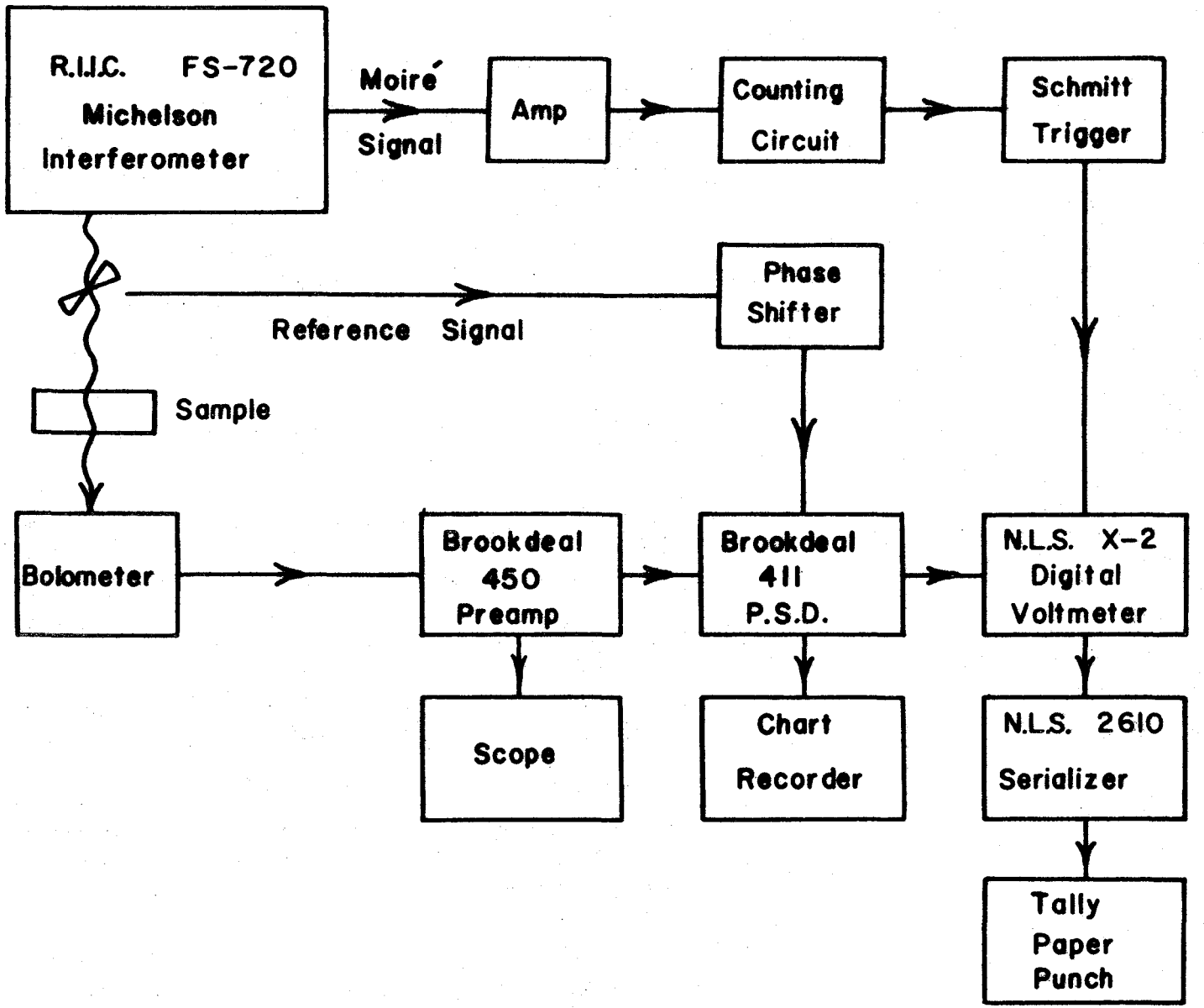
R.I.I.C. FS-720
Michelson
Interferometer
Moiré
Signal
Amp
Counting
Circuit
Schmitt
Trigger
Phase
Shifter
Reference Signal
Sample
Bolometer
Brookdeal
450
Preamp
Brookdeal
411
P.S.D.
N.L.S. X-2
Digital
Voltmeter
Scope
Chart
Recorder
N.L.S. 2610
Serializer
Tally
Paper
Punch

demodulated by a Brookdeal 411 phase sensitive detector. The output signal is measured by a Non-Linear Systems X-2 series digital voltmeter and fed through a Non-Linear Systems 2610 serializer to a Tally high speed paper tape punch. The phase sensitive detector output is also displayed on a pen recorder so that the signal level can be monitored during the course of a run. In order that the interferogram be sampled at regular intervals the Moiré fringe system is used to trigger the digital voltmeter. Included in this circuit are scale of two counting circuits, which enable every second or fourth pulse, etc., to be passed to the digital voltmeter. In this way, with a suitable use of filters, the spectral range can be reduced from 625 cm^{-1} to 312.5 cm^{-1}, or 156.25 cm^{-1}, etc., thus reducing the amount of information needed to be stored on tape. Fig. (4) shows typical interferograms of pure and doped KBr. They are direct chart recordings.

Procedure of a Run

The procedure of a run is as follows. Interferograms of both a doped and undoped sample of the same thickness are recorded under the same operating conditions. The paper tape is then converted to punched cards and the transformed spectra are calculated on a C.D.C. 6400 computer. Absorption coefficients are calculated by computing the negative logarithm of the ratio of the two spectra, the results

Figure 4

Two examples of interferograms measured with the interferometer. Curve (a) is the interferogram of a sample of pure Harshaw KBr, while curve (b) shows an interferogram of KBr doped with Tl^{+}. The curves are direct recorder tracings.

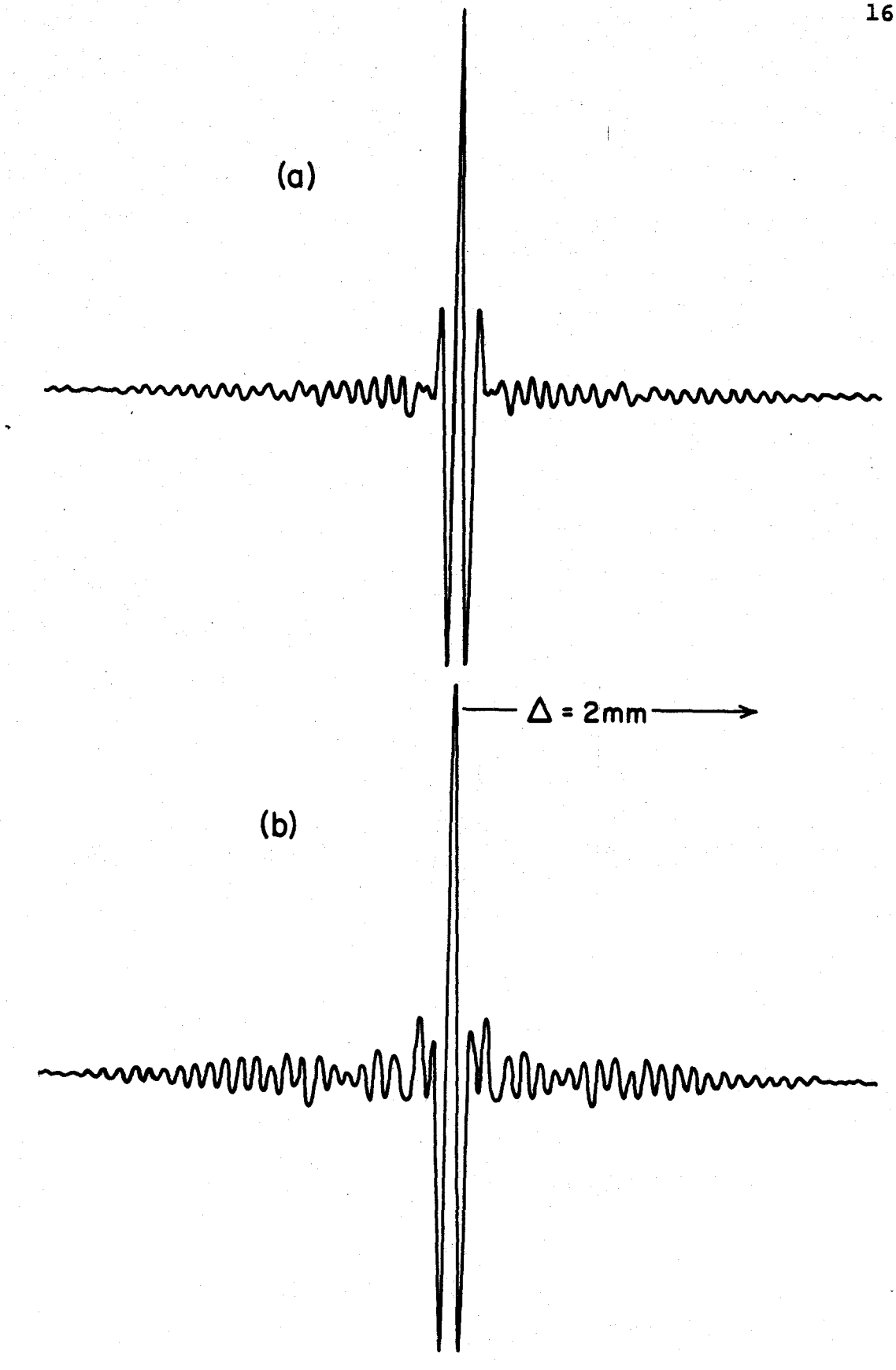
(a)
Δ = 2mm
(b)

being plotted by the computer line printer.

Two types of runs are usually made, one in which the interferogram is recorded on both sides of the central maximum. This enables accurate intensities to be calculated but reduces the effective resolution of the spectrum (Loewenstein 1963; Connes 1963). The second type of run is one-sided,with the first point starting on the central maximum. This type of operation introduces a phase error, pointed out by Loewenstein (1963), since it is usually difficult to start the first pulse accurately on the central maximum. However, the frequencies of the peaks are not affected; only the intensity is distorted (Bosomworth and Gush 1965). Thus one can perform high resolution one-sided runs and use the double-sided runs to check the relative intensities. In both cases the interferogram is multiplied by a linear apodization function (Vanasse 1962) to suppress the large side lobes of the scanning function.

B. SAMPLE PREPARATION

The single crystals used in this investigation came from several sources. The pure KBr and KCl crystals were obtained from the Harshaw Chemical Company, Cleveland, Ohio, and the KBr and KCl crystals doped with O_2^- were kindly provided by Dr. J. Rolfe of the National Research Council, Ottawa. Sm^{2+} and Eu^{2+} doped KBr and KCl crystals were ob-

tained from Dr. M. Buchanan, who has discussed their growth and analysis in some detail (Buchanan 1969).

All the other crystals used were grown in our laboratory by the Kryopoulos-Czochralski technique. The apparatus consisted of a vacuum tight Vycor chamber into which inert gases could be admitted. Metal parts were made of Inconel, and the crystals were grown in glazed porcelain #3 Coors crucibles.

The starting material for the melt was reagent grade chemicals from the Fisher Scientific Company. The dopants were also Fisher Reagent Grade. Usually 0.5 at.% dopant levels were added to the KBr melts, yielding about 0.1 at.% in the final crystals. KCl was found to require less dopant to reduce saturation of the transmission in the thickness used. Crystals of KCl, doped with 0.01 at.% impurity, were obtained from approximately 0.1 at.% impurity in the melt.

The melt mixture was usually dried under vacuum and then raised to the melting point. Ultra high purity argon gas was permitted to flow through the chamber at slightly above atmospheric pressure. This gas flow helped to carry away unwanted impurities and vaporized salt. Crystal boules of approximately 2.5 cm diameter and up to 6 cm in length could be pulled from the melt over a 3 to 4 hour period. Subsequent analysis showed that there was usually a gradation of impurity concentration through the length of the crystals,

the highest concentration being found at the bottoms of the crystals. In this manner samples of different impurity concentration could sometimes be obtained from the same boules.

Various techniques were used to determine the impurity concentrations of the different systems. The sodium and lithium concentrations in KBr and KCl were determined by atomic absorption and flame emission spectroscopy respectively. The concentration of OH^- in KBr was estimated from the far infrared results of Bosomworth (1967). Fluorine concentrations were measured using a specific ion electrode technique by Dr. R.G.V. Hancock, of the Department of Chemistry, McMaster University, who also determined the concentrations of Sm^{2+}, Eu^{2+} and Br^- in KCl by a neutron activation technique. This technique was also used to measure the iodine concentration in potassium chloride, however, the chlorine and iodine ions had first to be chemically separated since the radioactive isotopes of these two elements have similar half lives of approximately 25 min.

CHAPTER III

THEORY

In order to calculate the far-infrared absorption due to the addition of impurities, it is first important to know the dynamics of the unperturbed host crystal. We have used the ordinary shell model (Cowley et al. 1963) description of the lattice dynamics of KBr and KCl. The parameters for this model being determined from the results of inelastic neutron scattering experiments on KBr by Woods et al. (1963) and on KCl by Copley et al. (1969).

The model for the defect used in the perturbed calculations is the relaxation defect model of Woll, Gethins and Timusk (1968). This model is expected to be suitable when the impurity ions are smaller than the host ions they replace, when a different overlap of the ions and some relaxation of the lattice around the defect is expected.

The chapter is divided into three sections dealing with the unperturbed lattice, the lattice with impurities and finally the calculation of the far-infrared absorption line shape.

A. UNPERTURBED LATTICE

The vibrational Hamiltonain for the perfect lattice in the harmonic approximation can be written

$$H_o = \frac{1}{2} \sum_{L\alpha\kappa} M_\kappa \dot{X}_L^{\alpha\kappa 2} + \frac{1}{2} \sum_{\substack{L \\ L'}} \sum_{\substack{\beta\kappa \\ \beta\kappa'}} \Phi_{\alpha\beta}(L\kappa, L\kappa') X_L^{\alpha\kappa} X_{L'}^{\beta\kappa'} \quad \text{(III-1)}$$

where the quantity $X_L^{\alpha\kappa}$ is the displacement in the α-direction of the κth particle in the Lth unit cell. κ denotes the type of ion on the site L ($\kappa = \pm$ for the positive and negative ions) and M_κ is its mass. The interatomic force constant $\Phi_{\alpha\beta}$ is defined by

$$\Phi_{\alpha\beta}(L\kappa, L'\kappa') = \left| \frac{\partial^2 \Phi(X)}{\partial X_L^{\alpha\kappa} \partial X_{L'}^{\beta\kappa'}} \right| x = 0 \quad \text{(III-2)}$$

where $\Phi(x)$ is the potential energy of the crystal, consisting of two parts; a repulsive part Φ^R and an attractive Coulomb part Φ^C; the second derivative being evaluated at the equilibrium positions of the particles.

The equation of motion for the L^{th} ion can be reduced to a time independent form by making the substitution

$$X_L^{\alpha\kappa} = \frac{U_L^{\alpha\kappa}}{\sqrt{M_\kappa}} e^{-i\omega t} \quad \text{(III-3)}$$

where $U_L^{\alpha\kappa}$ is a time independent amplitude and ω is the frequency of vibration. The equation of motion then becomes

$$\sum_{L'\beta\kappa'} \left(\frac{\Phi_{\alpha\beta}(L\kappa,L'\kappa')}{\sqrt{M_\kappa M_{\kappa'}}} - \omega^2\delta_{L,L'}\delta_{\alpha,\beta}\delta_{\kappa,\kappa'}\right)u_L^{\beta\kappa'} = 0 \qquad \text{(III-4)}$$

which can be written in matrix rotation for all L as

$$(\underline{A} - \omega^2\underline{I})\underline{u} = 0 \qquad \text{(III-5)}$$

$$\text{where } A_{\alpha\beta}(L\kappa,L'\kappa') = \frac{\Phi_{\alpha\beta}(L\kappa,L'\kappa')}{\sqrt{M_\kappa M_{\kappa'}}} \qquad \text{(III-6)}$$

and $\underline{I}$ is the unit matrix.

Equation (III-5) can be diagonalized by making a unitary transformation, using the matrix $\underline{D}$ where

$$\underline{D}_{L\kappa\alpha,qj} = \frac{1}{\sqrt{N}}\,\varepsilon_\alpha(\kappa\underline{q}j)\exp(i\underline{q}\cdot\underline{R}(L\kappa)) \qquad \text{(III-7)}$$

into the representation of plane waves denoted by the wave vector $\underline{q}$ and polarization index j. In the alkali halides j labels the six normal modes of vibration which have characteristic frequencies $\omega_{\underline{q}j}$. $\underline{\varepsilon}(\kappa\underline{q}j)$ are the eigenvectors which give the vibrational directions and relative amplitudes of the $\underline{q}j$ mode.

For the alkali halides the $\underline{\varepsilon}(\kappa\underline{q}j)$ are real and the elements of the inverse transformation $\underline{D}^{-1}$ are

$$\underline{D}^{-1}_{L\kappa\alpha,\underline{q}j} = \frac{1}{\sqrt{N}}\,\varepsilon_\alpha(\kappa\underline{q}j)\exp(-i\underline{q}\cdot\underline{R}(L\kappa)). \qquad \text{(III-8)}$$

where N is the number of ions in the lattice.

The Green's function matrix for the unperturbed lattice, $\underline{G}(\omega^2)$, is defined by the equation

$$(\underline{A} - \omega^2\underline{I})\underline{G}(\omega^2) = \underline{I} \qquad \text{(III-9)}$$

In the $\{\underline{q}j\}$ representation $\underline{A}$ is diagonal with elements $\omega^2_{\underline{q}j}$ and therefore the elements of $\underline{G}$ are

$$\underline{G}(\omega^2;\underline{q}j,\underline{q}'j') = \frac{\delta_{\underline{q}\underline{q}'}\delta_{jj'}}{(\omega^2_{\underline{q}j}-\omega^2)} \qquad \text{(III-10)}$$

The Shell Model

Improvements to the previous model can be made if we take into account the effect of the valence electrons on the lattice vibrations. We have followed the procedure due to Woods et al. (1963) and Cowley et al. (1963). This shell model assumes that each ion consists of a heavy central core containing the nucleus and inner shell electrons surrounded by a rigid shell of valence electrons whose mass is negligible in the adiabatic approximation. Following the notation of MacPherson (1970) we label the isotropic force constant between the core and shell as G_K. We assume that short range repulsive over-lap forces act only between shells and extend out to second neighbours. The long range Coulomb forces between point dipoles are summed by the Ewald method (Kellerman, 1940).

In the $\{\underline{q}\kappa\alpha\}$-representation the equations of motion now become, in matrix notation

$$\omega^2 \underline{u} = (\underline{G} + \underline{X}\,\underline{C}\,\underline{X})\underline{u} + (\underline{X}\,\underline{C}\,\underline{Y} - \underline{G})\underline{s}$$

$$0 = (\underline{Y}\,\underline{C}\,\underline{X} - \underline{G})\underline{u} + (\underline{R}+\underline{G}+\underline{Y}\,\underline{C}\,\underline{Y})\underline{s} \qquad \text{(III-11)}$$

from which one can obtain the matrix appearing in equation (III-5)

$$\underline{A} = (\underline{G} + \underline{X}\,\underline{C}\,\underline{X}) - (\underline{X}\,\underline{C}\,\underline{Y}-\underline{G})(\underline{R} + \underline{G} + \underline{Y}\,\underline{C}\,\underline{Y})^{-1}(\underline{Y}\,\underline{C}\,\underline{X}-\underline{G}) \qquad \text{(III-12)}$$

$\underline{u}$ and $\underline{s}$ are 6 component vectors which contain the mass reduced coordinates for the ion cores and shells respectively. The core charges are $X_{\pm}e$ and the shell charges are $Y_{\pm}e$ with the total ionic charge being given by $Z_{\pm} = X_{\pm} + Y_{\pm}$. The components of the repulsive force constant matrix $\underline{R}$ are usually defined in terms of parallel and perpendicular second derivatives of the repulsive potentials which act between the nearest and second nearest neighbours.

The final eleven parameters of the shell model have been determined for KBr and KCl by least squares fitting to the inelastic neutron scattering results of Woods et al. (1963) and Copley et al. (1969). Calculations were made at 1505 $\underline{q}$-points in the irreducible 1/48th of the Brillouin zone. Utilizing the symmetry of the O_h group finally gives values of $\underline{q}, \omega(\underline{q}j)$ and $\underline{\varepsilon}(\kappa\underline{q}j)$ for KBr and KCl at 62,500 points in the full zone.

The unperturbed Green's function matrices were calculated by the method outlined by MacPherson (1970a).

B. PERTURBED LATTICE

The introduction of a single substitutional impurity into the lattice causes a change of mass and force constants which can be described by the equation

$$(\underline{A} + \underline{\Gamma} - \omega^2 \underline{I})u = 0 \qquad \text{(III-13)}$$

which is similar to equation (III-5) for the pure lattice. Here $\underline{\Gamma}$ is the matrix containing the mass and force constant changes due to the introduction of the impurity.

The perturbed Green's function $\bar{\underline{G}}$ can be related to the Green's function $\underline{G}$ for the unperturbed lattice by the Dyson equation

$$\bar{\underline{G}} = (\underline{I} + \underline{G}\,\underline{\Gamma})^{-1}\underline{G} \qquad \text{(III-14)}$$

rearranging gives

$$\bar{\underline{G}} = \underline{G} - \underline{G}\,\underline{T}\,\underline{G} \qquad \text{(III-15)}$$

where

$$\underline{T} = \underline{\Gamma}(\underline{I} + \underline{G}\,\underline{\Gamma})^{-1} \qquad \text{(III-16)}$$

$\underline{T}$ is the scattering matrix introduced by Klein (1963) and is non-zero only in the defect space of $\underline{\Gamma}$. The required matrix inversion is practicable, since we only need the elements of $\bar{\underline{G}}$ which are in the same space as $\underline{\Gamma}$.

The defect model is assumed to consist of a changed mass, Δm, and isotropic core-shell force constant Δk, at the site, changed longitudinal force constants to the nearest neighbours Δf, and changed longitudinal force constants between the shells of the first and fourth nearest neighbours Δg. These changes are shown in Fig. (5).

In the $\{L\underline{q}\alpha\}$ representation the matrices $\underline{T}$, $\underline{\Gamma}$ and $\underline{G}$ are block diagonal in the form

$$\underline{T} = \left[\begin{array}{c|c} t & 0 \\ \hline 0 & 0 \end{array}\right] \qquad \text{(III-17)}$$

$$\underline{\Gamma} = \left[\begin{array}{c|c} \gamma & 0 \\ \hline 0 & 0 \end{array}\right] \qquad \text{(III-18)}$$

$$\underline{G} = \left[\begin{array}{c|c} g & g_1 \\ \hline g_1 & g_2 \end{array}\right] \qquad \text{(III-19)}$$

and the equation for $\underline{T}$ reduces to

$$t = \gamma(1 + g\gamma)^{-1} \qquad \text{(III-20)}$$

where $\underline{\gamma}$ is an 18 dimensional submatrix given by

$$\gamma_{\alpha\alpha} = \begin{bmatrix} \frac{\Delta g}{M_-} & \frac{-\Delta g}{M} & 0 & 0 & 0 & 0 \\ \frac{-\Delta g}{M} & \frac{\Delta f+\Delta g}{M_+} & 0 & \frac{-\Delta k}{M} & 0 & 0 \\ 0 & 0 & \frac{\Delta k-\Delta m\omega^2}{M_-} & \frac{-\Delta k}{M_-} & 0 & 0 \\ 0 & \frac{-\Delta f}{M} & \frac{-\Delta k}{M_-} & \frac{\Delta k+2\Delta f}{M_-} & \frac{\Delta f}{M} & 0 \\ 0 & 0 & 0 & \frac{\Delta f}{M} & \frac{\Delta f+\Delta g}{M_+} & \frac{-\Delta g}{M} \\ 0 & 0 & 0 & 0 & \frac{-\Delta g}{M} & \frac{\Delta g}{M_-} \end{bmatrix} \qquad \text{(III-21)}$$

Figure 5

"Defect molecule" showing ions affected by changes introduced by the insertion of the impurity. The impurity ion is at the centre with Δm representing the change in mass at the defect site. Nearest neighbours are potassium metal ions located at $\pm r_o \hat{\alpha}$ and the fourth neighbours are halide ions at $\pm 2r_o \hat{\alpha}$, $\alpha = x,y,z$.

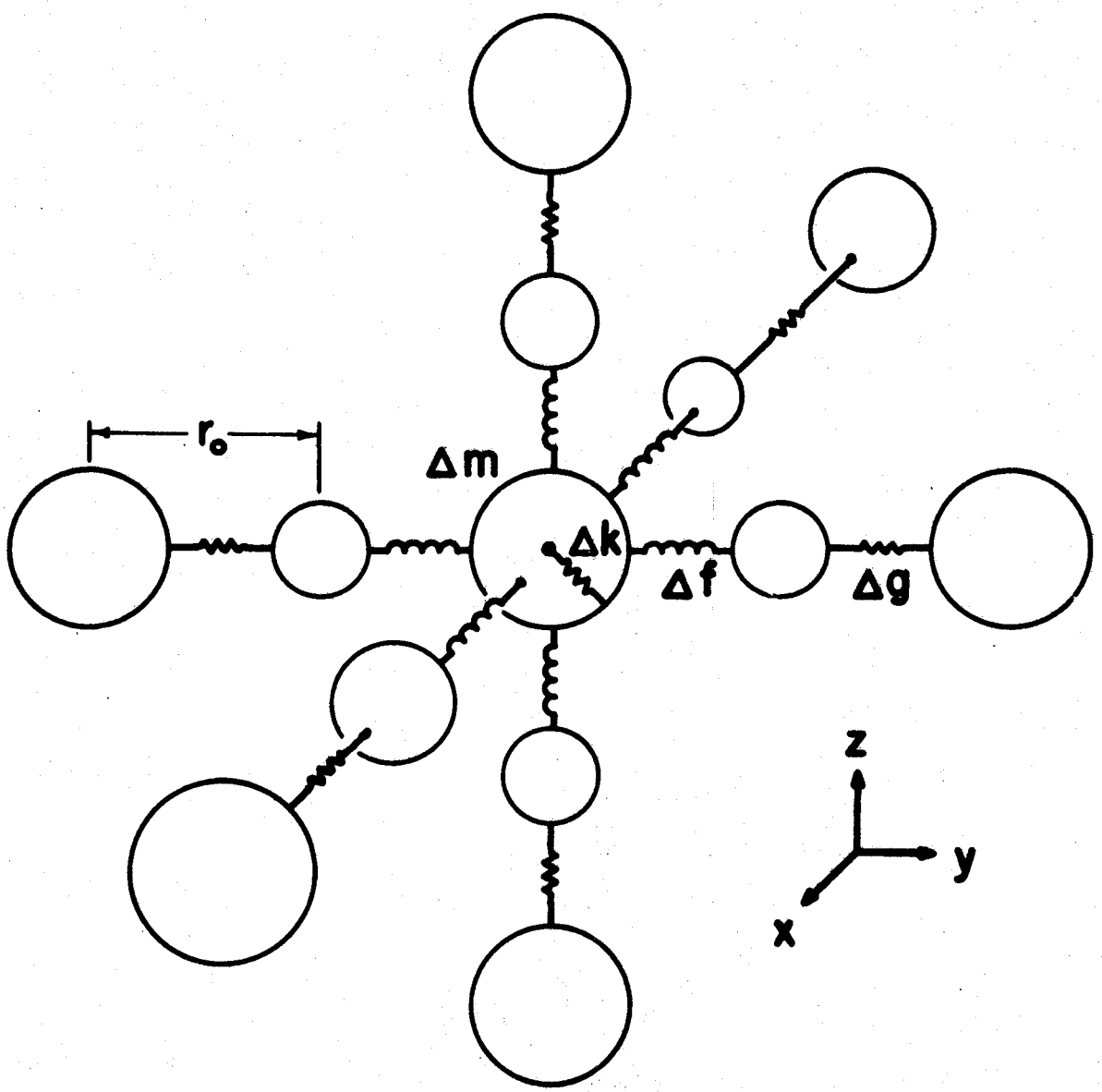
r_o
Δm
Δk
Δf
Δg
z
y
x

where $\alpha = x,y,z$ and $M = \sqrt{M_+ M_-}$. The rows and columns of this matrix are labeled in the defect space, $S_\alpha(-2r_o\hat{\alpha})$, $S_\alpha(-r_o\hat{\alpha})$, $U_\alpha(o)$, $S_\alpha(o)$, $S_\alpha(r_o\hat{\alpha})$ and $S_\alpha(2r_o\hat{\alpha})$ denoting displacements in the $\hat{\alpha}$ direction of the shells S, and the core U of the ions. The $\underline{\gamma}$ matrix may be reduced to block form by transforming to coordinates which form an irreducible basis of the O_h group.

The $\underline{\gamma}$ matrix retains the full point symmetry of the cubic lattice and the basis coordinates in this defect space are,

$$S(A_{1g};r) = (1/\sqrt{3})\{S_x(g;r) + S_y(g;r) + S_z(g;r)\}$$

$$S(E_g;r) = (1/\sqrt{2})\{S_x(g;r) - S_y(g;r)\}$$

$$S(E'_g;r) = (1/\sqrt{6})\{2S_z(g;r) - S_x(g;r) - S_y(g;r)\}$$

$$S_\alpha(T_{1u};r\hat{\alpha}) = S_\alpha(u;r\hat{\alpha})$$

$$u_\alpha(T_{1u};0) = u_\alpha(0) \qquad \text{(III-22)}$$

where $S_\alpha(g;r) = (1/\sqrt{2})\{S_\alpha(-r\hat{\alpha}) - S_\alpha(+r\hat{\alpha})\}$

$$S_\alpha(u;r) = (1/\sqrt{2})\{S_\alpha(-r\hat{\alpha}) + S_\alpha(+r\hat{\alpha})\}$$

$$S_\alpha(u;0) = S_\alpha(0)$$

with $r = r_o$ or $2r_o$ and $\alpha = x,y,z$.

With this basis the new non zero blocks along the diagonal are

$$\underline{\gamma}(E_g) = \underline{\gamma}(E'_g) = \underline{\gamma}(A_{1g}) = \begin{bmatrix} \frac{\Delta f+\Delta g}{M_+} & \frac{-\Delta g}{M} \\ \frac{-\Delta g}{M} & \frac{\Delta g}{M_-} \end{bmatrix} \qquad \text{(III-23)}$$

and

$$\underline{\gamma}(T_{1u\alpha}) = \begin{bmatrix} \frac{\Delta k-\Delta m\omega^2}{M} & \frac{-\Delta k}{M} & 0 & 0 \\ \frac{-\Delta k}{M} & \frac{2\Delta f+\Delta k}{M_-} & \frac{\sqrt{2}\Delta f}{M} & 0 \\ 0 & \frac{-\sqrt{2}\Delta f}{M} & \frac{\Delta f+\Delta g}{M_+} & \frac{-\Delta g}{M} \\ 0 & 0 & \frac{-\Delta g}{M} & \frac{\Delta g}{M} \end{bmatrix} \qquad \text{(III-24)}$$

The T_{2g} modes are not perturbed by this form of the defect model and consequently $\underline{\gamma}$ has no T_{2g} components. The rows and columns of $\underline{\gamma}(A_{1g})$ refer to the coordinates $S(A_{1g};r_o)$ and $S(A_{1g};2r_o)$ and similarly for $\underline{\gamma}(E_g)$ and $\gamma(E'_g)$. In the case of $\underline{\gamma}(T_{1u\alpha})$ the corresponding row and column indices are $u_\alpha(T_{1u};0)$, $S_\alpha(T_{1u};0)$, $S_\alpha(T_{1u};r_o)$ and $S_\alpha(T_{1u};2r_o)$.

C. FAR-INFRARED INDUCED ABSORPTION

Absorption of far-infrared radiation in pure alkali halide crystals is restricted to excitation of only zero wave vector phonons, that is the well known reststrahlen absorption. When impurities are introduced into such a crystal it

loses its translational symmetry, and the restrictive $\underline{q} \approx 0$ selection rule is relaxed. Radiation can now interact with all vibrational modes that have the appropriate symmetry. These modes are visible in measurements of the far-infrared absorption as structure in addition to the reststrahlen absorption. This absorption can be calculated using the model developed in the preceeding sections by a method similar to that described by MacPherson and Timusk (1970b).

A theoretical expression for the absorption constant as a function of angular frequency ω is given by Klein (1968);

$$\alpha(\omega) = \frac{(n_\infty^2+2)^2 4\pi\omega}{N v c 9 n(\omega)} Im(\underline{Z}_x^\dagger \underline{M}^{-\frac{1}{2}} \underline{G}\ \underline{T}\ \underline{G}\ \underline{M}^{-\frac{1}{2}} \underline{Z}_x) \qquad \text{(III-25)}$$

where $n(\omega)$ is the index of refraction of the crystal at frequency ω and is assumed constant over the frequency range of interest, n_∞ is the index of refraction in the high frequency limit, N is the number of unit cells of volume v and c is the velocity of light. $\underline{G}$ is the unperturbed Green's function matrix and $\underline{T}$ is the "scattering" matrix of equation (III-16). The quantities $\underline{Z}_x$, $\underline{Z}_y$ and $\underline{Z}_z$ are vectors with components

$$Z_\beta^\alpha(L\kappa) = Z_\kappa\ \delta_{\alpha\beta} \qquad \alpha,\beta = x,y,z. \qquad \text{(III-26)}$$

The charge on the κ ion in the L^{th} unit cell is $Z_x e$ and $\underline{M}^{-\frac{1}{2}}$ is a diagonal matrix with elements $1/\sqrt{M}_\kappa \delta_{LL'} \delta_{\kappa\kappa'} \delta_{\alpha\beta}$. In the case of the rigid ion model $Z_+ = -Z_- = Z$ and the vector

$\underline{M}^{-\frac{1}{2}}\underline{Z}_x$ is proportional to the $\underline{q} = 0$ transverse optical phonon eigenvector polarized in the x-direction. In the case of the shell model however, both ion cores and shells, have individual charges and the situation is not so simple . MacPherson and Timusk (1970a) have shown that the Green's function matrix can be written in separated form. Then the vector $\underline{R}_x(\omega) = \underline{G}\,\underline{M}^{-\frac{1}{2}}\underline{Z}_x$ in equation (III-25) is modified and becomes

$$\underline{R}_x(\omega) = \begin{bmatrix} \underline{G}_{uu} & \underline{G}_{us} \\ \underline{G}_{su} & \underline{G}_{ss} \end{bmatrix} \begin{bmatrix} \underline{M}^{-\frac{1}{2}} & 0 \\ 0 & \underline{M}^{-\frac{1}{2}} \end{bmatrix} \begin{bmatrix} \underline{X}_x \\ \underline{Y}_x \end{bmatrix} \qquad \text{(III-27)}$$

where the vectors $\underline{X}_x$ and $\underline{Y}_x$ are similar to $\underline{Z}_x$ except that they refer to the core and shell charges respectively.

Denoting the core and shell polarization vectors by $\underline{\varepsilon}$ and $\underline{\eta}$ and the eigenfrequencies by $\omega_{\underline{q}j}$, the components of $\underline{R}_x(\omega)$ can be written as

$$\{R_x(\omega)\}^u_{L\kappa\alpha} = \{\underline{G}_{uu}\underline{M}^{-\frac{1}{2}}\underline{X}_x + \underline{G}_{us}\underline{M}^{-\frac{1}{2}}\underline{Y}_x\}_{L'\kappa\alpha} \qquad \text{(III-28)}$$

$$= \sum_{L'\kappa'\beta}\frac{1}{N}\sum_{\underline{q}j}\frac{\varepsilon_\alpha(\kappa;qj)\,[\varepsilon^\dagger_\beta(\kappa;qj)X_{\kappa'} + \eta^\dagger_\beta(\kappa';qj)Y_{\kappa'}]\,\delta_{\beta\kappa}\exp(iq\cdot(R_{L\kappa}-R_{L'\kappa'}))}{(\omega^2_{qj}-\omega-\omega^2)\sqrt{M_{\kappa'}}}$$

$$= \sum_{\kappa' j}\frac{\varepsilon_\alpha(\kappa;oj)}{\omega^2_{oj}-\omega^2}\,\frac{[\underline{\varepsilon}^\dagger(\kappa';oj)\,\underline{X}_x + \underline{\eta}^\dagger(\kappa';ok)\,\underline{Y}_x]}{\sqrt{M_{\kappa'}}}$$

and

$$\{R_x(\omega)\}^S_{L\kappa\alpha} = \sum_{\kappa' j}\frac{\eta_\alpha(\kappa;oj)\,[\underline{\varepsilon}^\dagger(\kappa';oj)\cdot\underline{X}_x + \underline{\eta}^\dagger(\kappa';oj)\cdot\underline{Y}_x]}{(\omega^2_{oj}-\omega^2)\sqrt{M_{\kappa'}}} + \sum_{\kappa'} A^{-1}_{ss}\binom{\kappa\kappa'}{LL'}\frac{\underline{Y}_{\kappa'}}{\sqrt{M_{\kappa'}}}$$

where $A_{ss} = R + G + YCY$. The $\underline{q} = 0$ vectors $\underline{\varepsilon}(\kappa;oj)$ and $\underline{\eta}(\kappa;oj)$ have non-zero x components only for the transverse optic (TO) and transverse acoustic (TA) modes polarized in the X direction. These components are

$$\eta_x(\pm;0,TA) = \varepsilon_x(\pm;0,TA) = [M_\pm/(M_+ + M_-)]^{\frac{1}{2}}$$

$$\varepsilon_x(\pm;0,TO) = \pm[M_\mp/(M_+ + M_-)]^{\frac{1}{2}}$$

and $\eta_x(\pm;0,TO)$ which is obtained from $\varepsilon_x(\pm;0,TO)$ by means of equation (III-11). The acoustic mode coefficients in equation (III-27) are zero so that only the x-polarized transverse optic modes contribute to the sum over the polarization index j. In the required combination of matrix elements for $R_x(\omega)$ it can be seen that the elements referring to neighbours in the $\pm x$ direction have the same sign. The combination of matrix elements is therefore "odd" in symmetry with respect to the position of the impurity ion. Thus if we apply the same transformation to $R_x(\omega)$ as was applied to $\underline{\gamma}$ to obtain the independent symmetrized blocks, only elements of T_{lux} symmetry appear. The elements of $\underline{t}(T_{lux})$ are given by

$$\underline{t}(T_{lux}) = \underline{\gamma}(T_{lux})[\underline{I}+\underline{g}(T_{lux})\underline{\gamma}(T_{lux})]^{-1} \qquad \text{(III-29)}$$

The components for $R_x(\omega)$ in the same representation are

$$R_x(T_{lux};\omega) = \frac{p}{\omega_{TO}^2-\omega^2} \begin{bmatrix} \varepsilon_x(-,0,TO) \\ \eta_x(-0,TO) \\ \sqrt{2}\eta_x(+,0,TO) \\ \sqrt{2}\eta_x(-,0,TO) \end{bmatrix} + \begin{bmatrix} 0 \\ R_x^-(0) \\ \sqrt{2}R_x^+(0) \\ \sqrt{2}R_x^-(0) \end{bmatrix} \qquad \text{(III-30)}$$

where

$$p = \sum_{\kappa} \frac{\underline{\varepsilon}^{\dagger}(\kappa,0,TO)\cdot\underline{X}_{\kappa}+\underline{\eta}^{\dagger}(\kappa,0,TO)\ \underline{Y}_{\kappa}}{\sqrt{M_{\kappa}}}$$

and

$$R_x^{\kappa}(0) = \sum_{\kappa'} \frac{A_{ss}^{-1}{}_{LL'}^{(\kappa\kappa')}Y_{\kappa'}}{\sqrt{M_{\kappa'}}}$$

Finally the total induced absorption can be written as

$$\alpha(\omega) = \frac{4\pi(n_\infty^2+2)^2\omega N}{9cn(\omega)} \left(R_x^{\dagger}(\omega)\,\mathrm{Im}\ t(\omega^2-io^+)R_x(\omega)\right)_{T_{lux}} \qquad \text{(III-31)}$$

where N is the number of non interacting impurities per unit volume and NNv is the total number of impurities. The induced far-infrared absorption below the reststrahlen frequency was calculated using this expression.

CHAPTER IV

RESULTS AND DISCUSSION OF KBr IMPURITY SPECTRA

A. GENERAL REMARKS

In a study of the induced single phonon continuous absorption, it is important that structure in the host lattice absorption, be unambiguously distinguished from band-mode resonances and gap modes that may occur due to a particular impurity. This problem can be resolved by using accurate models for the phonons of the host crystal and by studying the spectra due to a variety of strong and weakly perturbing impurities. One can then attempt to identify critical points of the host lattice that are common to all the defect spectra, (Timusk and Ward 1969, Macdonald et al. 1969).

In KBr all the impurities used, with the exception of Cl^-, produce a similar continuous absorption spectrum from 40 to 93 cm^{-1}. All the spectra are interrupted by several very sharp discontinuities that can indeed be identified with Van Hove singularities (Van Hove 1953) of KBr. The positions of the singularities are found to vary slightly with impurity concentration. Fig. (6) shows the typical absorption in KBr with Na^+ as the impurity. The two curves are for different impurity concentrations. The discontinuities

FIGURE 6

Far-infrared absorption between 60 and 95 cm^{-1} of KBr containing two different concentrations of Na^{+}. The discontinuities in the spectrum are marked A, B, C and D and one can see from the vertical dashed line at B that the positions of these discontinuities move to higher frequencies as the concentration is increased. The resolution of the interferometer is given by the frequency interval between the arrows.

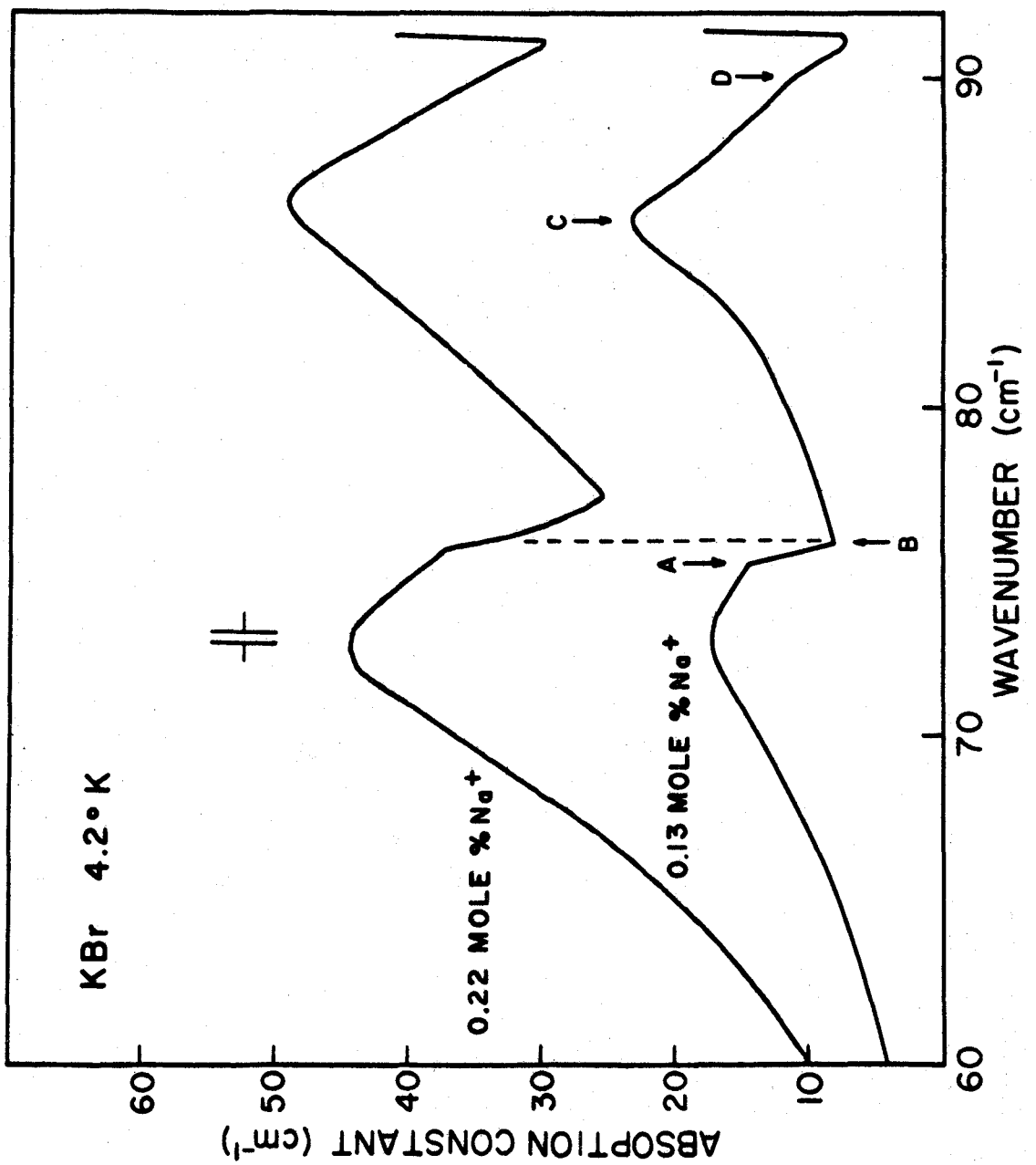
KBr 4.2° K
0.22 MOLE % Na+
0.13 MOLE % Na+
A
B
C
D
ABSORPTION CONSTANT (cm-1)
WAVENUMBER (cm-1)
10
20
30
40
50
60
70
80
90

in the spectrum are marked A, B, C and D and one can see from the vertical dashed line at B that the positions of these discontinuities move to higher frequencies as the concentration is increased. We take the extrapolated zero-concentration value for the position of the singularity in the pure crystal.

Other impurities in KBr show similar structure, the only difference is the change in relative intensities of the various peaks. Table (1) summarizes the positions of the singularities for all the impurities studied in KBr. Strongly perturbing impurities that require large changes of mass and force constants in contrast to the weakly perturbing isotopic impurities, produce an absorption which is proportional to a more strongly modified density of states.

In KBr several of the impurities, namely, Li^+, OH^- and F^- produce band-mode resonances below 40 cm^{-1} where the density of states is low. In addition Na^+, Tl^+ and O_2^- show evidence of gap modes, (absorption in the gap between the acoustic and optical modes).

As pointed out by Van Hove (1953) the singularities in the unperturbed density of states, that is points in the Brillouin zone where the gradient of frequency as a function of wave vector $\underline{q}$ vanishes, are due to saddle points and maxima and minima in the frequency surfaces. Neutron diffraction

TABLE 1

Positions of the observed singularities in KBr crystals with different impurities at 11°K. The Na^+, Sm^{++} and Li^+ data have been extrapolated to zero defect concentration. The other impurity concentrations are as listed.

	Mole % impurity	A (cm^{-1})	B (cm^{-1})	C (cm^{-1})	D (cm^{-1})
Li^+	0	74.71	75.1	85.67	89.56
Na^+	0	74.68	75.2	85.22	89.73
Tl^+	<.5	74.8	75.2	86.36	89.57
Sm^{++}	0	74.91	75.22	85.49	89.8
Cl^-	≈ 2.0	74.7*	76.0*		
F^-	.001	74.84	75.53	85.67	90.17
OH^-	.013	74.6	75.5	85.6	90.15
O_2^-	≈ .001	74.76	75.38	85.8	89.3
Shell Model		70.0	73.0	83.0	88.0

*High concentration metamorphosed singularities.

experiments are usually performed in directions of high symmetry and critical points in these directions have been determined fairly accurately using this technique. In general these frequencies agree well with the infrared results. In off-symmetry directions however, where neutron measurements have not been made, the infrared measured critical points are not in such good agreement with the interpolated shell model frequencies. Similar observations have been made by Timusk and Buchanan (1967) who studied the vibronic side band of Sm^{2+} electronic transitions in KBr.

A change of shape or metamorphism of Van Hove singularities has been predicted theoretically by Okazaki et. al. (1967). These predictions have been confirmed in this thesis for the KBr:Cl^- system with the first direct experimental observation of metamorphism. The singularities A and B are seen to undergo change from a step of type ⌐ in the normal spectra to a type ⌐ in KBr:Cl^-. This effect will be discussed in more detail when individual impurity spectra are considered.

Estimates of the force constant changes needed for a particular impurity were obtained by considering a rigid ion picture of the defect and its immediate neighbours. The relative sizes of the defect ion and the ion it replaces give some indication of the amount of inward and outward relaxation of the neighbours. In the cases where resonant modes are

present, the force constant change between first neighbours, Δf, was adjusted to give a resonant mode peak at the experimentally determined frequency. The force constant change between first and fourth neighbours Δg, was then adjusted to give an overall fit to experiment.

Not all defects produced resonances and in general force constant changes were chosen so that the shape and relative intensities of the various peaks could be reproduced. Whenever possible force constant changes determined by other experiments were compared with our results, notable among these are the work of Buchanan and Woll (1969), on the vibronic side band of Sm^{2+} in KBr, Rolfe (1970) on similar experiments of O_2^- in KBr and the Raman work of Harley et al. (1969,1971) on the KBr Tl^+ system. In this manner the effectiveness of the defect model in describing the local environment of the impurity ion could be tested.

The polarizability of the defect ion, which is related to Δk, the change in the core-shell force constant, is found to have little effect on the calculated absorption in KBr and KCl. In each of the systems studied decreasing k only tended to slightly reduce the overall absorption. This is in agreement with the far-infrared calculations of MacPherson (1970), and the side band calculations of Buchanan and Woll (1969). With $\Delta k = 0$, the shell model defect is almost equivalent to

the rigid ion defect model used by Woll et al. (1968).

Comparison of the theoretical calculations with the experimental results for each specific impurity in KBr will be described in greater detail in the next section.

B. SPECIFIC ABSORPTION SPECTRA

1. Sodium

Baumann and Pohl (1967) have previously studied the KBr:Na^+ system through thermal conductivity experiments. Their measurements indicate a resonance at 72 cm^{-1}, this resonance however was not observed in our infrared measurements and did not appear in our calculations of the T_{1u} modes, the only ones that can be seen in the far-infrared.

The far infrared absorption consists of four sharp peaks in the gap in addition to the broad one phonon continuum, see the full line in Fig. (7). Several sharp discontinuities are seen to interrupt the continuous absorption and these have been designated A, B, C and D, as mentioned in the last section. In addition to the sharp drop in intensity at the step A→B there is a broad peak C, centred at 85.2 cm^{-1} with a shoulder D at 89.7 cm^{-1}. The four peaks in the gap occur at 91.6, 93.4, 94.6 and 98.3 cm^{-1}. The peak at 94.6 cm^{-1} has previously been identified by Levine (Klein 1968) and by Grisar et al. (1967) to be a gap mode of Cl^-.

FIGURE 7

Induced far-infrared absorption due to Na^+ ions in KBr. The experimental absorption shows evidence of modes in the gap. The calculated curve is based on the shell model for the defect with the force constant changes $\Delta f = -7{,}500$ dyn/cm, $\Delta g = -2000$ dyn/cm and $\Delta k = 0$.

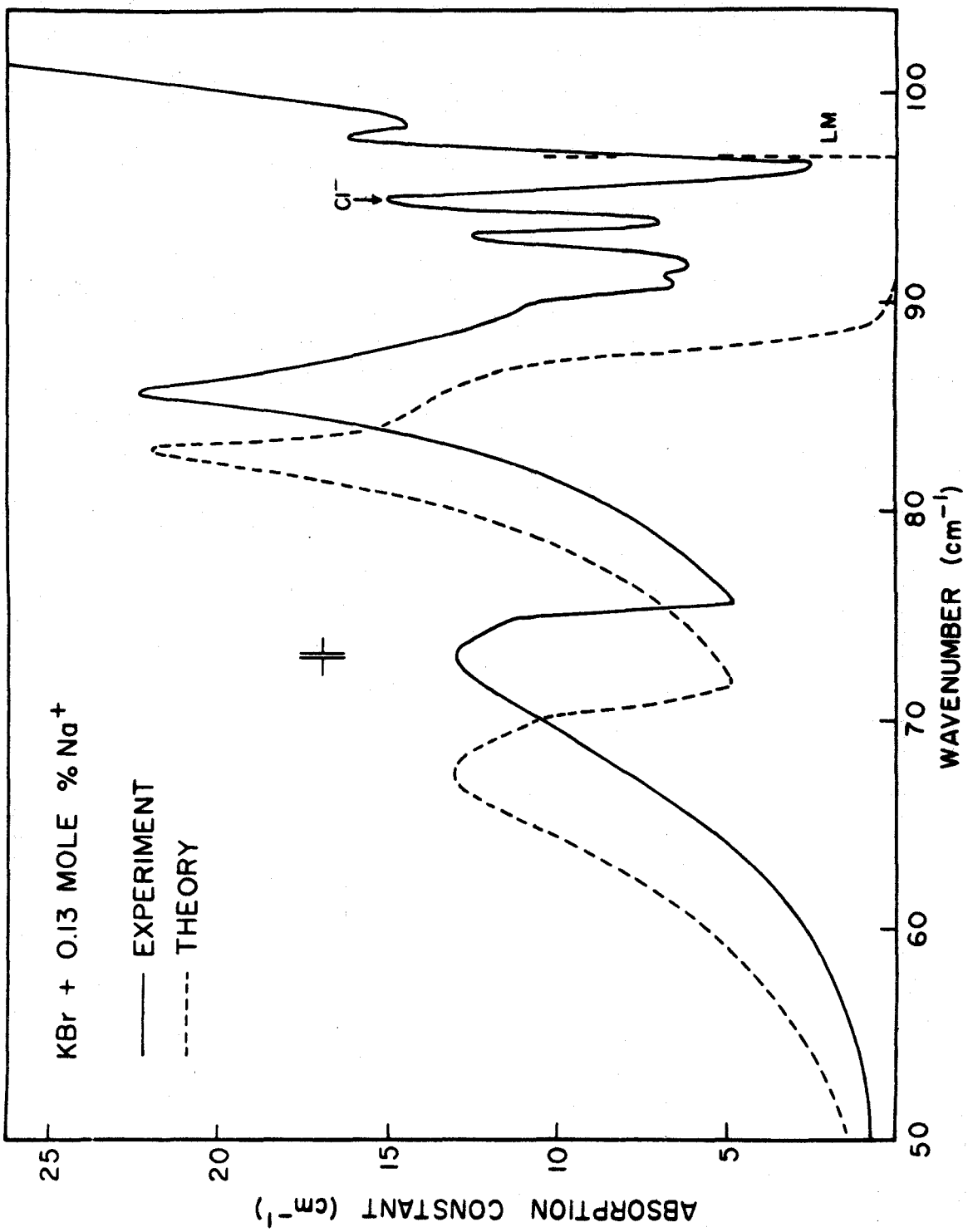
KBr + 0.13 MOLE % Na+
EXPERIMENT
THEORY
Cl⁻
LM
ABSORPTION CONSTANT (cm⁻¹)
WAVENUMBER (cm⁻¹)
25
20
15
10
5
50
60
70
80
90
100

This peak occurred in all the KBr samples studied, even in the nominally pure Harshaw crystals. Examination of the 91.6 and 93.4 cm^{-1} peaks shows that their line strength appears to vary as the square of the sodium ion concentration, thus indicating that these absorption peaks may be due to pairs of sodium ions (Tsvetov et al. 1967). However this is only a tentative suggestion since the peaks occur very close together and difficulty is encountered in deciding the zero level. The peak at 98.3 cm^{-1} occurs on the steeply rising resstrahlen edge making its positive identification difficult.

Low resolution transmission measurements on KBr:Na^+ crystals have been previously made by Hadni et al. (1967) using a CN laser. They observed a peak at 93 cm^{-1} and three bands at 101, 83.5 and 71.5 cm^{-1}. The 93 cm^{-1} peak is identified by them to be the Cl^- resonance, however their measurements place it approximately 2 cm^{-1} low in frequency. The bands at 71.5 and 83.5 cm^{-1} appear to be the same as our two principle bands A and C, but again they appear low in energy. Because of low resolution these workers were unable to observe structure due to other impurities in KBr.

The positions of the singularities vary slightly with dopant concentration. Figs. (8), (9) and (10) show this dependence for the singularities A, B and C as a function of concentration. Increasing the Na^+ concentration produces a shift to higher frequencies of the position of the step A→B,

FIGURE 8

The frequency of the singularity A as observed in the far infrared plotted as a function of Na^+ impurity concentration. The straight line was fitted by eye.

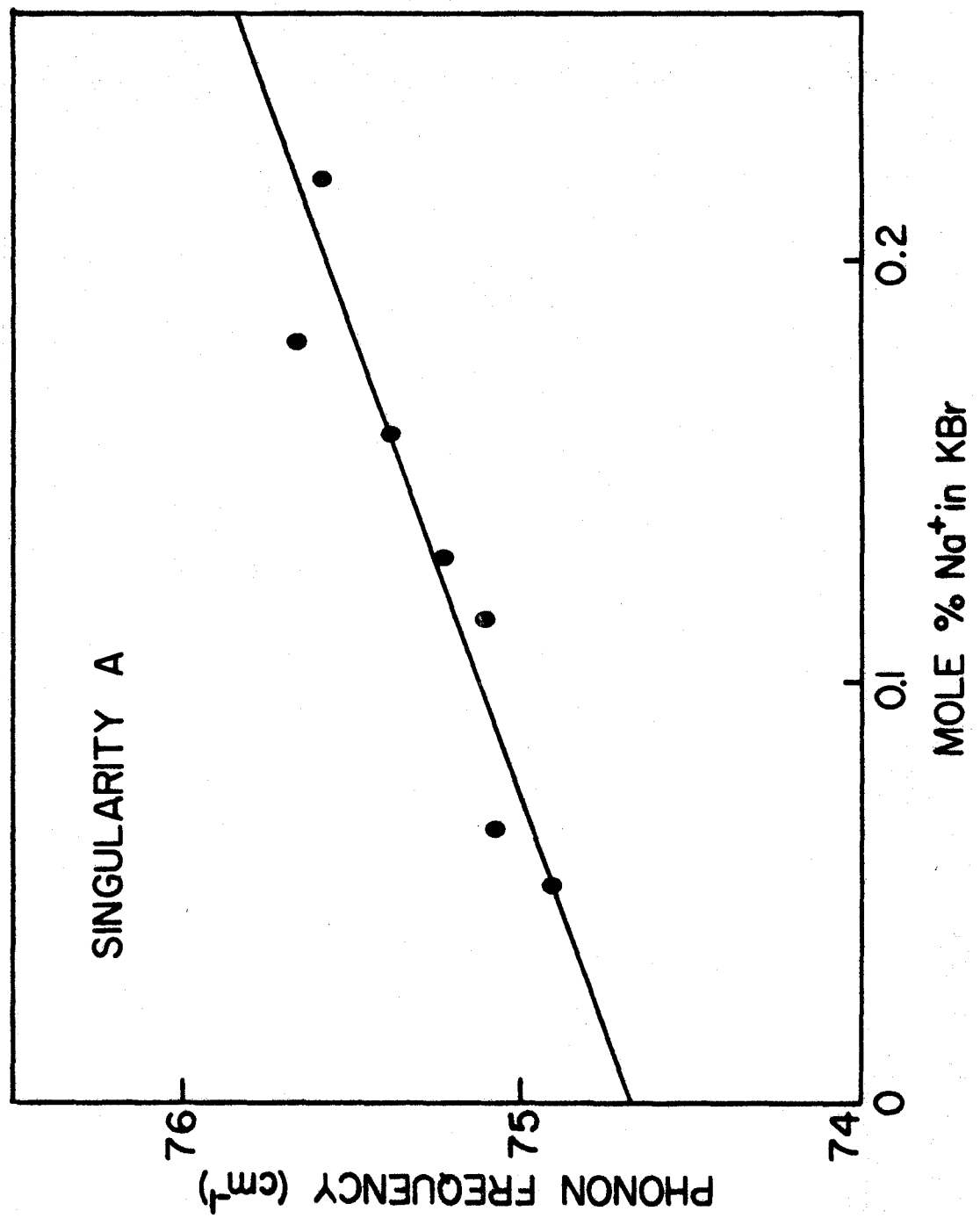
SINGULARITY A
PHONON FREQUENCY (cm⁻¹)
76
75
74
0
0.1
0.2
MOLE % Na⁺ in KBr

FIGURE 9

The frequency of the singularity B as observed in the far-infrared plotted as a function of Na^+ impurity concentration.

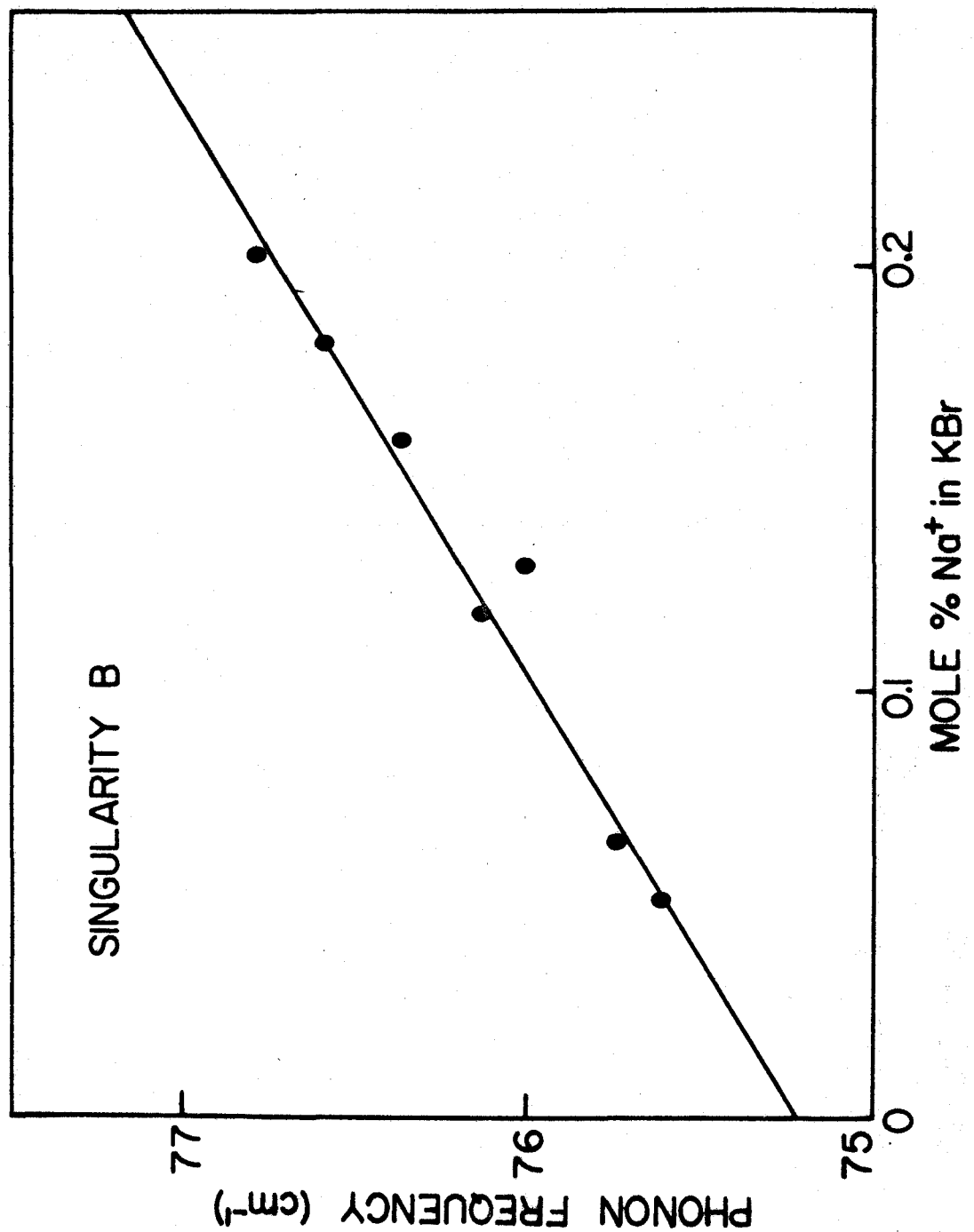
SINGULARITY B
PHONON FREQUENCY (cm⁻¹)
77
76
75
0
0.1
0.2
MOLE % Na⁺ in KBr

FIGURE 10

The frequency of the singularity C as observed in the far-infrared plotted as a function of Na^+ impurity concentration.

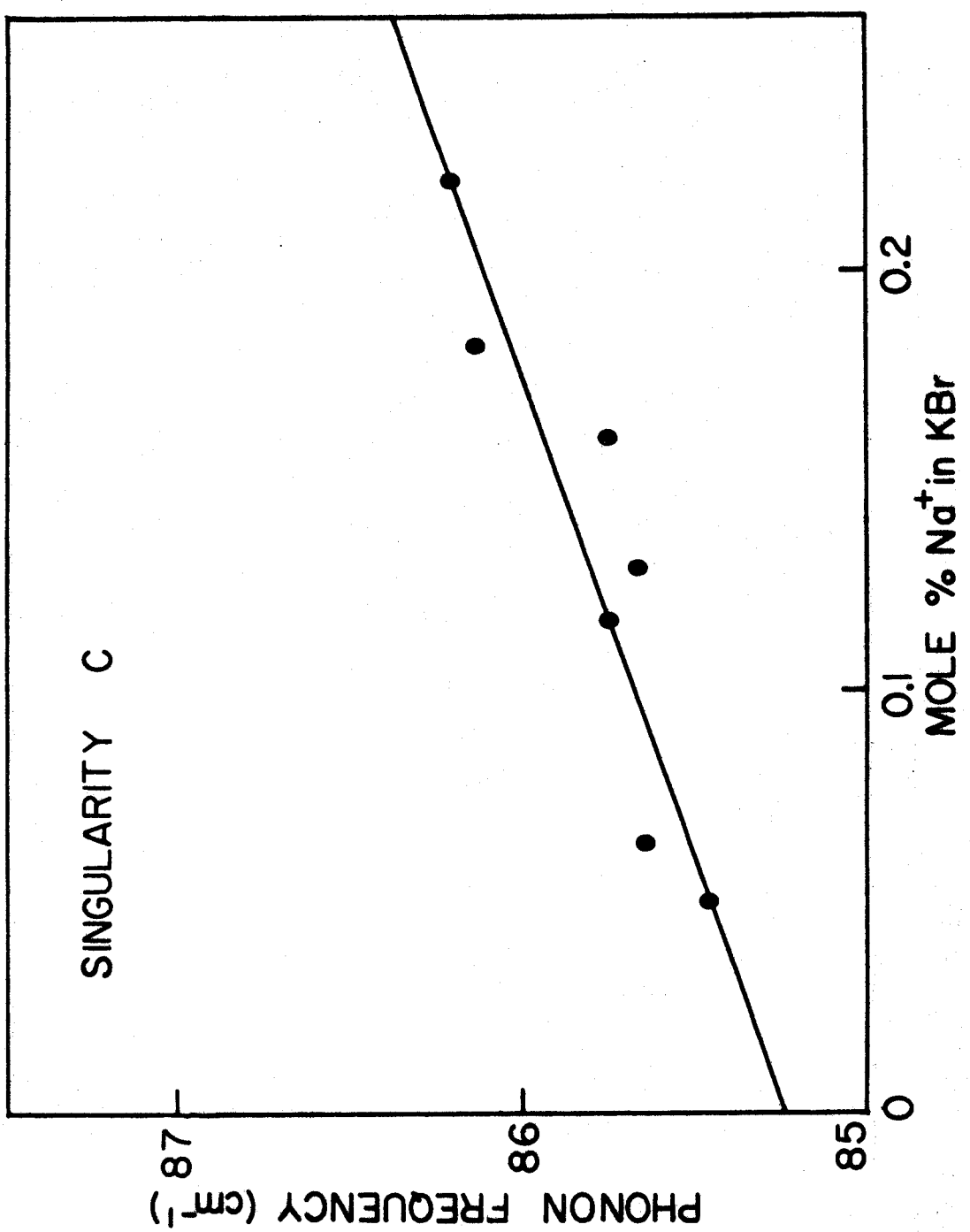
SINGULARITY C
PHONON FREQUENCY (cm⁻¹)
87
86
85
0
0.1
0.2
MOLE % Na⁺ in KBr

the slope of the step becoming less sharp and eventually disappearing. An extrapolation of these curves to zero defect concentration gives the positions of Van Hove singularities of the unperturbed KBr lattice at 11°K. These extrapolated values are given in Table (1). The singularities C and D may be affected by the nearness of the Cl^- resonance, variation of the concentration of some residual impurities such as calcium might cause frequency shifts. It is known that such shifts are particularly strong near resonances (Svensson et al. 1965).

Difficulty was encountered in measuring the higher Na^+ concentration crystals due to the very strong absorption. This was overcome to some extent by mounting the doped crystals on pure KBr substrates and grinding the samples down to approximately 100 microns thickness. However this difficulty did place an upper concentration limit on the measurements.

Some indication of the change of force constants needed to fit the experimental curve, can be obtained by considering the relative sizes of the Na^+ and the K^+ ion it replaces. The sodium impurity has an ionic radius approximately 37% less than that of potassium. Hence one would expect a reduction of the first neighbour central force constant and also some inward relaxation of the nearest neighbour bromine ions. This is indeed found to be the case, the best fit to the experimental

curve is obtained with $\Delta f = -7500$ dynes/cm and $\Delta g = -2000$ dynes/cm where f is the defect nearest neighbor for a constant and g nearestfourth neighbor force constant. Fig. 7(a) shows the comparison between experiment and theory. The model reproduces the overall shape of the absorption, including the relative intensities of the two peaks. A resonance is also predicted at 97 cm^{-1} in the gap. The positions of the singularities in the calculated curve are independent of the change of force constants and it is reasonable to identify the observed and predicted singularities as the same.

From the shell model calculation, Fig. (11), it is found that the singularities A B C and D occur at 70.0, 73.0, 83.0 and 88.0 cm^{-1} respectively. In the region of the step AB the shell model critical points are predicted 6% low in frequency. This disagreement between experiment and theory was also found in the same region by Buchanan and Woll (1969). They point out, that in this region the critical points arise at $\underline{q}$ vectors not measured by neutron diffraction. The few neutron measurements made near this region, indicate that the actual phonons appear higher in frequency than those predicted by the shell model, in agreement with the far-infrared measurements.

From inspection of the shell model dispersion surfaces it is found that the 75 cm^{-1} step (A and B) arises from a near

FIGURE 11

Unperturbed phonon density of states for KBr. The upper curves are the individual frequency distributions for the six phonon polarization branches and the lower curve is the total density of states. The curves have been normalized so that $\int \rho_{total}(\omega) d\omega = 1$ and were produced by sorting frequencies at 625000 wave vectors into 0.5 cm^{-1} wide bins by the method developed by Gilat and Raubenheimer (1966).

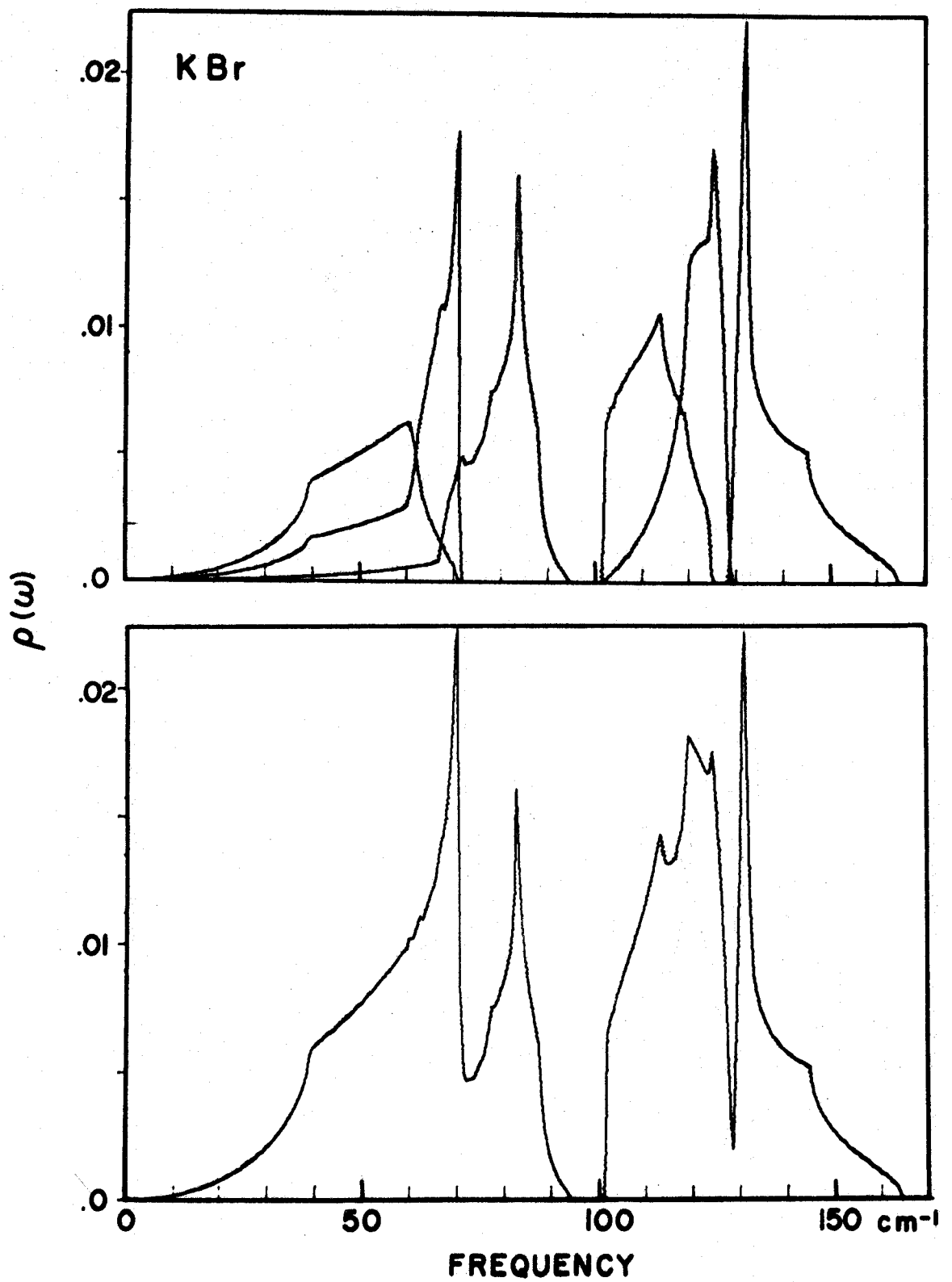
KBr
.02
.01
.0
ρ(ω)
.02
.01
.0
0
50
100
150 cm-1
FREQUENCY

degeneracy of a saddle point on the [110] axis at [0.52, 0.52,0] and a maximum at [0.65,0.35,0.35] of the second highest acoustical branch. Between these points the eigenvectors are normal to the $q_x = q_y$ plane and the potassium ion is almost stationary. The singular points C and D are saddle points in the highest acoustical branch at [0.6,0.6,0] and [0.65,0,0], respectively.

2. Lithium

Lithium doped potassium bromide has been extensively studied. Sievers and Takeno (1965) observed a very sharp absorption line at 16.07 cm^{-1} for $^7Li^+$ and at 17.71 cm^{-1} for $^6Li^+$. This low frequency absorption was originally thought to be a defect induced lattice resonant mode with the Li^+ ion occupying a normal lattice site. However theoretical calculations on the minimum emergy configurations for Li^+ in KBr by Wilson et al. (1967) and by Quigley and Das (1967), have shown that it is possible for the Li^+ ion to occupy off-centre positions in the [111] directions. Tunneling between the eight equivalent [111] sites should lead to low lying states with splittings of the order of 1 cm^{-1}.

Attempts to observe these low lying states by measurements of the low temperature dielectric constant (Bogardus and Sack 1966), ultrasonic absorption (Byer and Sack 1966, 1967), thermal conductivity (Baumann et al. 1967) and specific

heat (Harrison et al. 1968) have shown that no such states occur between 0.01 and 10°K. Measurements, by Sievers' group at Cornell, of the electric field (Kirby and Sievers 1968) and stress induced (Nolt and Sievers 1966, 1968) frequency shifts of the Li^+ resonant mode are consistent with the on-centre configuration.

Recent calculations of the effect of the lattice parameter on the KBr:Li^+ system by Quigley and Das (1968) have indicated that when the low temperature lattice parameter is used in their previous calculations, the off-centre well depths are reduced to 0.002 ev, favouring an on-centre configuration for the Li^+ ion. However these authors also point out that the existence of the shallow off-centre wells in the potential, illustrate the weakness of the restoring forces, which helps to account for the large isotope shift observed by Sievers and Takeno (1965) and by Kirby et al. (1967). New infrared measurements on the KBr:Li^+ system by Clayman et al. (1971) have shown that the Li^+ resonant mode is shifted only slightly by the application of an electric field. This result together with the large isotope shift have been explained in terms of an harmonic potential containing a central barrier. The barrier is found to be small compared to the zero-point energy of the resonant mode and hence the impurity still appears to occupy the normal lattice site.

In addition to the lithium resonant mode, Sievers and

Takeno also observed prominent bands at 43 and 83 cm^{-1}. High resolution far-infrared measurements were made on Li^+ doped KBr single crystals, in the hope of resolving the single phonon induced absorption in the 83 cm^{-1} region. Measurements were made from 30 cm^{-1} to 100 cm^{-1} and the results are shown in Fig. (12). Except for the addition of the 43 cm^{-1} band, the absorption spectrum is very similar to the KBr:Na^+ system. The sharp step A→B occurs at the same frequency as before, however the 83 cm^{-1} peak is much stronger. The origin of the 43 cm^{-1} peak is uncertain. It could be, as pointed out by Sievers and Takeno (1965), the second overtone of the low frequency absorption.

The concentration dependence of the singularities A and B was determined using three different Li^+ concentrations and the results are shown in Fig. (13) and Fig. (14). Comparison with Figs. (8) and (9) for the sodium case, shows that the frequency shifts for the Li^+ impurity are much smaller. However extrapolation to zero concentration yields frequency values for the singularities A and B that are the same as for the Na^+ impurity within 0.2%. This lends strong support to the view that these features are singularities of the KBr host lattice.

Recently, Klein (1968) has presented a review of theoretical calculations on the KBr:Li^+ system. In particular he compares results of calculations by Benedek and Nardelli

FIGURE 12

Experimental induced far-infrared absorption due to Li^+ ions in KBr. Measurements were made between 30 and 100 cm^{-1}. Note the sharp step at 75 cm^{-1}. The resolution of the interferometer is given by the frequency interval between the arrows.

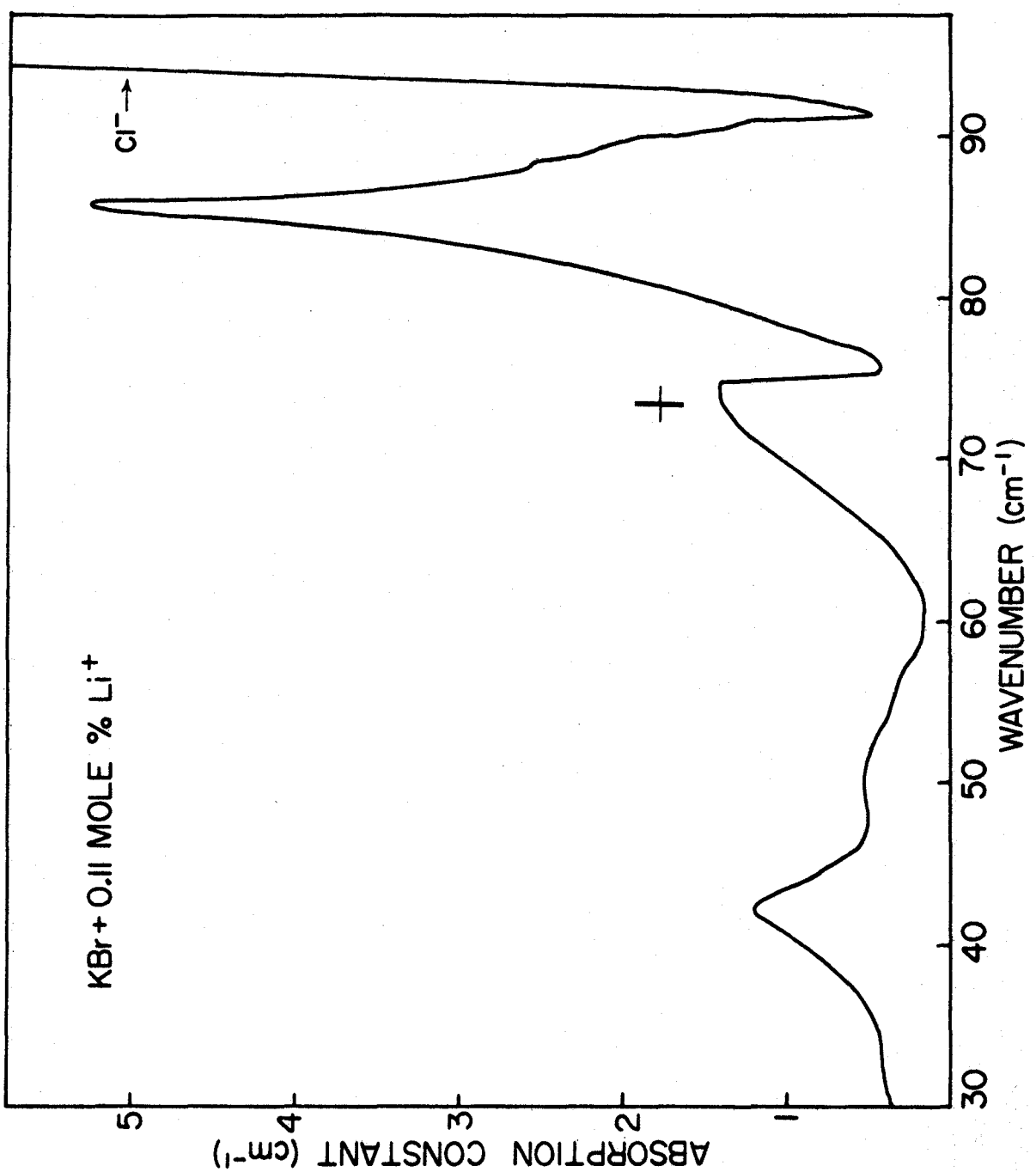
KBr + 0.11 MOLE % Li+
Cl−
+
ABSORPTION CONSTANT (cm-1)
WAVENUMBER (cm-1)
1
2
3
4
5
30
40
50
60
70
80
90

FIGURE 13

The frequency of the singularity A as observed in the far-infrared plotted as a function of Li^+ impurity concentration. The straight line is a best fit by eye.

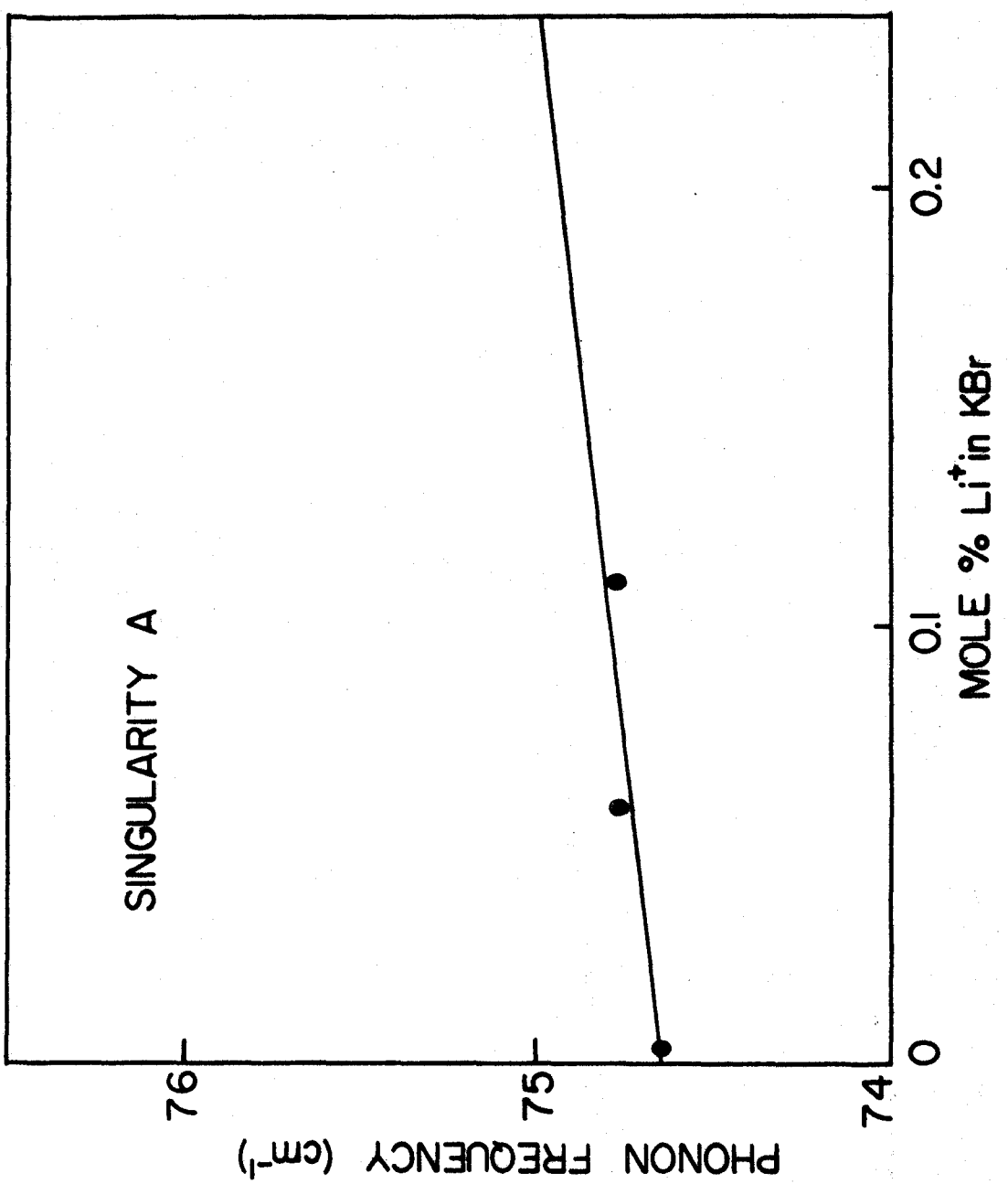
SINGULARITY A
PHONON FREQUENCY (cm⁻¹)
76
75
74
0
0.1
0.2
MOLE % Li⁺ in KBr

FIGURE 14

The frequency of the singularity B as observed in the far-infrared plotted as a function of Li^+ impurity concentration.

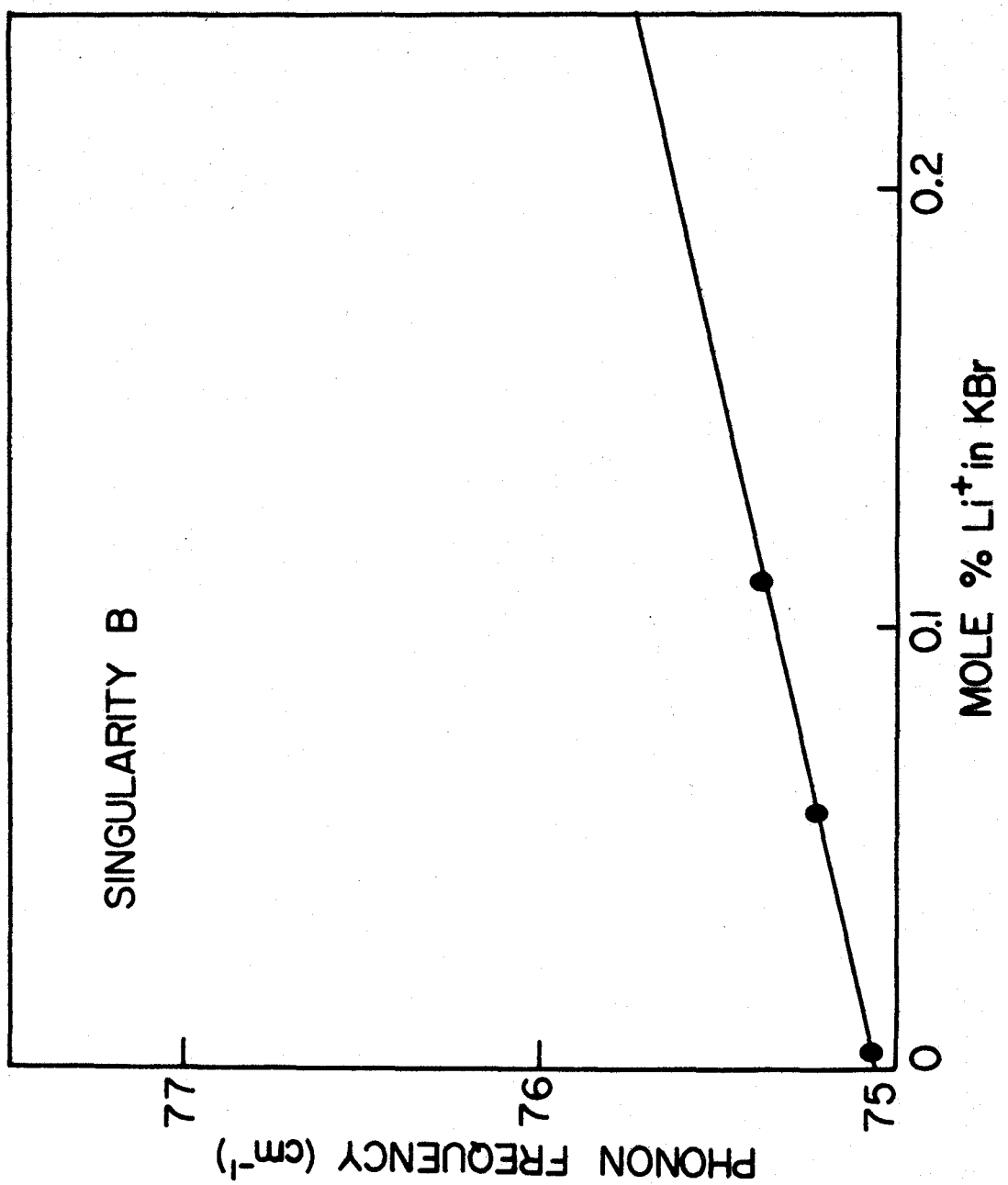
SINGULARITY B
PHONON FREQUENCY (cm⁻¹)
77
76
75
0
0.1
0.2
MOLE % Li⁺ in KBr

(1967) and by Klein and Gould (1967). Nearest neighbour force constant changes of the order of 90%, in agreement with the simplified calculations of Sievers and Takeno (1965), are required to fit the lithium resonance.

Attempts to fit the experimental curve in Fig. (12) with our model have met with little success. With force constant changes of $\Delta f = -12{,}350$ and $\Delta g = -2000$ dynes/cm it is possible to predict the resonant mode absorption at 17.7 cm^{-1}, but the intensity of this peak was found to be grossly overestimated. In addition the strong absorption at 74 cm^{-1} and 85 cm^{-1} in the experimental curve could not be adequately reproduced by the model. A similar situation was encountered by Macdonald et al. (1968) when they attempted to fit the absorption due to lithium in NaCl.

In an attempt to improve our fit to the experimental spectrum we have performed calculations with small reductions in Δf and larger reductions in Δg. We indeed found the position of theLi^+ resonant mode to be very sensitive to changes in Δg. With values of $\Delta f = -5000$ dyn/cm and $\Delta g = -14{,}300$ dyn/cm the resonant mode can be placed at its experimentally determined position, however no improvement of the absorption intensity was found. Further calculations with Δf slightly increased and Δg decreased, giving a picture of the Li^+ ion and its surrounding Br^- ions moving as a rigid "molecule", did not substantially improve the relative intensities of the

resonant mode and higher frequency peaks.

3. Thallium

Considerable interest has been generated concerning Tl^+ doped potassium halide crystals, since it is believed that the Tl^+ ion acts as an isotopic impurity. Harley et al. (1969, 1970, 1971) have studied the first order Raman spectrum for Tl^+ doped KBr and conclude that the spectrum is best fitted with zero force constant changes between the defect and its neighbours. Such an isotopic impurity is valuable in the study of vibrational modes of crystals since the perturbation it produces is small and the induced absorption should be free of resonances and gap modes.

The far-infrared absorption due to Tl^+ in KBr is shown as the full curve in Fig. (15). A broad band extends from 44 to 76 cm^{-1} with the usual peak C and shoulder D occurring at 86.36 and 89.57 cm^{-1} respectively. No band mode resonances were observed, in contrast to the 72 cm^{-1} resonance indicated by the thermal conductivity measurements of Baumann and Pohl (1967), however several sharp peaks are seen in the gap. These may be single defect gap modes or modes produced by pairs of Tl^+ ions. They have not been studied in detail.

Following the suggestion of Harley et al. the absorption was calculated with no force constant changes, only a change of mass at the defect site. The result is shown in

FIGURE 15

Induced far-infrared abosprion due to Tl^{+} ions in KBr. Several peaks are seen in the gap in addition to the local mode of Cl^{-}. The calculated absorption is based on the shell defect with force constant changes $\Delta f = 8000$ dyn/cm, $\Delta g = \Delta k = 0$.

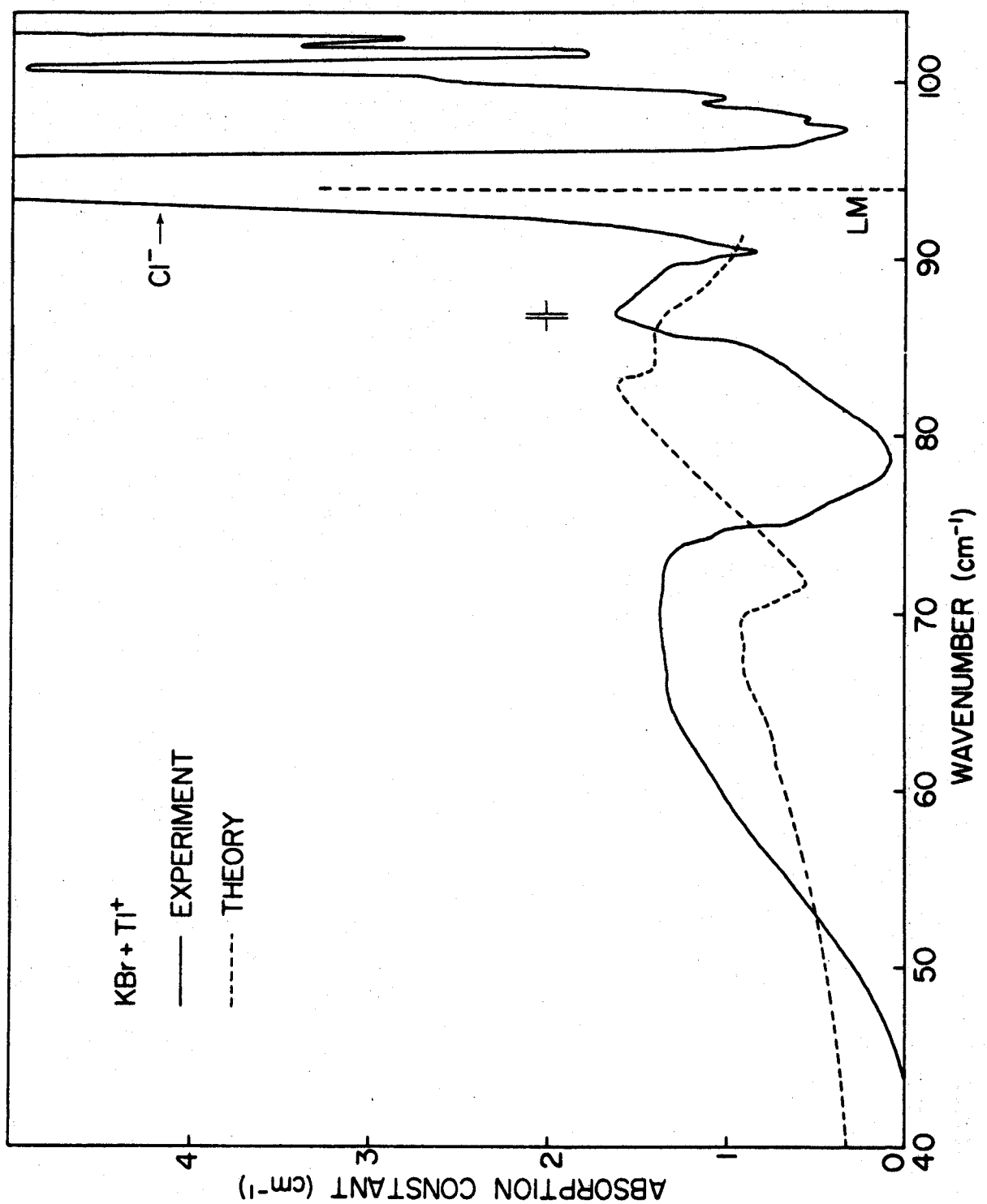
KBr + Tl+
EXPERIMENT
THEORY
Cl⁻
LM
ABSORPTION CONSTANT (cm⁻¹)
WAVENUMBER (cm⁻¹)
0
1
2
3
4
40
50
60
70
80
90
100

Fig. (16). A strong resonance is found to occur at 75 cm^{-1} obscuring the shell model step at 70 cm^{-1}. Increasing Δf, moves the resonance to higher frequencies and eventually into the gap. T_{1u} symmetry resonances are not expected to be observed in Raman spectra since only even modes are Raman active.

Our results seem to indicate that Tl^+ does not act as a complete isotopic impurity, indeed our best fit to the experimental curve was obtained using $\Delta f = 8000$ dynes/cm and $\Delta g = 0$. Even with this force constant change the comparison between experiment and theory is not good, see Fig. (15). The peak C in the calculation appears much broader than the same peak in the experimental absorption, however the shoulder D, corresponding to the saddle point in the highest acoustical branch, is very pronounced, both in experiment and theory.

Because of the relatively poor agreement between experiment and theory the answer as to whether Tl^+ acts as an isotopic impurity or not is still in some doubt. Further far-infrared experiments on Tl^+ in other potassium halides are needed before any real conclusions can be made.

4. Samarium

The full curve in Fig. (17) shows the far-infrared absorption due to Sm^{2+} in KBr. No resonant mode or gap modes are observed, except for the Cl^- local mode. The now familiar absorption was observed and the frequencies of the singularities

FIGURE 16

Calculated far-infrared induced absorption due to Tl^{+} ions in KBr using zero force constant changes. A strong resonance occurs at 75 cm^{-1} obscuring the shell model step at 60 cm^{-1}. Increasing Δf moves the resonance to higher frequencies and eventually into the gap.

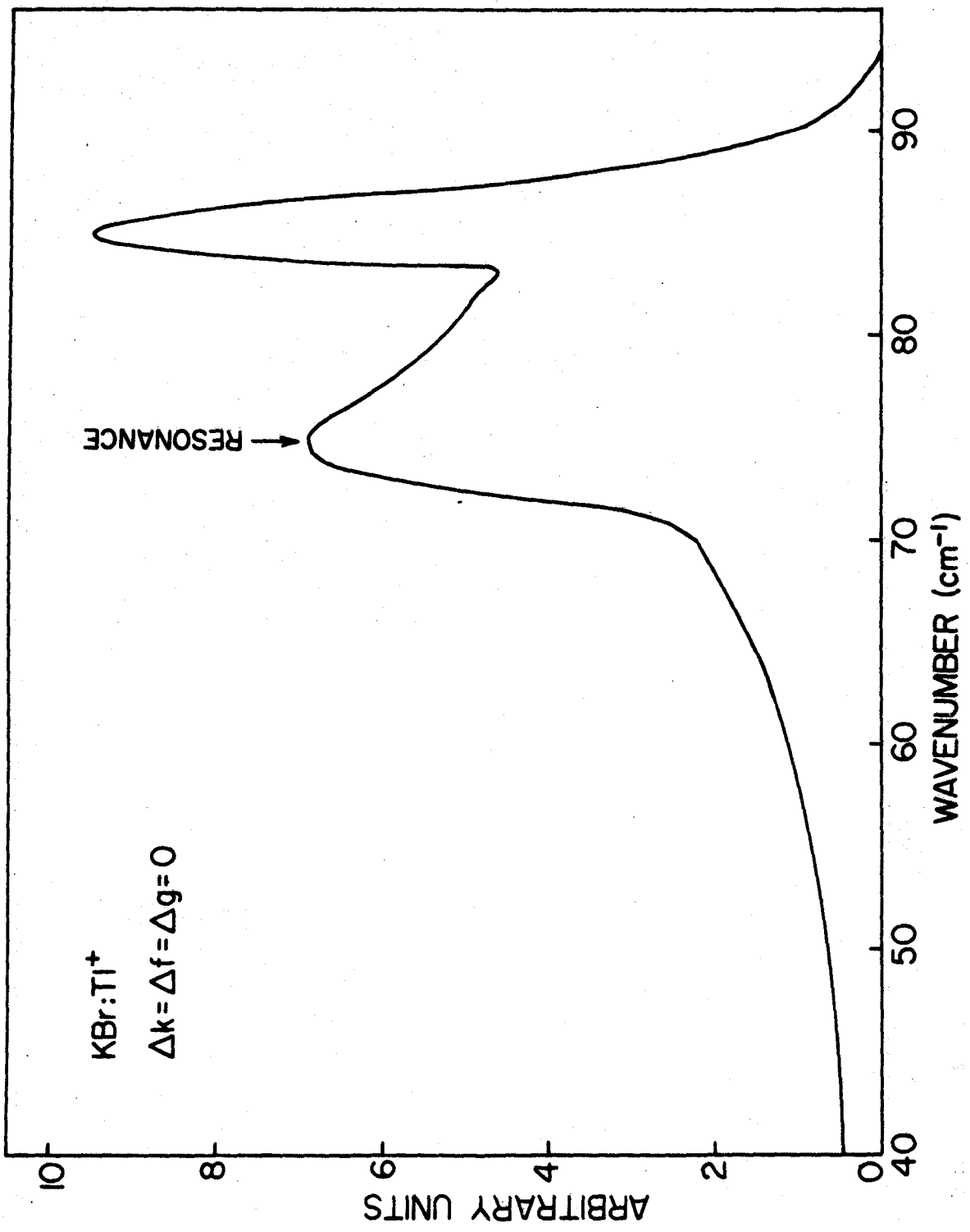
KBr:Tl+
Δk=Δf=Δg=0
RESONANCE
ARBITRARY UNITS
WAVENUMBER (cm-1)
0
2
4
6
8
10
40
50
60
70
80
90

FIGURE 17

Induced far-infrared absorption due to Sm^{2+} ions in KBr. There is no evidence of resonances in the experimental curve. The calculated absorption is from the shell model for the defect with the force constant changes Δf = 14,500 dyn/cm, Δg = -1500 dyne/cm, Δk = 0. These same force constant changes were used to fit the Sm^{2+} fluorescent side band by Buchanan and Woll (1969). The resolution of the experimental curve as indicated by the arrows is .15 cm^{-1}.

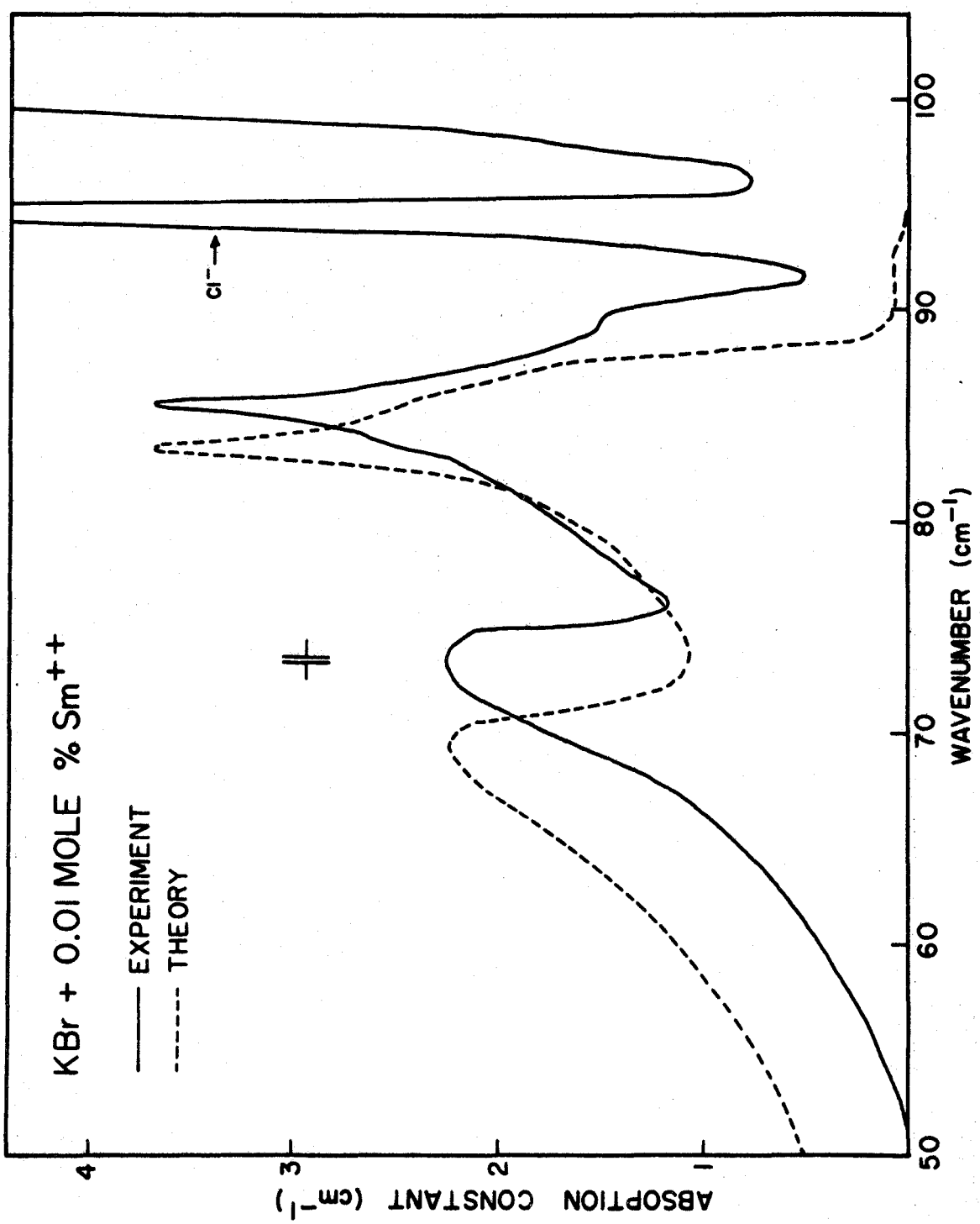
KBr + 0.01 MOLE % Sm++
EXPERIMENT
THEORY
Cl⁻
ABSORPTION CONSTANT (cm⁻¹)
WAVENUMBER (cm⁻¹)
1
2
3
4
50
60
70
80
90
100

A, B, C and D are listed in Table 1. Measurements were made on two crystals of different Sm^{2+} concentration and the slight variation of the positions of the singularities A and B with Sm^{2+} concentration are shown in Fig. (18). Extrapolating to zero impurity concentration gives values for the frequencies of the singularities A and B that are within 0.1 cm^{-1} of the values determined from the Li^{+} and Na^{+} curves.

In the case of the Sm^{2+} the rigid ion picture would indicate a reduction of the first neighbour force constant change Δf, due to the ionic radius of Sm^{2+} which is about 36% smaller than the potassium ion it replaces. However, as pointed out by Buchanan and Woll (1969), because of the increased Coulomb field the first neighbours will tend to move toward the Sm^{2+} ion. This will result in a large increase in Δf and a smaller decrease in Δg.

The experimental curve was fitted using the values of Δf and Δg determined by Buchanan and Woll (1969) from vibronic side band calculations. The calculated curve is compared with experiment in Fig. (17). It can be seen that there is good overall agreement between theory and experiment. The relative heights of the peaks are well reproduced.

The ability of the calculation to give satisfactory fits to both the far-infrared absorption and the one-phonon side band indicate that the choice of Γ, the force constant matrix for the case of Sm^{2+} in KBr reasonably describes the

FIGURE 18

The frequencies of singularities A and B as observed in the far-infrared plotted for two impurity concentrations of Sm^{2+}.

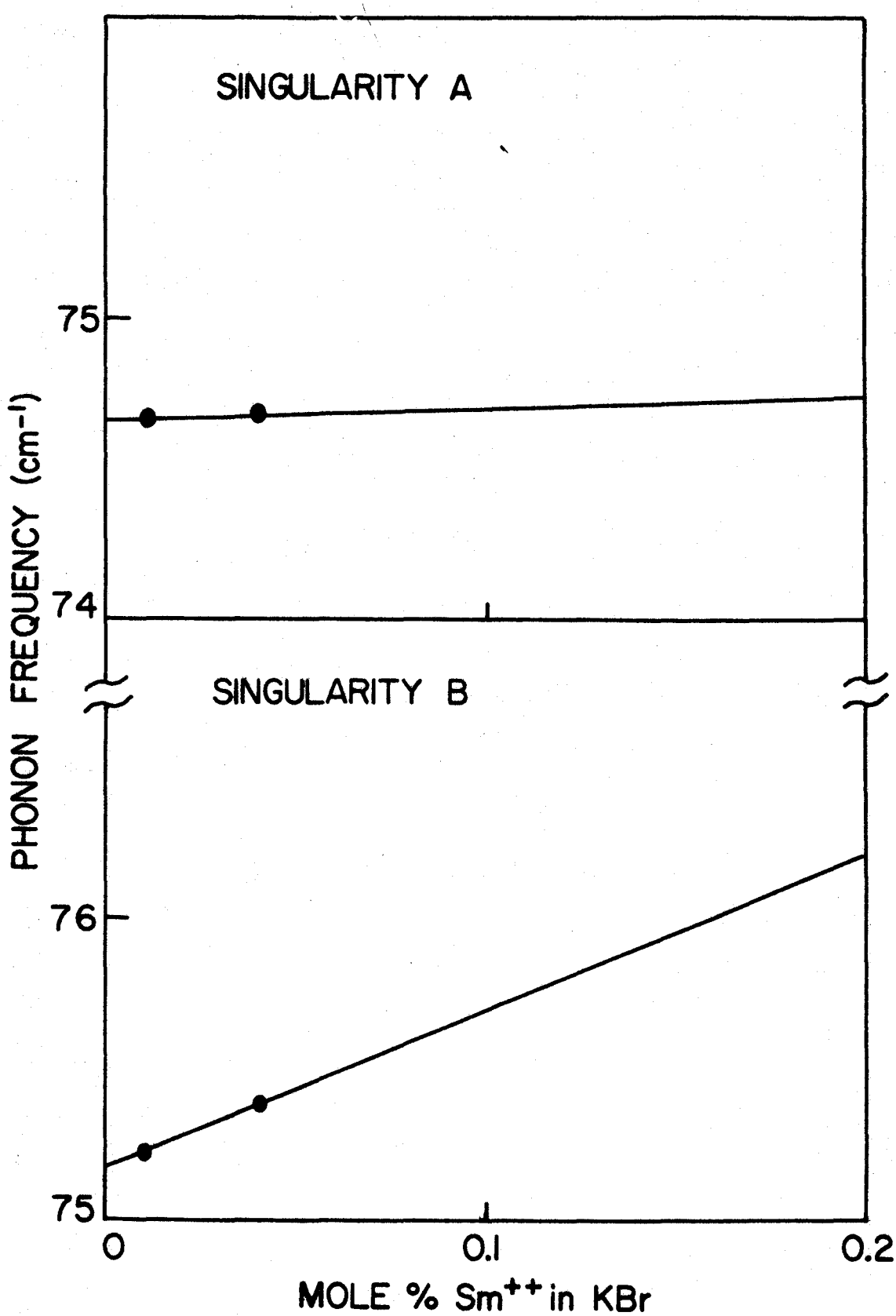
SINGULARITY A
SINGULARITY B
PHONON FREQUENCY (cm⁻¹)
75
74
76
75
0
0.1
0.2
MOLE % Sm++ in KBr

defect environment. The effect of compensating lattice vacancies has been assumed to be small. The vacancies are assumed to be sufficiently far away so that the Sm^{2+} site is considered to be cubic (Buchanan and Woll 1969).

5. Chlorine

Chlorine appears as an unwanted impurity in all the KBr crystals studied. Fig. (19) shows the absorption due to Cl^- in a sample of Harshaw KBr. The most striking feature is the local mode in the gap at 94.6 cm^{-1}. This peak has been identified as being due to Cl^- by Levine (Klein 1968) and by Grisar et al. (1967). Similar gap mode absorption due to Cl^- in KI has been previously reported by Sievers et al. (1965) and Nolt et al (1967). The experimental curve shows no structure in the region of the single-phonon critical points of KBr.

The experimental curve was fitted using $\Delta f = -2000$ and $\Delta g = -250$ dynes/cm and as can be seen from Fig. (19) comparison between theory and experiment is quite good. With zero force constant change a local mode is predicted at 95.5 cm^{-1}. The small reduction in Δf and Δg was required to place the peak at its experimentally determined position. The magnitude of the force constant changes required are consistent with the slightly smaller ionic radius of the Cl^- ion than the Br^- ion it replaces. Additional support for this picture comes from the work of Hurrell at al (1967), who found that a small de-

FIGURE 19

Far-infrared absorption due to Cl^- in KBr. No structure is seen in the region of the single-phonon crutucal points, however a local mode appears in the gap at 94.6 cm^{-1}. The calculated curve is from the shell model for the defect with force constant changes $\Delta f = -2000$ dyn/cm, $\Delta g = -250$ dyn/cm, $\Delta k = 0$.

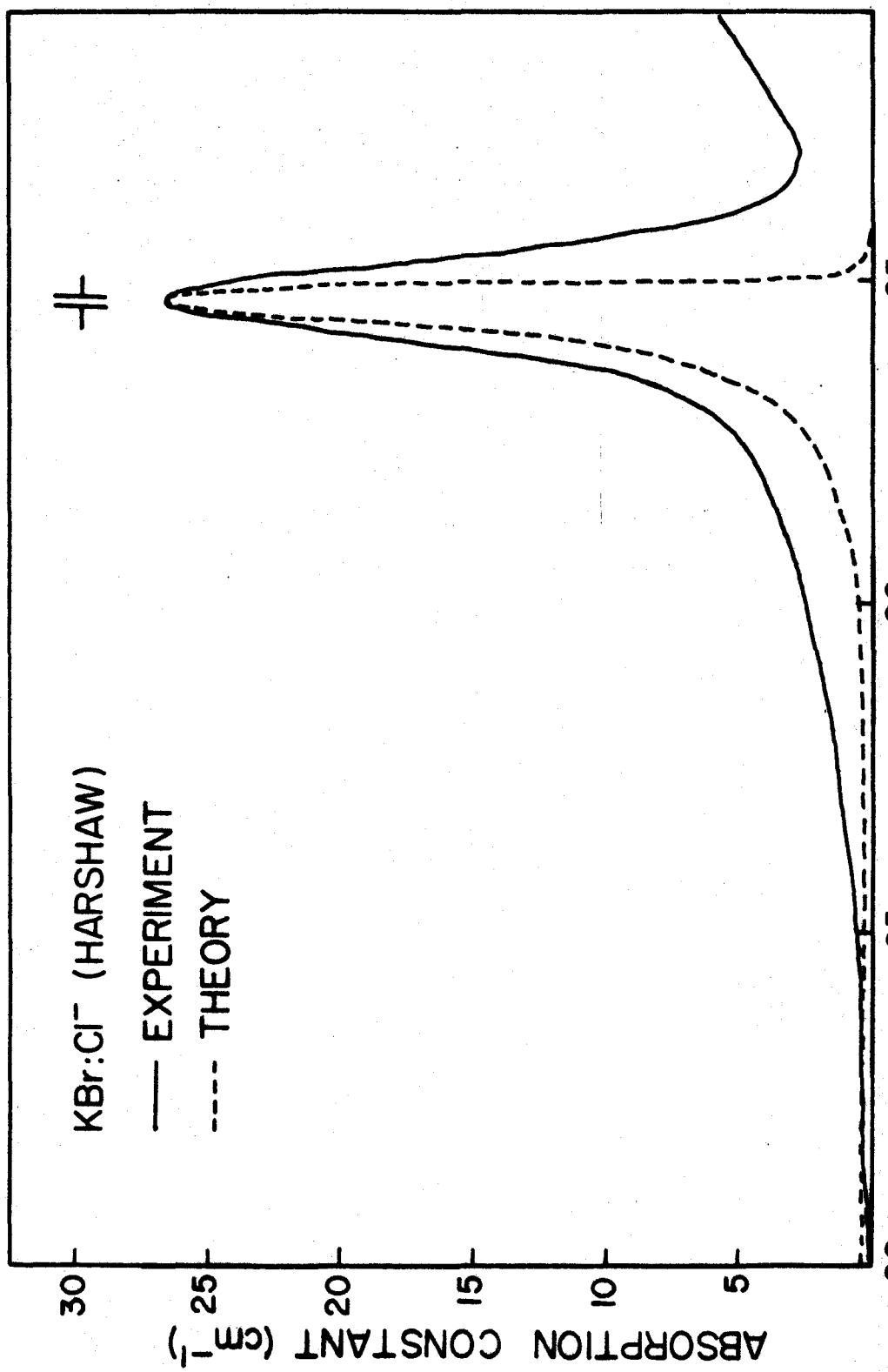
KBr:Cl⁻ (HARSHAW)
EXPERIMENT
THEORY
ABSORPTION CONSTANT (cm⁻¹)
30
25
20
15
10
5
80
85
90
95
WAVENUMBER (cm⁻¹)

decrease in the nearest neighbour force constant was required to fit their first order Raman spectra of mixed KBr:KCl crystals.

In an attempt to observe single phonon induced absorption due to Cl^-, far infrared measurements were made on single crystals of KBr containing approximately 2 mole % Cl^-. As the Cl^- concentration is increased the low frequency tail of the gap mode peak at 94.6 cm^{-1} becomes observable and extends to below 70 cm^{-1}. The interesting feature of this curve is the sharp increase in absorption between 74.7 cm^{-1} and 76.0 cm^{-1} shown in Fig. (20). These two frequencies are found to correspond closely to the frequencies of the singularities A and B in the defect spectra previously studied. However in the case of Cl^- the step A B has reversed slope.

This metamorphism of Van Hove singularities had been previously predicted theoretically by Okazaki et al. (1968), but had never been experimentally confirmed until the present time. The theoretical calculations were made using a simple model of the defect with two parameters, namely a nearest neighbour scalar force constant change λ' and a change of mass M' at the defect site. Okazaki et al. found that by decreasing λ' or by increasing M' metamorphism takes place in the direction indicated in Fig. (21). Using the notation shown in Fig. (21) the singularity A is found to change from type M_2 to M_0 and singularity B changes from type M_3 to M_1 in agreement with theory.

FIGURE 20

Far-infrared absorption due to approximately 2 mole % Cl^- in KBr. As the Cl^- concentration is increased the low frequency tail of the gap mode peak at 94.6 cm^{-1} extends to 70 cm^{-1} with a sharp increase in absorption between 74.7 cm^{-1} and 76.0 cm^{-1}. These frequencies correspond closely to the frequencies of the singularities A and B, however, they have changed type.

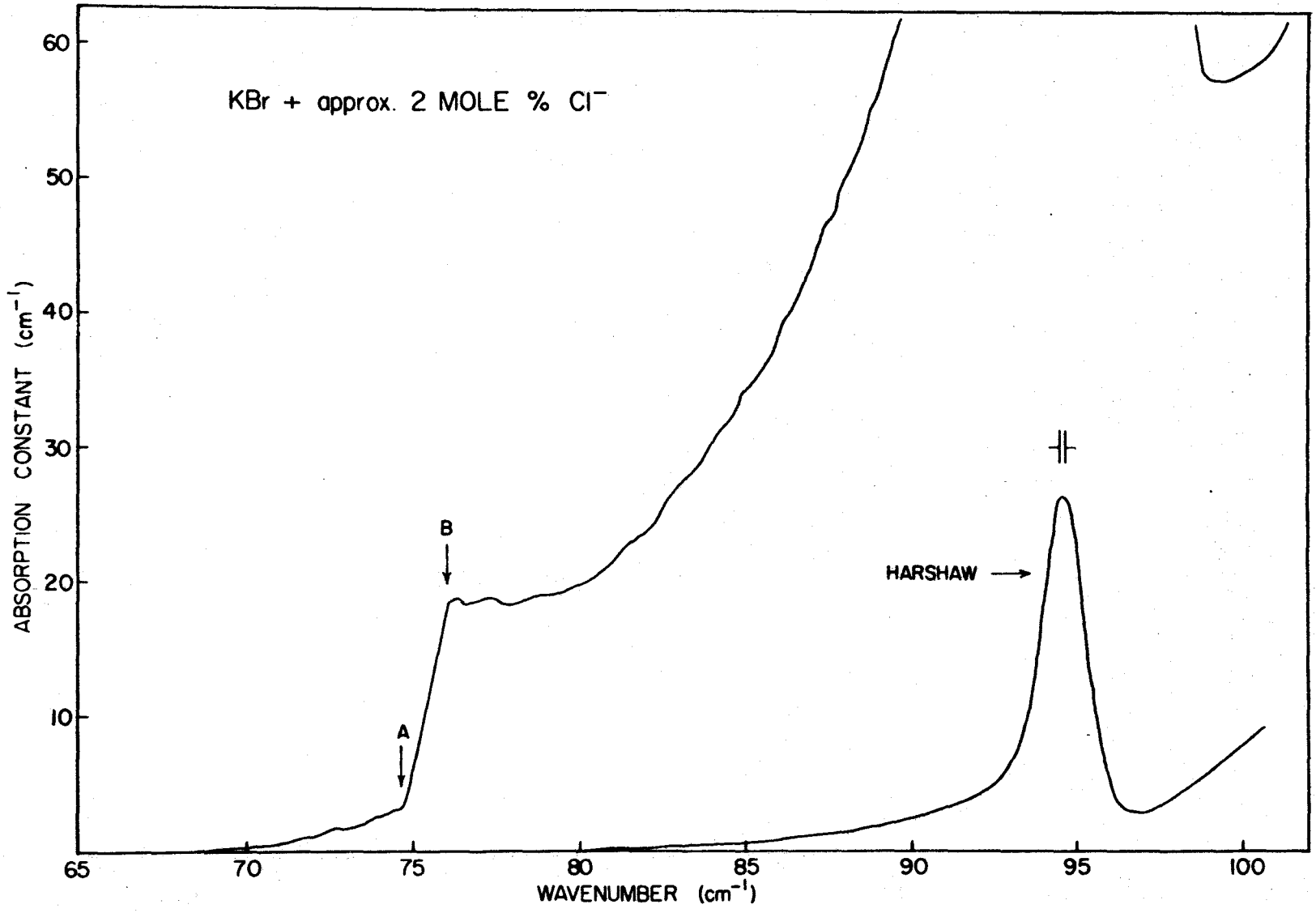
KBr + approx. 2 MOLE % Cl⁻
ABSORPTION CONSTANT (cm⁻¹)
WAVENUMBER (cm⁻¹)
60
50
40
30
20
10
65
70
75
80
85
90
95
100
A
B
HARSHAW

FIGURE 21

Metamorphism of Van Hove singularities (taken from Okasaki et al. 1967). As the impurity mass is increased or the nearest neighbour force constant is decreased, the shape of the singularity corresponding to any of the four types (M_0, M_1, M_2 and M_3) can change in the direction indicated.

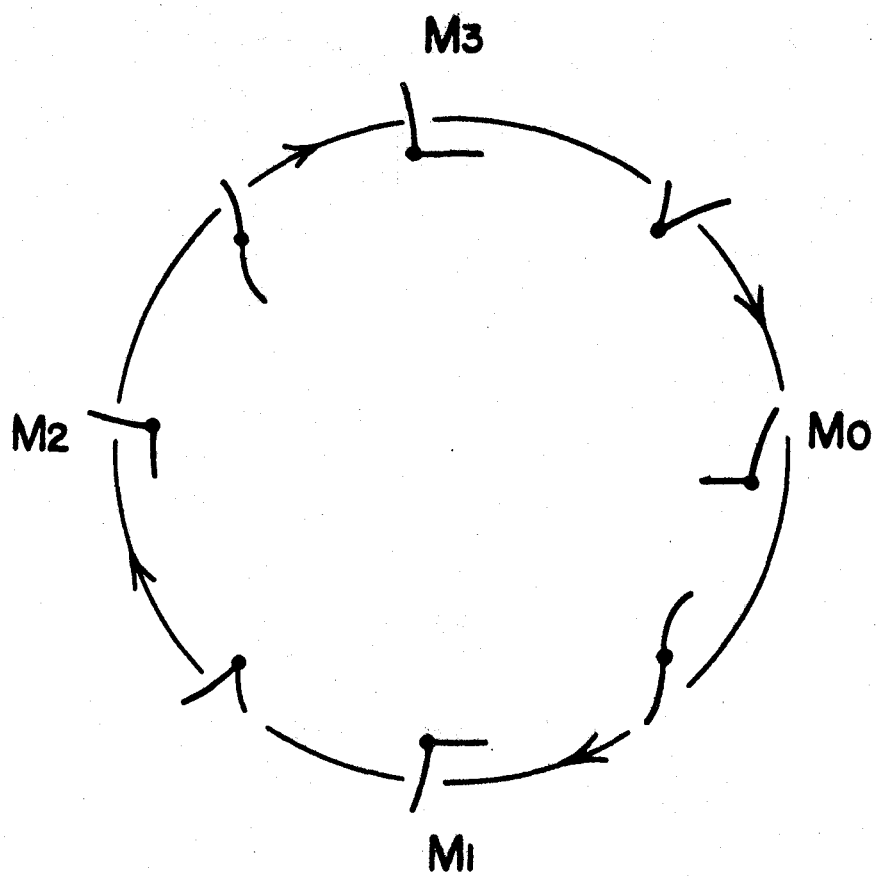

Singularity 'A' changes from type $M_2 \rightarrow M_0$

" 'B' " " " $M_3 \rightarrow M_1$

6. Fluorine

A resonant band mode absorption has been found previously by Levine (1966) due to F^- in KBr, at 37 cm^{-1}. This resonance has also been observed through thermal conductivity measurements by Pohl (1966). Similar resonances due to F^- ions have been observed in NaCl (Macdonald et al. 1968) and KCl (next chapter).

The far-infrared absorption spectrum from 30 cm^{-1} to 100 cm^{-1} is shown as the full curve in Fig. (22). The resonant peak is centred at 37.4 cm^{-1} and has a full width at half maximum of 5 cm^{-1}. Toward higher frequencies there are two absorption peaks at 72 and 85.6 cm^{-1}. A weak shoulder is seen at 90.2 cm^{-1}.

The calculated absorption is compared with experiment in Fig. (22). The first neighbour force constant change Δf was adjusted to give the resonant mode peak at its experimentally observed position of 37.4 cm^{-1}. Δg was adjusted to give the best fit to the higher frequency peaks. The values of Δf and Δg used were -11,000 and -8000 dynes/cm in qualitative agreement with the rigid ion picture of an inward relaxation of the nearest neighbour potassium ions due to the 32% reduction in ionic radius when a Br^- ion is replaced by a F^- ion.

With the values used for Δf and Δg the calculation predicts an incipient T_{1u} resonance at 83 cm^{-1}, however this

FIGURE 22

Induced far-infrared absorption due to F^- ions in KBr. An impurity resonance is seen at 37.4 cm^{-1}. The calculated absorption is from the shell model for the defect with force constant changes Δf = -11000 dyn/cm, Δg = -8000 dyn/cm, Δk = 0. The first neighbour force constant change Δf was adjusted to give the resonant mode peak at its experimentally observed position and Δg was adjusted to give the best fit to the higher frequency peaks. The experimental resolution is given by the frequency interval between the arrows.

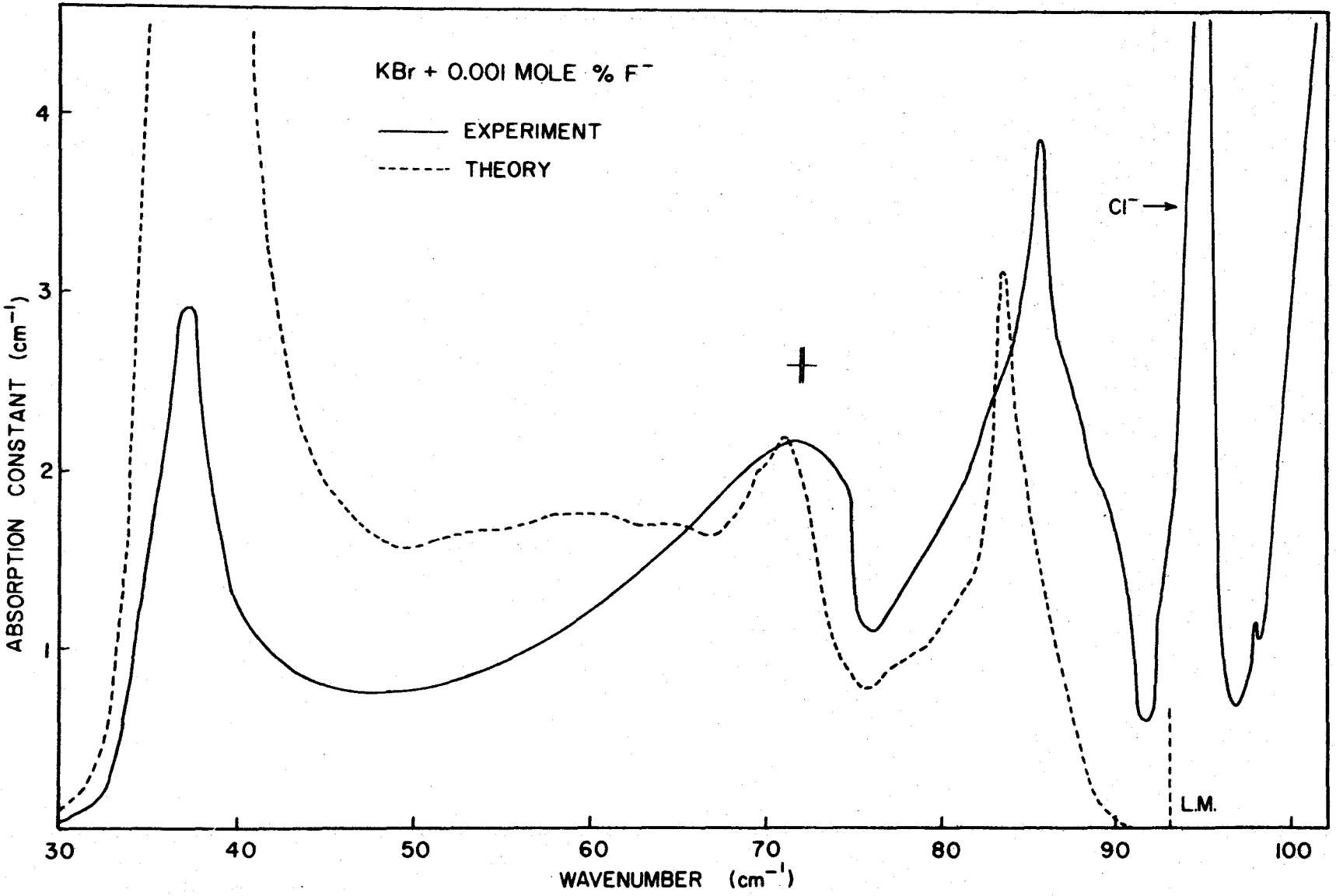
KBr + 0.001 MOLE % F⁻
EXPERIMENT
THEORY
Cl⁻
L.M.
ABSORPTION CONSTANT (cm⁻¹)
WAVENUMBER (cm⁻¹)
1
2
3
4
30
40
50
60
70
80
90
100

is also the position of the saddle point C in the density of states of KBr. It is probable that this resonance enhances the absorption of the 83 cm^{-1} peak, but it is experimentally difficult to distinguish the resonance because of the strong host lattice absorption in this region. The model also predicts a local mode at 93 cm^{-1}. A weak peak in the gap at 98 cm^{-1} was observed experimentally but the strong Cl^- resonance obscures any peaks that might be identified with the 93 cm^{-1} absorption.

As can be seen from Fig. (22) the calculation overestimates the strength of the 37.4 cm^{-1} resonance but the intensity of the structure at higher frequencies it not as greatly diminished as the lithium case. Similar calculations on F^- in NaCl have been performed by Macdonald et al. (1968) using the same model of the defect and very good agreement with experiment was obtained.

7. Hydroxide

The absorption due to the dipolar diatomic impurity OH^- in KBr has been studied previously both in the near and far infrared. The O-H stretching modes in KBr have been studied by Wedding and Klein (1969) and by Klein et al. (1969). The far-infrared OH^- induced absorption in KBr has been measured by Bosomworth (1967), however no direct correlation with host lattice singularities was made at that time. We have made new high resolution far-infrared measurements on KBr:KOH

and the results are shown in Fig. (23).

A resonant band mode peak is observed at 37.5 cm^{-1} in agreement with the previous results of Bosomworth. This resonance has also been observed by Rosenbaum et al (1969) in thermal conductivity measurements. The usual structure is seen close to the gap, but in addition the peak at 85.6 cm^{-1} has a slightly shoulder on the low frequency side at about 82 cm^{-1}. The shoulder D is very pronounced in the KBr:KOH absorption.

In order to determine the orientation of the hydroxyl ion in the KBr lattice, Lüty and Weinmann (1967) have made measurements of the electric field induced dichroism of the ultraviolet OH band. Their results indicate that the hydroxyl ion goes into the lattice substantially with its axis along the [100] direction.

It has been pointed out by Wedding and Klein (1969) that the OH^- ion can be regarded in a first approximation as a distorted F^- ion with dimensions perpendicular to its axis comparable to the F^- dimensions and with larger dimensions parallel to the axis. The similarity between the observed spectra for these two ions in KBr, especially the appearance of the resonant peak at almost the same position, certainly supports this view.

The experimental curve was fitted using the same force constant changes used previously for the F^- calculation.

FIGURE 23

Induced far-infrared absorption due to the dipolar diatomic impurity OH^- in KBr. A resonant mode peak is seen at 37.5 cm^{-1}. The calculated curve is based on the shell model for the defect with the same force constant changes used for the KBr:F^- calculation. Note the calculation overestimates the intensity of the resonant mode peak.

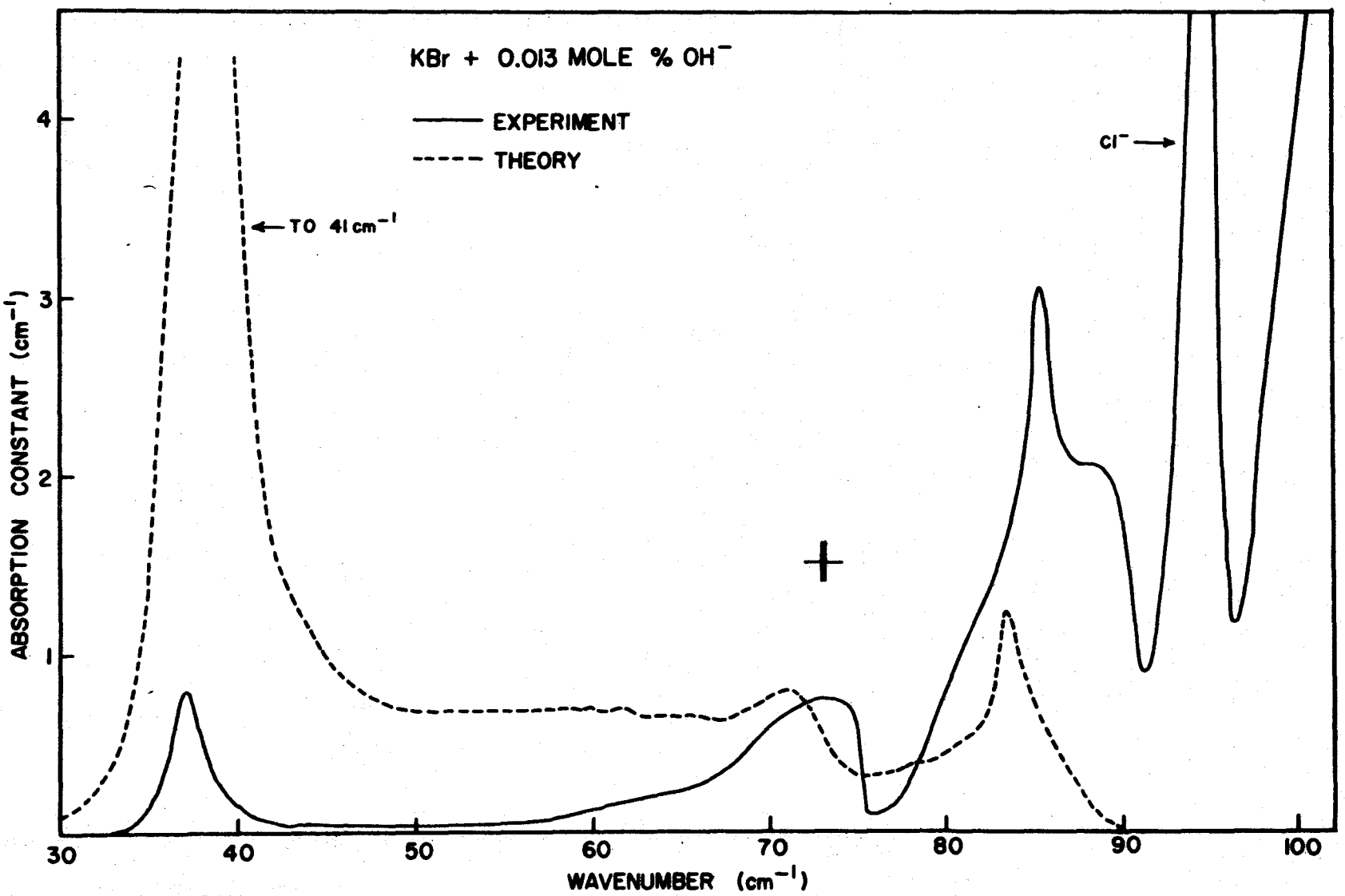
KBr + 0.013 MOLE % OH⁻
EXPERIMENT
THEORY
TO 41 cm⁻¹
Cl⁻
ABSORPTION CONSTANT (cm⁻¹)
WAVENUMBER (cm⁻¹)
1
2
3
4
30
40
50
60
70
80
90
100

See Fig. (23). Only the defect mass was changed to that of OH^-. The low frequency resonance was predicted at the correct frequency, while the shoulder at 82 cm^{-1} in the experimental curve can now be tentatively identified with the incipient resonance predicted by the calculation at 83 cm^{-1}. This shoulder can also be seen in the curve of Bosomworth. The calculation also predicts a local mode at 95 cm^{-1}. Although no gap modes were observed in our low concentration crystals, Bosomworth's experimental curve shows a small peak in the region of 97 cm^{-1}.

8. Oxygen

The O_2^- molecule was the last impurity in KBr to be studied. Measurements were made on a crystal containing between 10^{17} and 10^{18} molecules/cc and the results are shown in Fig.(24). The experimental curve is similar to all the other defect spectra studied, the singularities A, B, C, and D are prominently displayed. In addition to the continuum absorption, four sharp peaks are observed in the gap.

The orientation of the O_2^- molecule in the potassium halides was determined using paramagnetic resonance techniques by Kanzig and Cohen (1959). It is found to substitute for the anion with its axis pointing in the <110> direction. The optical absorption and fluorescence of this impurity in KBr has been studied by Rolfe et al. (1961).

FIGURE 24

Induced far-infrared absorption due to O_2^- in KBr. In addition to the continuum absorption, four sharp peaks are observed in the gap. The calculated absorption is from the shell model for the defect with the force constant changes $\Delta f = -5000$ dyn/cm, $\Delta g = 600$ dyn/cm and $\Delta k = 0$, in agreement with the fluorescent side band results of Rolfe (1970).

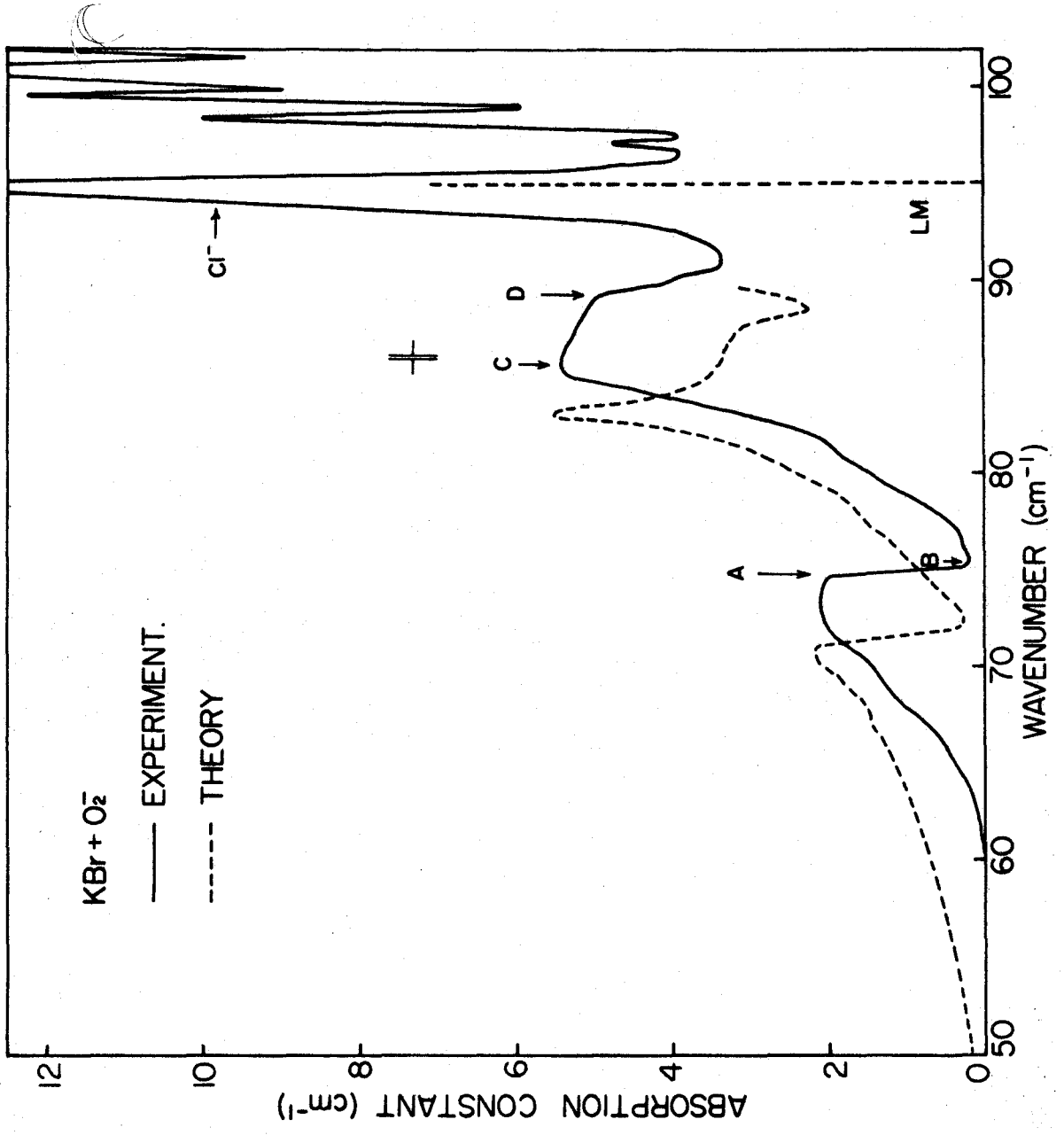
KBr + O_2^-
EXPERIMENT.
THEORY
Cl^-
A
B
C
D
LM
ABSORPTION CONSTANT (cm^{-1})
WAVENUMBER (cm^{-1})
0
2
4
6
8
10
12
50
60
70
80
90
100

Theoretical fits to the O_2^- fluorescent side band results of Rolfe (1970) indicate that a small reduction in both Δf and Δg are required to fit the data. This is in qualitative agreement with our own calculations. Values of $\Delta f = -5000$ and $\Delta g = -600$ dynes/cm were used to give the best fit to the infrared curve. See Fig. (24). The calculated curve reproduces the relative heights of the two main peaks and displays a prominent shoulder at 88 cm^{-1}. With our choice of force constants a gap mode is predicted at 95 cm^{-1}. Since the experimental curve shows evidence of absorption in the gap it is probable that the 95 cm^{-1} absorption corresponds to one of the observed peaks. However these have not been studied in detail.

Table II summarizes the force constant changes used for each impurity in KBr.

TABLE 2

Force constant changes used to fit the impurity induced far-infrared absorption in KBr. The core-shell force constant change Δk was put equal to zero.

Impurity	Δf (dynes/cm)	Δg (dynes/cm)
Na^+	-7,500	-2,000
Tl^+	8,000	0
Sm^{++}	14,500	-1,500
Cl^-	-2,000	- 250
F^-	-11,000	-8,000
OH^-	-11,000	-8,000
O_2^-	- 5,000	- 600

Note: The accuracy of the force constant changes is of the order ± 2000 dynes/cm.

CHAPTER V

RESULTS AND DISCUSSION OF KCl IMPURITY SPECTRA

A. GENERAL REMARKS

The recent publication of phonon dispersion curves for KCl by Copley et al (1969), and the successful fitting of these curves by their shell model VI has encouraged the present investigation into the defect induced absorption in this material. With the availability of neutron measured phonons one is able to interpret features in the induced absorption with Van Hove singularities of the unperturbed density of states, and compare them with similar features seen in KBr.

Unlike KBr, KCl has no gap between the acoustic and optical phonon branches, see Fig. (25). In general the impurity induced spectra of KCl show a continuous absorption ranging from 60 to 120 cm^{-1} superimposed on the sloping reststrahlen background, corresponding to the high frequency portion of the acoustic phonon spectrum. Two principle peaks are observed in this continuum at 108 cm^{-1} and 117 cm^{-1}. The peak at 108 cm^{-1} has been recently observed through first order Raman experiments on KCl:Tl^{+} by Harley et al (1969, 1971) and

FIGURE 25

Unperturbed phonon density of states for KCl. Upper curves are branch frequency distributions and the lower curve is the total density of states.

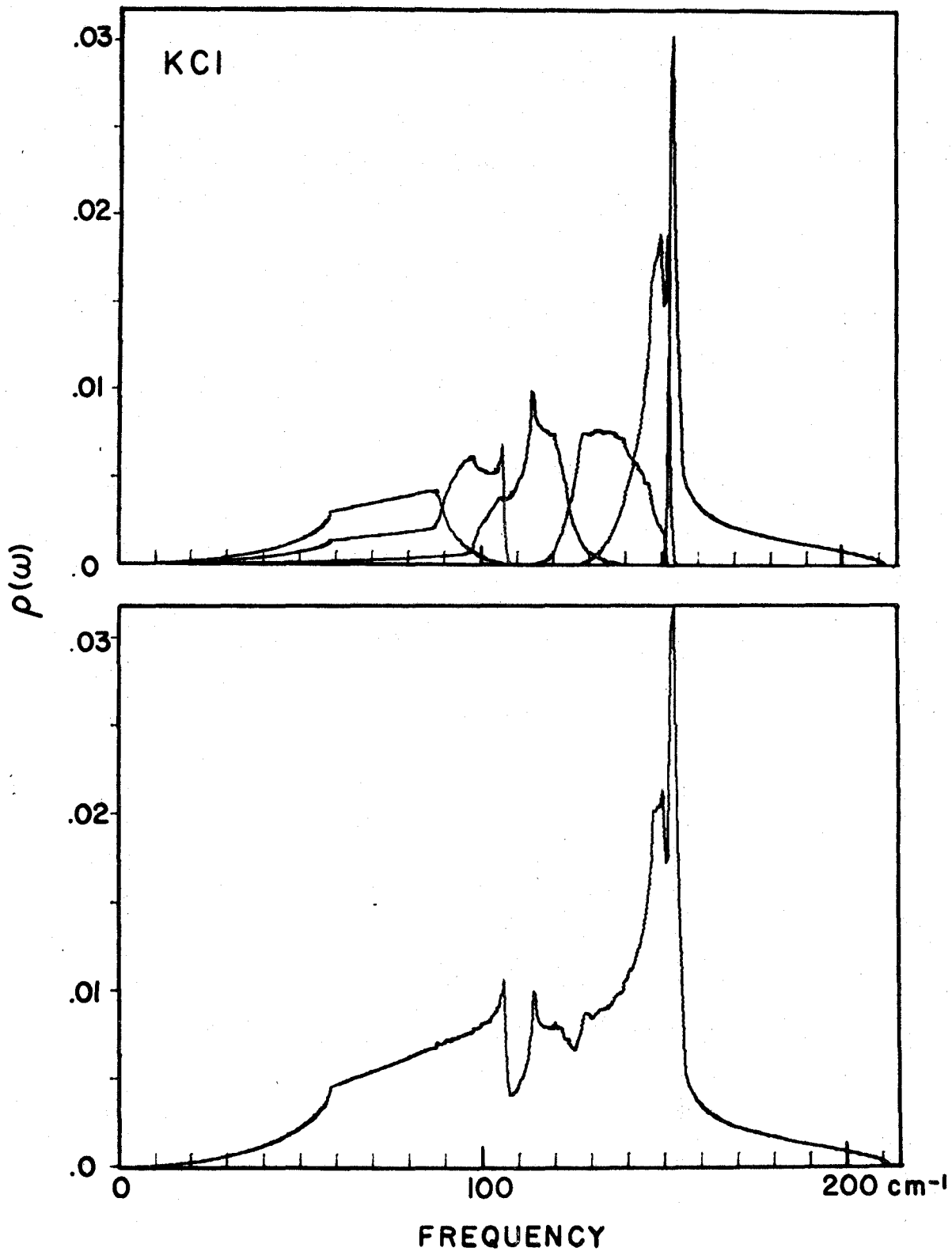
KCl
.03
.02
.01
.0
ρ(ω)
.03
.02
.01
.0
0
100
200 cm-1
FREQUENCY

Harley and Walker (1970). The shape of the absorption is very similar to the infrared results with a sharp drop in intensity at about 108 cm^{-1} and a low frequency tail extending to 60 cm^{-1}. This 108 cm^{-1} peak is also found to shift to higher frequencies with increasing impurity concentration in a similar fashion to the singularities in KBr. Low frequency resonant models due to Li^{+} and F^{-} were also observed.

Another major reason for studying KCl is that one can observe the induced absorption due to the naturally occurring Cl^{35} and Cl^{37} isotopes. These weakly perturbing isotopic defects are expected to reveal critical points in the phonon spectrum. They also enable a direct test of the defect model to be made since no force constant changes are introduced. Similar experiments on the chlorine and lithium isotopes in sodium chloride and lithium fluoride were first performed by Klein and Macdonald (1968).

In the next section specific impurity spectra are discussed and compared with theoretical calculations.

B. SPECIFIC ABSORPTION SPECTRA

1. Chlorine Isotope

The far-infrared absorption spectrum due to the stable Cl^{35} and Cl^{37} isotopes acting as simple mass defects in KCl is shown in Fig. (26). Measurements were made on a single crystal

FIGURE 26

Induced far-infrared absorption due to the stable isotopes Cl^{35} and Cl^{37} in KCl. Measurements were made on a single crystal of nominally pure Harshaw KCl. The calculated curve is based on the shell model of the defect with zero force constant changes, The experimental resolution is .15 cm^{-1}.

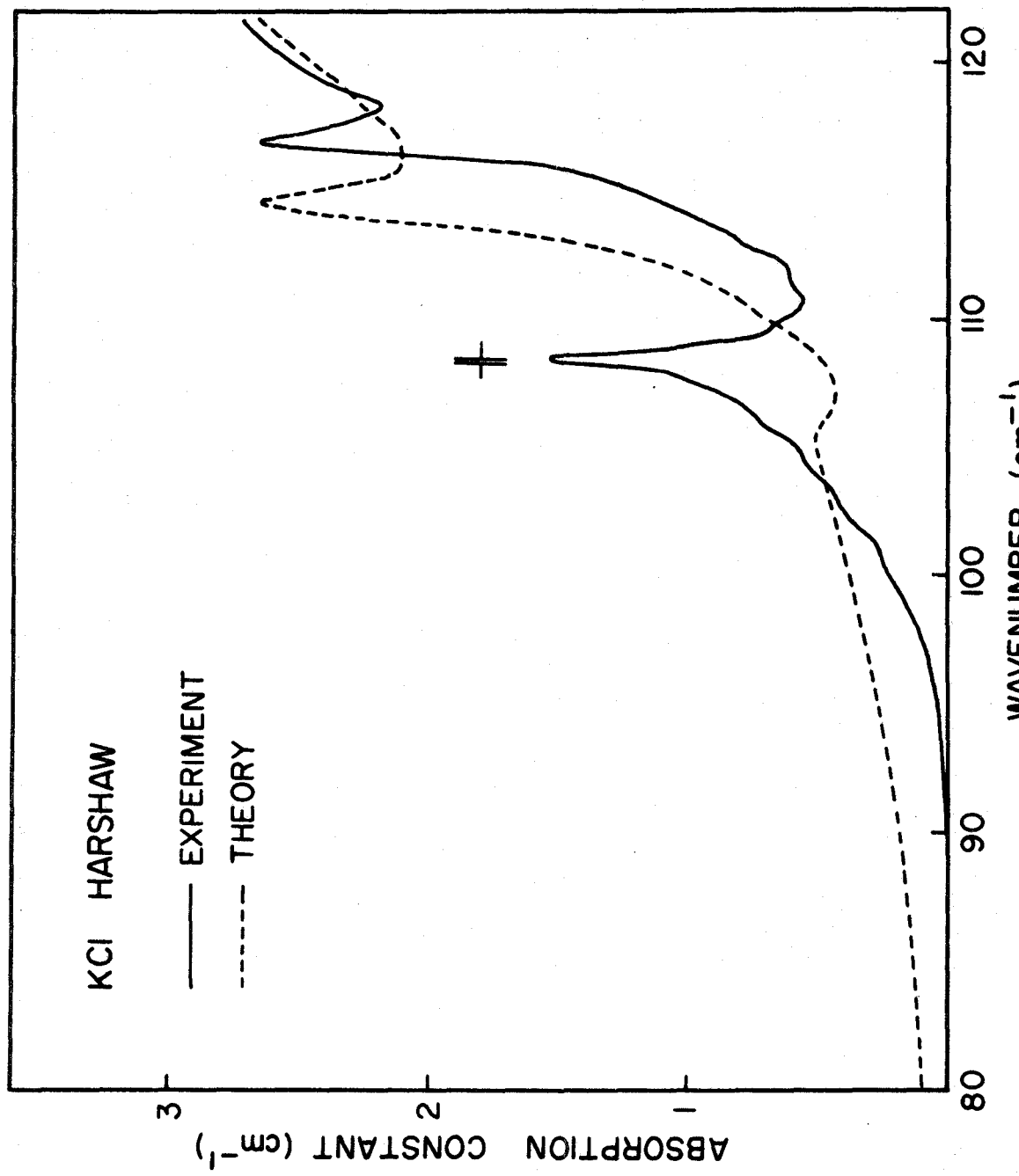
KCl HARSHAW
EXPERIMENT
THEORY
ABSORPTION CONSTANT (cm⁻¹)
WAVENUMBER (cm⁻¹)
80
90
100
110
120
1
2
3

of nominally pure Harshaw KCl. Two peaks were observed at 108.26 cm^{-1} and 117 cm^{-1}. No other absorption was observed down to 30 cm^{-1}. The 108 cm^{-1} peak is seen to fall off sharply on the high frequency side.

The dashed curve in Fig. (26) is the result of a calculation with zero force constant changes. Only the impurity mass was changed, from the average value of 35.45 to 36.96 a.m.u. The two main peaks in the calculated spectrum are found to agree to within 2% of the experimentally determined frequencies. The shape of the 117 cm^{-1} peak is correctly reproduced by the calculation, but the 108 cm^{-1} absorption in the experimental curve appears too strong in comparison with the calculation. This may be due to the presence of small amounts of unwanted impurities, such as calcium etc. in the sample, which would tend to increase the strength of the absorption.

Because of the weak perturbation of the isotope defect, identification of Van Hove singularities is not complicated with the appearance of band-mode resonances. The step in the calculated spectrum arises from critical points in the dispersion surface of the second acoustical branch. The top of the step at 106.3 cm^{-1} is due to a saddle point at approximately (0.52,0.52,0) and the bottom at 107 cm^{-1} is due to a nearly degenerate maximum at (0.65,0.35,0.35) in the Brillouin zone. The corresponding frequencies in the experimental curve

are listed in Table (3), however in some of the spectra the bottom of the step is not very distinct. These results may help to clarify the far-infrared work of MacPherson and Timusk (1970b) on the induced absorption due to H^- ions in KCl. They observed two peaks at 99 and 108 cm^{-1}, and it now appears that their 99 cm^{-1} peak is a resonance of the H^- ion or some unknown impurity, since the 108 cm^{-1} peak appears in all the KCl defect spectra studied. With our assignment of the critical points the calculated frequencies appear 2% low in agreement with frequencies measured in the nearby region of the zone along the [111] direction by Copley et al. (1969) using neutron spectroscopy. However more recent neutron results by Raunio and Almqvist (1969) in this region indicate that the unperturbed phonon energies tend to a higher value in agreement with the infrared results. It is interesting to note that these critical points correspond to similar features already seen in KBr.

The peak at 114.5 cm^{-1} in the calculated spectrum is due to a saddle point in the third acoustical branch at (0.5,0.5,0.5).

2. Sodium

The experimental absorption due to KCl doped with Na^+ ions is shown in Fig. (27). Measurements were made from 30 cm^{-1} up to the reststrahlen absorption and no resonant modes

TABLE 3

Positions of the observed singularities in KCl with different impurities at 11°K. The Na^+ values have been extrapolated to zero defect concentration.

	Mole % impurity	cm^{-1}	cm^{-1}	cm^{-1}
Li^+	.001	108.72	109.41	117.3
Na^+	0	108.65		117.18
Sm^{++}	.01	108.3		117.4
Eu^{++}	.04	108.87	110.9	117.49
Cl^- isotope		108.56	109.2	116.96
F^-	.0015	108.4	109.9	117.34
O_2^-	≈.001	108.64	109.8	117.18
Br^-	.064	108.79	109.4	117.9
I^-	.05	108.0	111.2	117.19
Shell Model		106.3	107	114.5

FIGURE 27

Induced far-infrared absorption due to Na^+ ions in KCl. The calculated curve is from the shell model of the defect with force constant changes $\Delta f = -500$ dyn/cm, $\Delta g = \Delta k = 0$. Recent measurements by Templeton and Clayman (1970) on high concentration samples has revealed a resonant pair mode peak at 44 cm^{-1}.

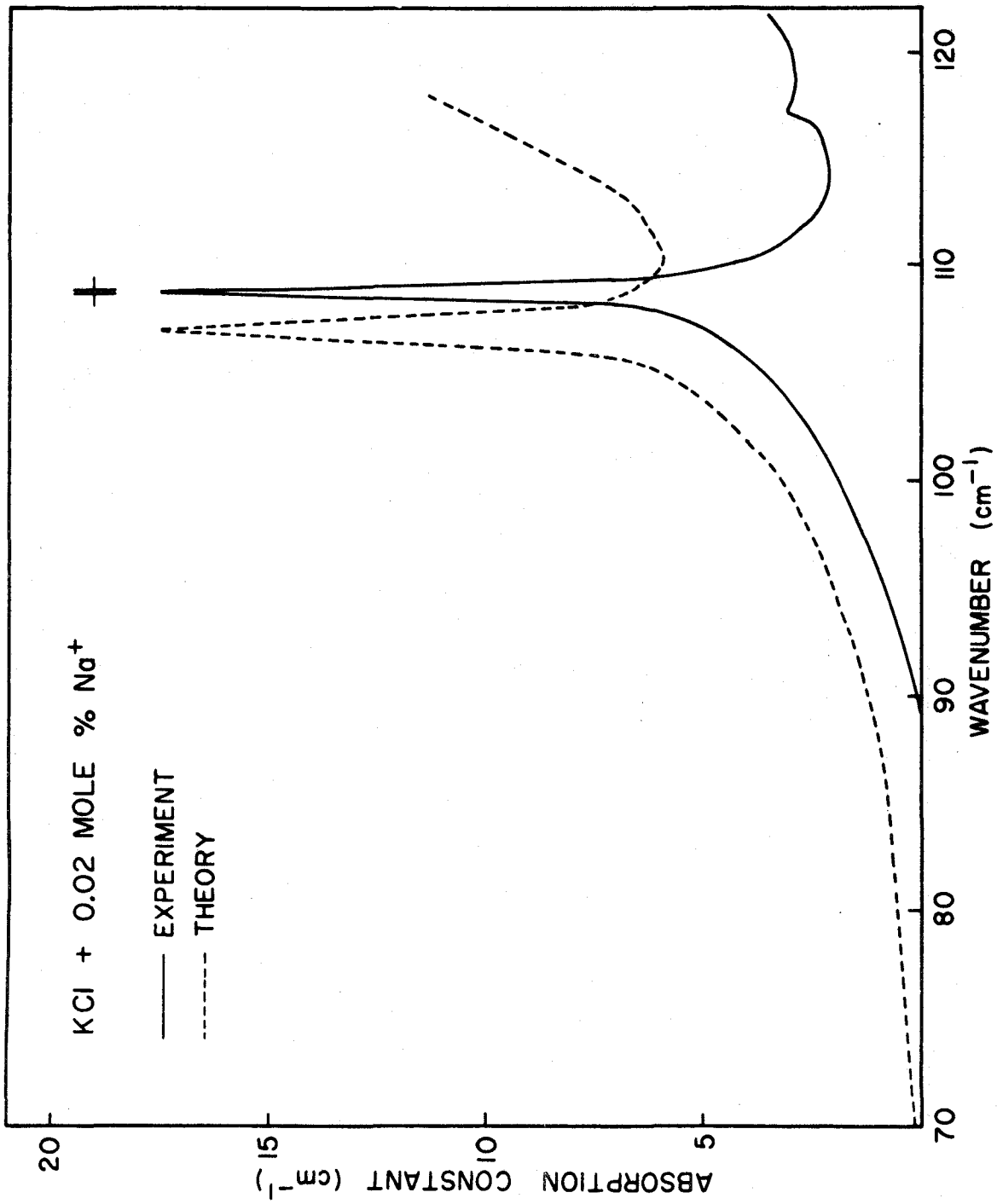
KCl + 0.02 MOLE % Na^+
EXPERIMENT
THEORY
ABSORPTION CONSTANT (cm^{-1})
WAVENUMBER (cm^{-1})
20
15
10
5
70
80
90
100
110
120

were observed. However recent measurements by Templeton and Clayman (1970) on KCl crystals containing approximately eight times our Na^+ concentration have revealed a weak resonant peak at 44 cm^{-1}. These authors attribute this resonance as being due to absorption by pairs of Na^+ ions.

Our measurements reveal a sharp absorption at 108.29 cm^{-1}. A weak peak at 117.19 cm^{-1} is also observed. These peaks are at the same positions as those previously observed in the Harshaw KCl measurements, however the introduction of Na^+ into the lattice causes the 108 cm^{-1} peak to grow in intensity and shift to higher frequencies. The frequency dependence of this peak on Na^+ concentration is shown in Fig. (28), the rate of increase being 2 cm^{-1}/0.1% Na^+ which is four times the rate of the similar feature A seen in KBr. The curve has been extrapolated to zero defect concentration and the position of the singularity for pure KCl is given in Table (3). The position and strength of the 117 cm^{-1} peak was not affected by the addition of Na^+ ions into the KCl lattice.

The best fit to the experimental curve was obtained with a small reduction in the defect-first neighbour force constant. Decreasing Δf still further produced a reduction in strength and a broadening of the 107 cm^{-1} peak. A small change of slope at 114.5 cm^{-1} can also be seen in the calculated spectrum. Agreement between experiment is good, and

FIGURE 28

The frequency of the saddle point singularity at (0.52,0.52,0) in the second acoustical branch of KCl, as observed in the far-infrared, plotted as a function of Na^+ concentration. The straight line is the best fit by eye.

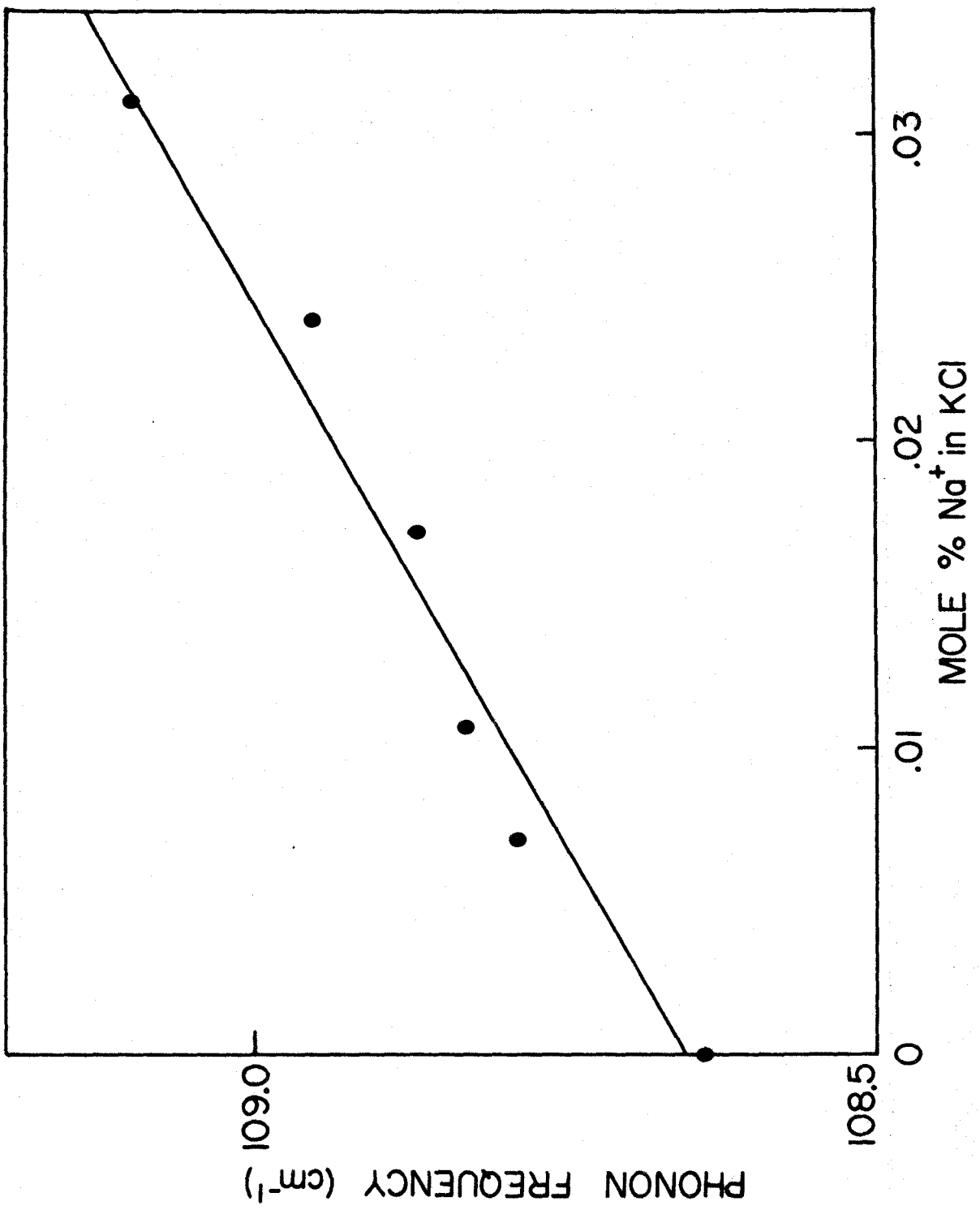
PHONON FREQUENCY (cm⁻¹)
109.0
108.5
0
.01
.02
.03
MOLE % Na⁺ in KCl

the overall shape of the absorption is reproduced well.

3. Lithium

Potassium chloride doped with lithium is one of the most thoroughly studied defect systems. The reason for such interest in this system is that the Li^+ ion enters the KCl lattice substitutionally but enters in an off-centre position. Tunneling between equivalent positions is then possible. This has been confirmed by a variety of experiments. In particular measurements of the dielectric constant (Sack and Moriarity 1965), electro-caloric effect (Lombardo and Pohl 1965, 1966), ultrasonic velocity and attenuation (Byer and Sack 1966, 1967), specific heat (Harrison et al. 1968) paralectric resonance (Kirby et al.1970) and thermal conductivity (Baumann et al. 1967, Walton 1967), indicate the existence of defect energy states in the region of 1°K. Higher energy states have been observed through far infrared absorption measurements by Nolt and Sievers (1966) who found an absorption band at 40 cm^{-1}. In a recent paper by Kirby, Hughes and Sievers (1970) new absorption measurements on the 40 cm^{-1} band were presented and compared with the tunneling model of Gomez, Bowen and Krumhansl (1967).

Early calculations by Matthews (1965) using a one dimensional model showed that an impurity could be in an off-

centre equilibrium position. Subsequent calculations using three dimensional models by Quigley and Das (1967), Wilson et al. (1967) and by Gomez, Bowen and Krumhansl (1967) have established that the Li^+ ion can exist in any one of eight equivalent equilibrium sites in the [111] directions. The latter model of Gomez,Bowen and Krumhansl, which assumes that the Li^+ ion moves in a multiple-well harmonic-oscillator potential, has been partially successful in fitting the tunneling splitting and resonant mode.

Because of the instability of the KCl:Li^+ system no attempt was made to calculate the one phonon absorption using our model of the defect. A more sophisticated model is needed which takes into account the off-centre character of the Li^+ ion. However far infrared measurements on a single crystal of KCl doped with Li^+ were made from 30 cm^{-1} to 120 cm^{-1}. The experimental curve is shown in Fig. (29). The low frequency band at 40 cm^{-1} was observed in addition to a sharp peak centred at 108.22 cm^{-1}. A weaker peak at 117.3 cm^{-1} was also observed. The absorption on the high frequency side of the 108 cm^{-1} peak falls off sharply in agreement with the shell model assignment of Van Hove singularities in this region. The frequencies of the singularities are listed in Table (3) and one can see the close agreement between the values measured using the on-centre impurities.

FIGURE 29

Experimental far-infrared induced absorption of Li^+ ions in KCl. The band at 40 cm^{-1} is due to tunneling between the eight equivalent off-centre equilibrium sites of the Li^+ ion. The structure at higher frequencies is due to the host lattice absorption.

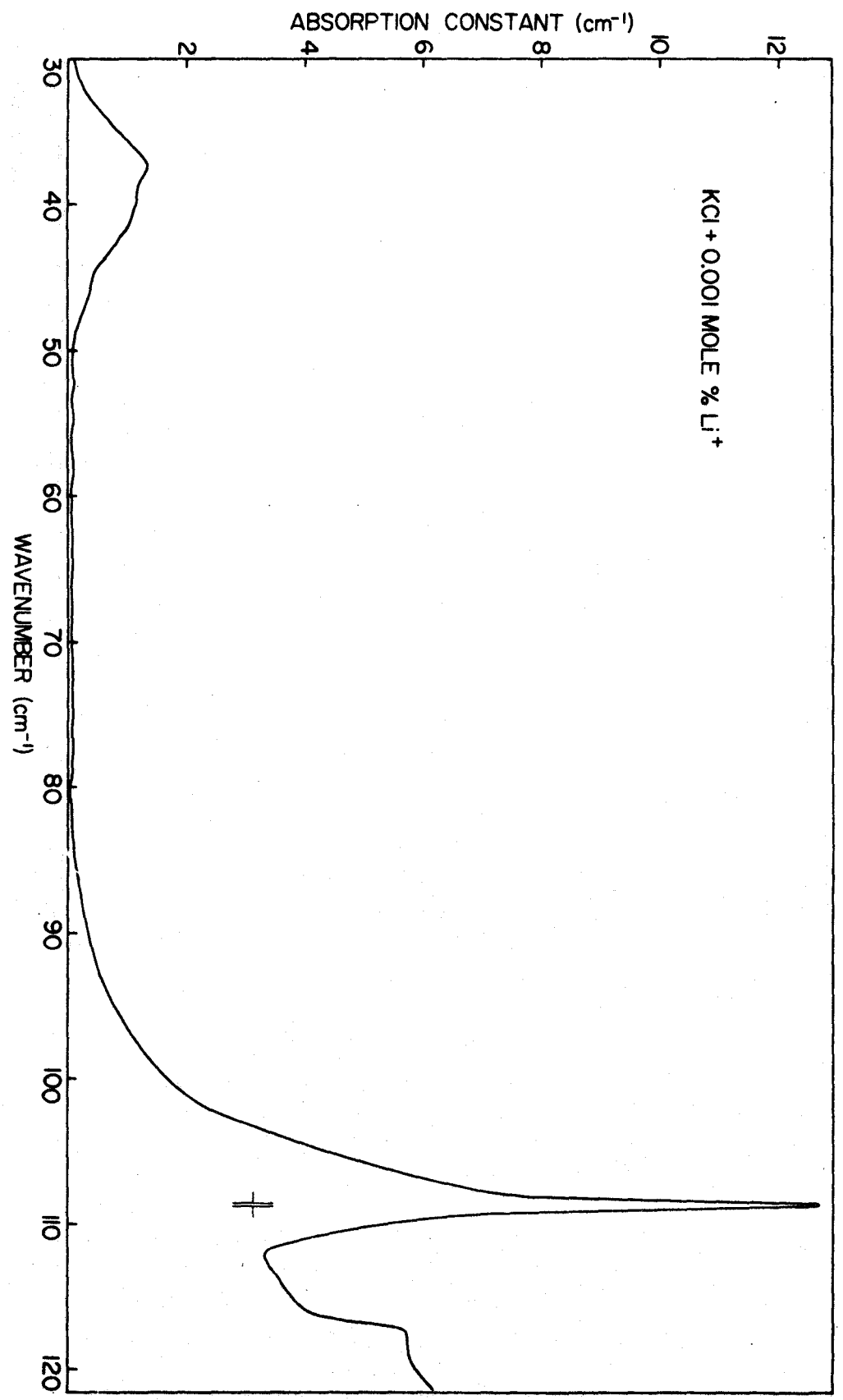
ABSORPTION CONSTANT (cm⁻¹)
2
4
6
8
10
12
KCl + 0.001 MOLE % Li⁺
WAVENUMBER (cm⁻¹)
30
40
50
60
70
80
90
100
110
120

4. Samarium

Fig. (30) shows the experimental absorption due to Sm^{2+} in KCl. The familiar 108 cm^{-1} peak appears broader and more symmetrical than in previous spectra, the step on the high frequency side appearing less sharp. A shoulder at 117.5 cm^{-1}, due to the third branch saddle point, can be clearly seen.

The experimental curve is compared with the model using force constant changes determined by Buchanan and Woll (1969) from fits to their fluorescent side band spectra. The values of Δf and Δg are the same as used previously to fit the KBr:Sm^{2+} spectra, a large increase in Δf being required due to the effect of the increased Coulomb field.

It can be seen that overall agreement between experiment and theory is good, with the general shape of the absorption being reproduced. The 106.3 cm^{-1} peak in the calculation however appears somewhat narrower than the same experimental absorption. But in general the model appears to be adequate in accounting for both side band and far infrared absorption due to Sm^{2+} in KBr and KCl.

5. Europium

The far-infrared absorption spectra due to Eu^{2+} in KCl appears very similar in all respects to the previous spectrum for

FIGURE 30

Induced far-infrared absorption due to Sm^{2+} ions in KCl. The experimental curve is compared with the shell model defect calculation using force constant changes determined by Buchanan and Woll (1969) from fits to their fluorescent side band spectra. The values of Δf and Δg are the same as used to fit the KBr:Sm^{2+} curve, i.e. Δf = 14,500 dyn/cm, Δg = -1500 dyn/cm, Δk = 0.

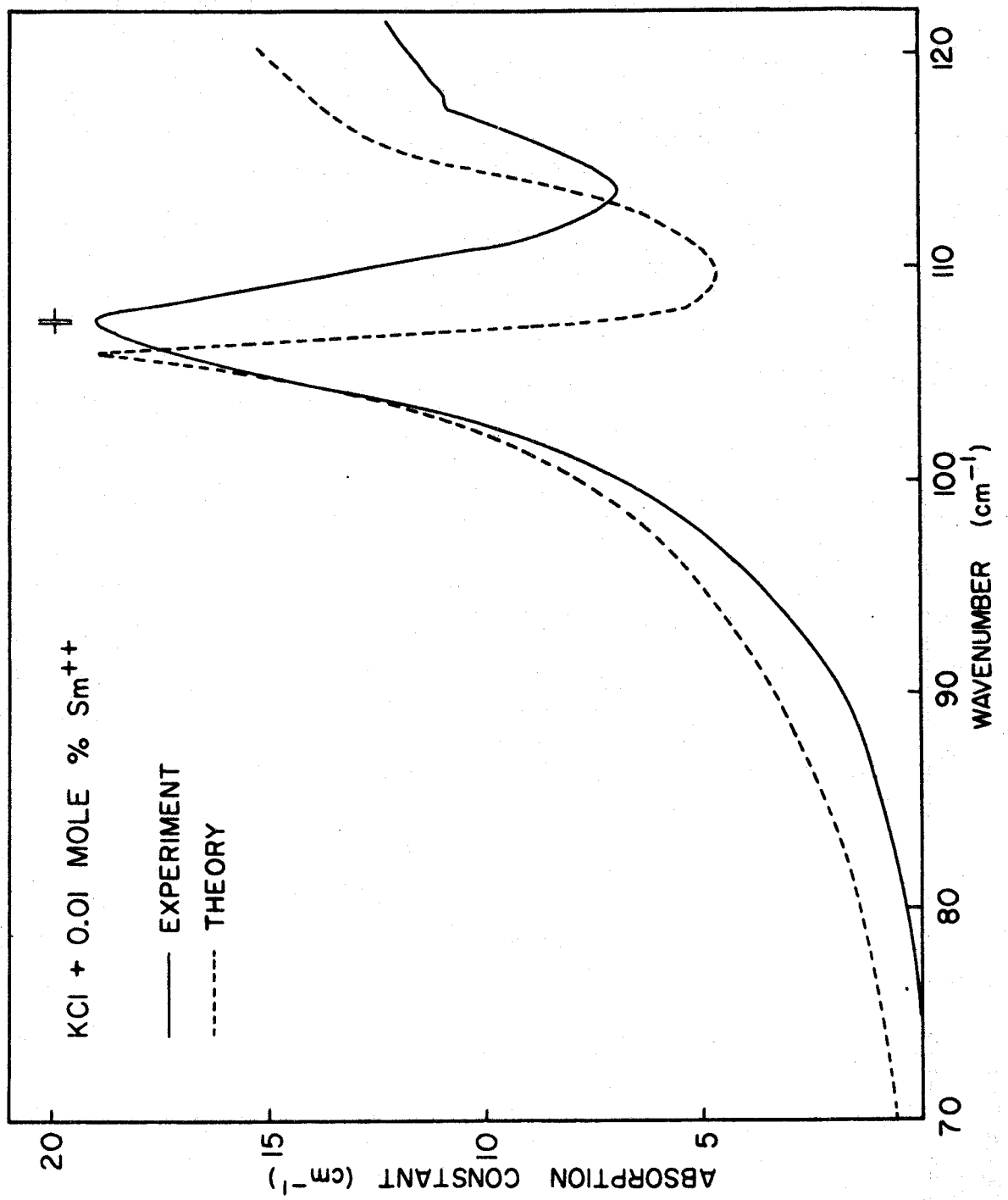
KCl + 0.01 MOLE % Sm++
EXPERIMENT
THEORY
ABSORPTION CONSTANT (cm⁻¹)
WAVENUMBER (cm⁻¹)
20
15
10
5
70
80
90
100
110
120

KCl:Sm^{2+}, the only difference being a narrowing of the 108 cm^{-1} peak in better agreement with the calculation. See Fig. (31). Because of the similarity between these two rare earths the same force constant changes were used in the calculation. The main peak in the experimental curve was found at a slightly higher frequency. This is probably due to the Eu^{2+} concentration being four times that of the Sm^{2+} doped sample. No resonant modes were observed down to 30 cm^{-1}.

Schwartz and Walker (1966,1967) have observed a resonant mode in thermal conductivity measurements on single crystals of KCl containing Eu^{2+}. They observed a prominent dip at 30°K corresponding to a resonant state. However these authors conclude that the positive ion vacancy that accompanies the Eu^{2+} ion is the dominent phonon scatterer. The Eu^{2+} ion appears to act as a small perturbation on the vacancy effect.

6. Fluorine

A resonant band mode absorption due to F^- in KCl has been found at 77 cm^{-1}. This absorption seems to be the direct analog of the KBr:F^- resonance encountered in the last chapter. The usual structure is observed at higher frequencies, that is a sharp peak at 108.4 cm^{-1} and a shoulder at 117.34 cm^{-1}, see the full curve in Fig. (32).

In order to place the resonant mode peak at its experimentally determined position of 77 cm^{-1}, the nearest

FIGURE 31

Induced far-infrared absorption due to Eu^{2+} ions in KCl. The calculated absorption is from the shell model for the defect using the same force constant changes as the KCl:Sm^{2+} system

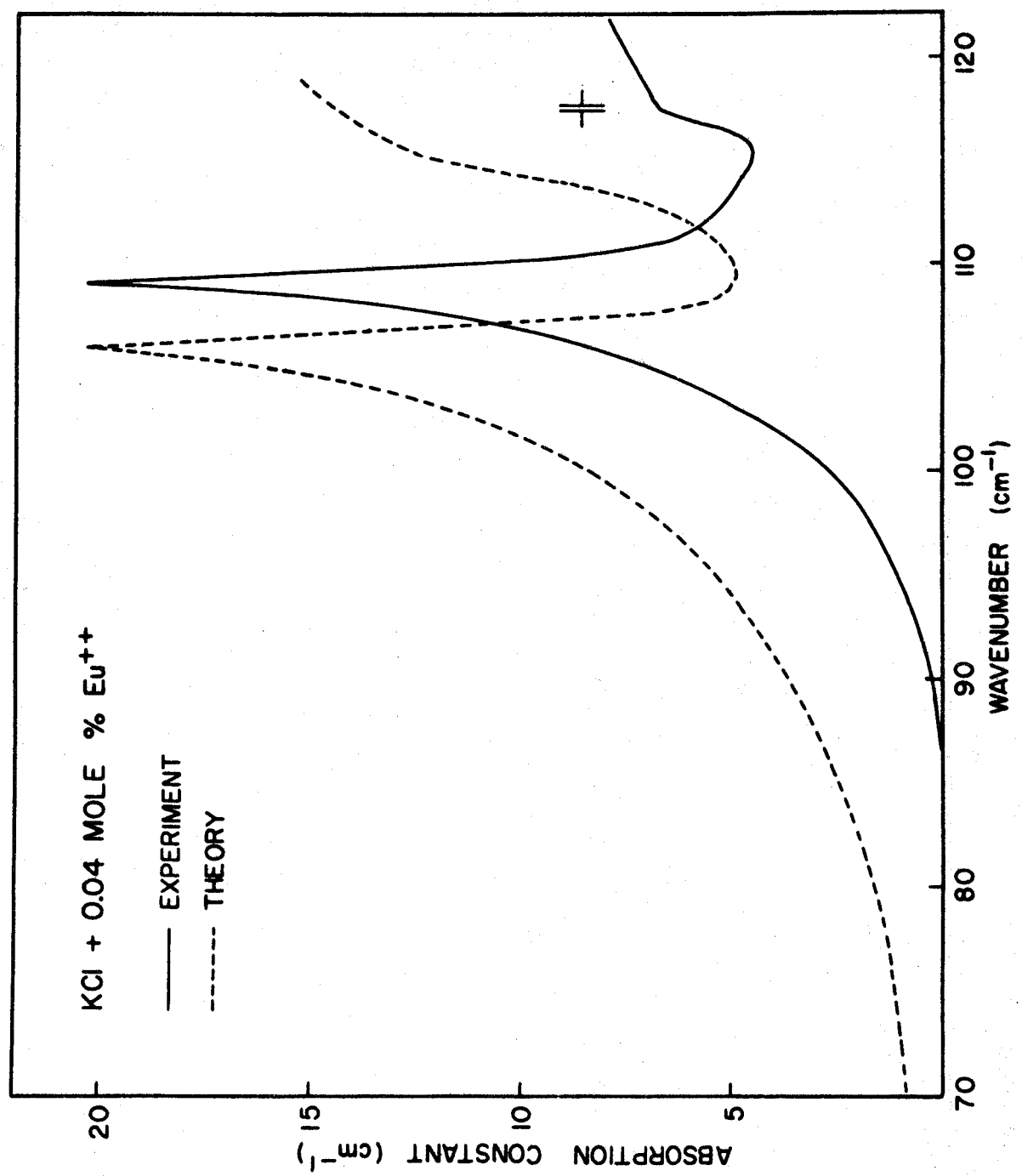
KCl + 0.04 MOLE % Eu++
EXPERIMENT
THEORY
ABSORPTION CONSTANT (cm⁻¹)
WAVENUMBER (cm⁻¹)
20
15
10
5
70
80
90
100
110
120

FIGURE 32

Induced far-infrared absorption due to F^- ions in KCl. A resonant band mode absorption can be seen at 77 cm^{-1}. The calculated curve is based on the shell model for the defect with the first neighbour force constant being reduced by $\Delta f = -10{,}900$ dyn/cm in order to fit the resonant mode peak. With $\Delta g = -1000$ dyn/cm and $\Delta k = 0$ the higher frequency structure can be seen but reduced in intensity.

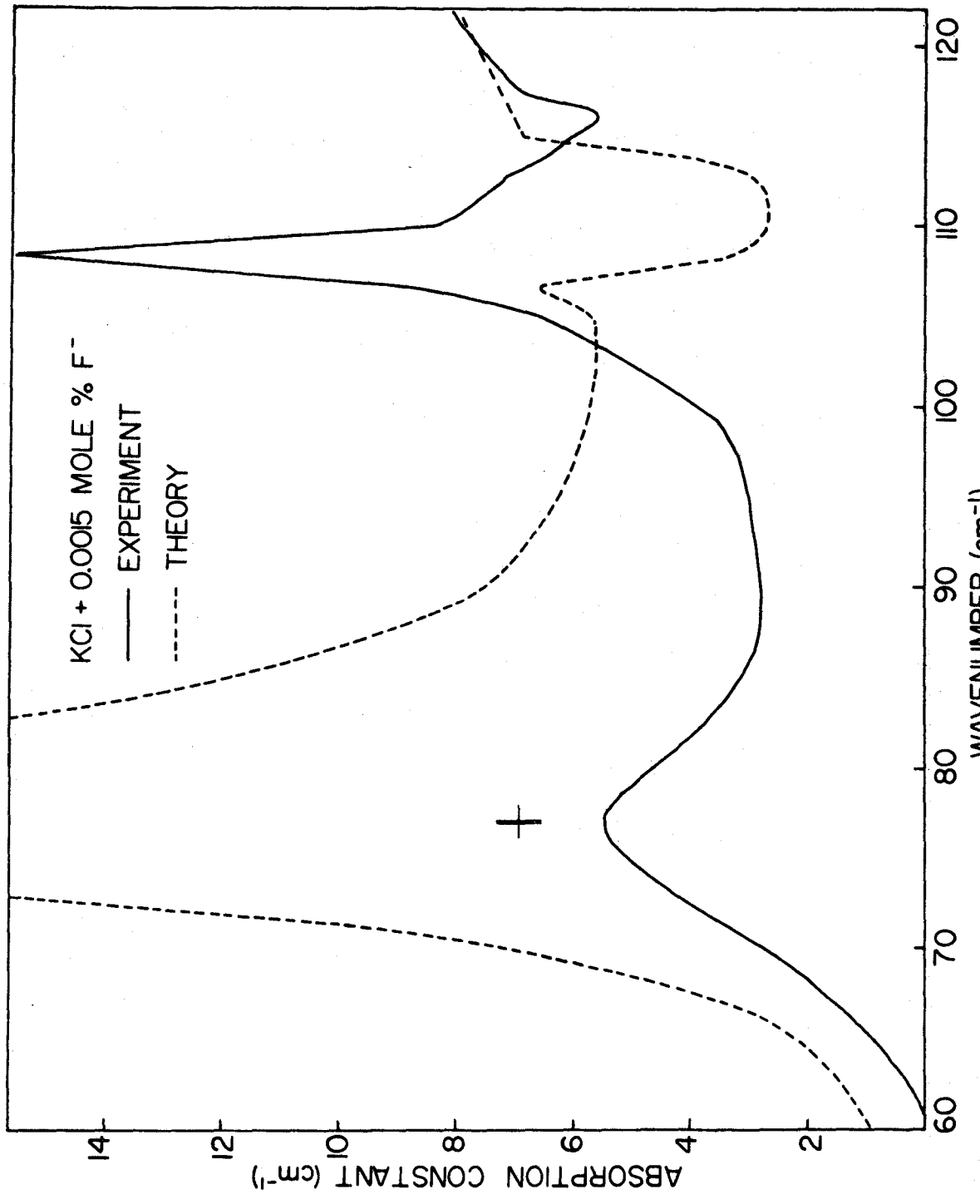
KCl + 0.0015 MOLE % F⁻
EXPERIMENT
THEORY
ABSORPTION CONSTANT (cm⁻¹)
WAVENUMBER (cm⁻¹)
2
4
6
8
10
12
14
60
70
80
90
100
110
120

neighbour force constant was reduced until $\Delta f = -10{,}900$ dynes/cm. Comparison between experiment and theory can be seen in Fig. (32). A situation similar to that encountered in the KBr:F^- system occurs in which the strength of the resonant absorption is overestimated by the calculation with a subsequent loss of intensity at higher frequencies. The 106.3 cm^{-1} peak in the calculation appears at its correct position but greatly reduced in intensity. Some improvement is found by putting $\Delta g = -1000$ dynes/cm. Even though the reduction in force constants is in qualitative agreement with the reduced ionic radius of the F^- ion, the present model fails to reproduce correct intensities when resonant modes are present.

7. Bromine

The far-infrared absorption spectrum due to Br^- ions in KCl is shown in Fig. (33). No resonant band mode absorption was found down to 30 cm^{-1} in agreement with previous infrared measurements of Weber and Siebert (1968). However a region of strong absorption was found centred at 108.8 cm^{-1}. A weaker peak is seen at 117.5 cm^{-1}. Indications of this peak are also seen in the spectrum of Weber and Siebert. Nair and Walker (1971) have recently made Raman measurements on KCl, KBr mixed crystals but found no structure below 120 cm^{-1}. However analysis of their results was complicated by

FIGURE 33

Induced far-infrared absorption due to Br^- in KCl. No resonant band modes were observed down to 30 cm^{-1}. The calculated spectrum is from the shell model for the defect with force constant changes $\Delta f = -3000$ dyn/cm, $\Delta g = 300$ dyn/cm, $\Delta k = 0$. The experimental resolution is .15 cm^{-1}.

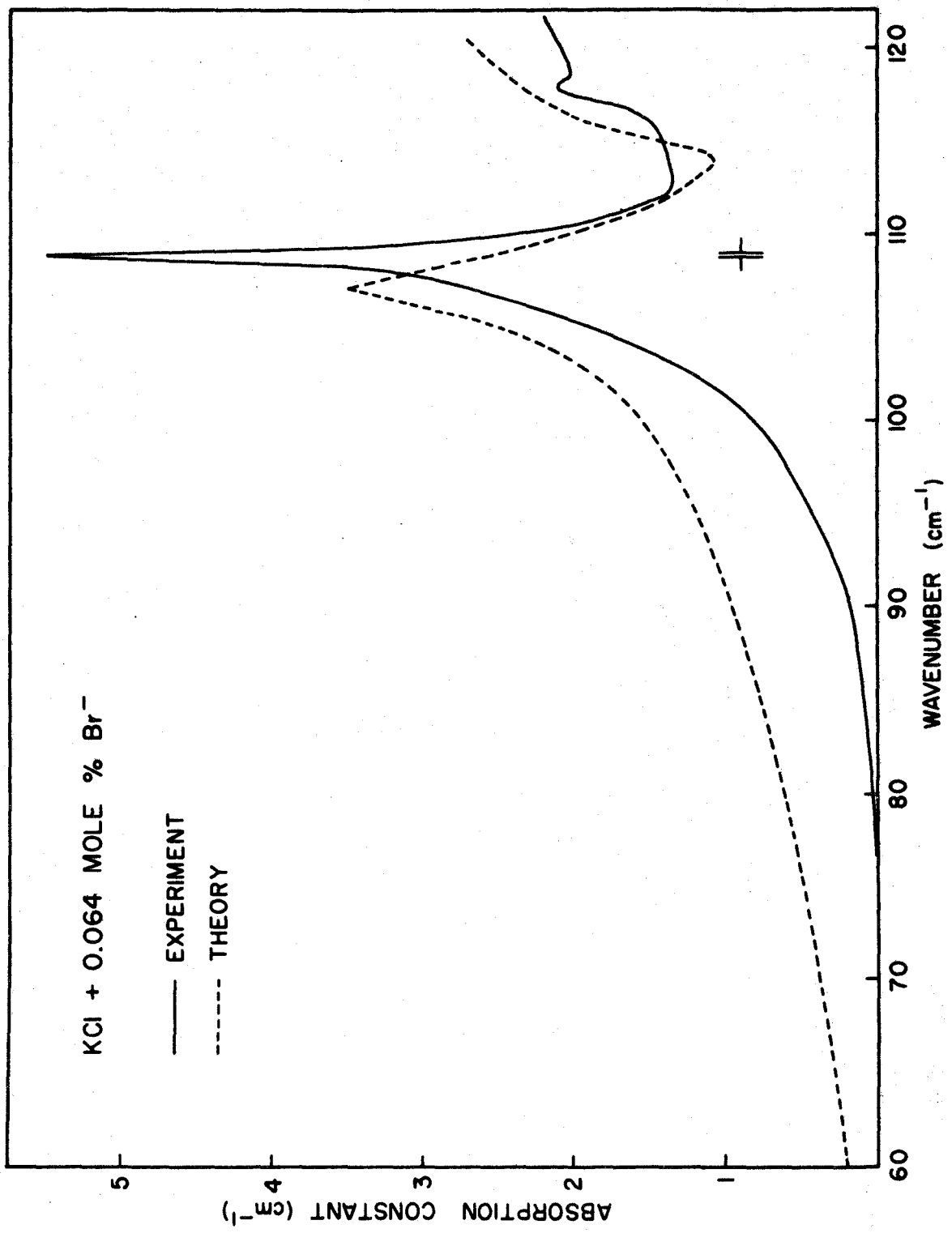
KCl + 0.064 MOLE % Br⁻
EXPERIMENT
THEORY
ABSORPTION CONSTANT (cm⁻¹)
WAVENUMBER (cm⁻¹)
1
2
3
4
5
60
70
80
90
100
110
120

the comparable intensities of the first- and second-order spectra.

Thermal conductivity measurements on the KCl:Br^- system have been made by Baumann and Pohl (1967) and their results show a dip at 36°K corresponding to a resonance at 86 cm^{-1}.

Recent measurements of the specific heat enhancement of the KCl:Br^- system by Karlsson (1970) have been interpreted as being due to a lattice resonant mode at 110±10 cm^{-1}. However we attribute the infrared absorption at 108.8 cm^{-1} as being due to singularities in the single phonon density of states of KCl in agreement with the conclusion of Weber and Siebert. These authors also measured the absorption due to Cu^+ in KCl and found a similar peak at 108 cm^{-1}. Indeed this peak occurs in all the KCl spectra studied and is independent of the impurity used, indicating that the absorption is due to the host lattice.

The result of a calculation for Br^- ions in potassium chloride using a small reduction in f and a smaller increase in g is given in Fig. (33). The calculated peak at 106.3 cm^{-1} is too broad in comparison with the experimental absorption. The rigid ion picture would indicate a small increase in the first neighbour force constant since the slightly larger Br^- ion would tend to push the nearest neighbour K^+ ions outwards. However when Δf is increased a strong resonance moves across

the region of interest and obscures the continuous structure. With the force constants used a shoulder is seen at 114.5 cm^{-1} but the overall agreement between experiment and calculation is poor. It is probable that improvements could be made by including the effects of second neighbours, This has been found to be the case for Br^- in NaCl (Macdonald and Klein 1968).

8. Iodine

I^- in KCl produces a far-infrared absorption which is very similar to the KCl:Br^- system discussed in the last section. The main peak at 108 cm^{-1} however is broader than the similar Br^- absorption in better agreement with the calculation. No resonances were observed. A resonance at 57 cm^{-1} has been observed through measurements of thermal conductivity by Baumann and Polh (1967) and has been interpreted as being similar to the KCl:Br^-system in which the resonance is essentially due to the increase of the impurity mass.

Comparison between the experimental and calculated spectra are shown in Fig. (34). The agreement is good, the height and width of the main absorption are well reproduced, with the shoulder at 117 cm^{-1} appearing prominently in both curves. Δg was increased to 1500 dynes/cm while Δf was kept at the same value as used for KCl:Br^-.

FIGURE 34

Induced far-infrared absorption due to I^- ions in KCl. The calculated spectrum is based on the shell model for the defect with force constant chantes $\Delta f = -3000$ dyn/cm, $\Delta g = 1{,}500$ dyn/cm, $\Delta k = 0$. This system is essentially the same as the KCl:Br^- system except for the increase in mass of the I^- ion.

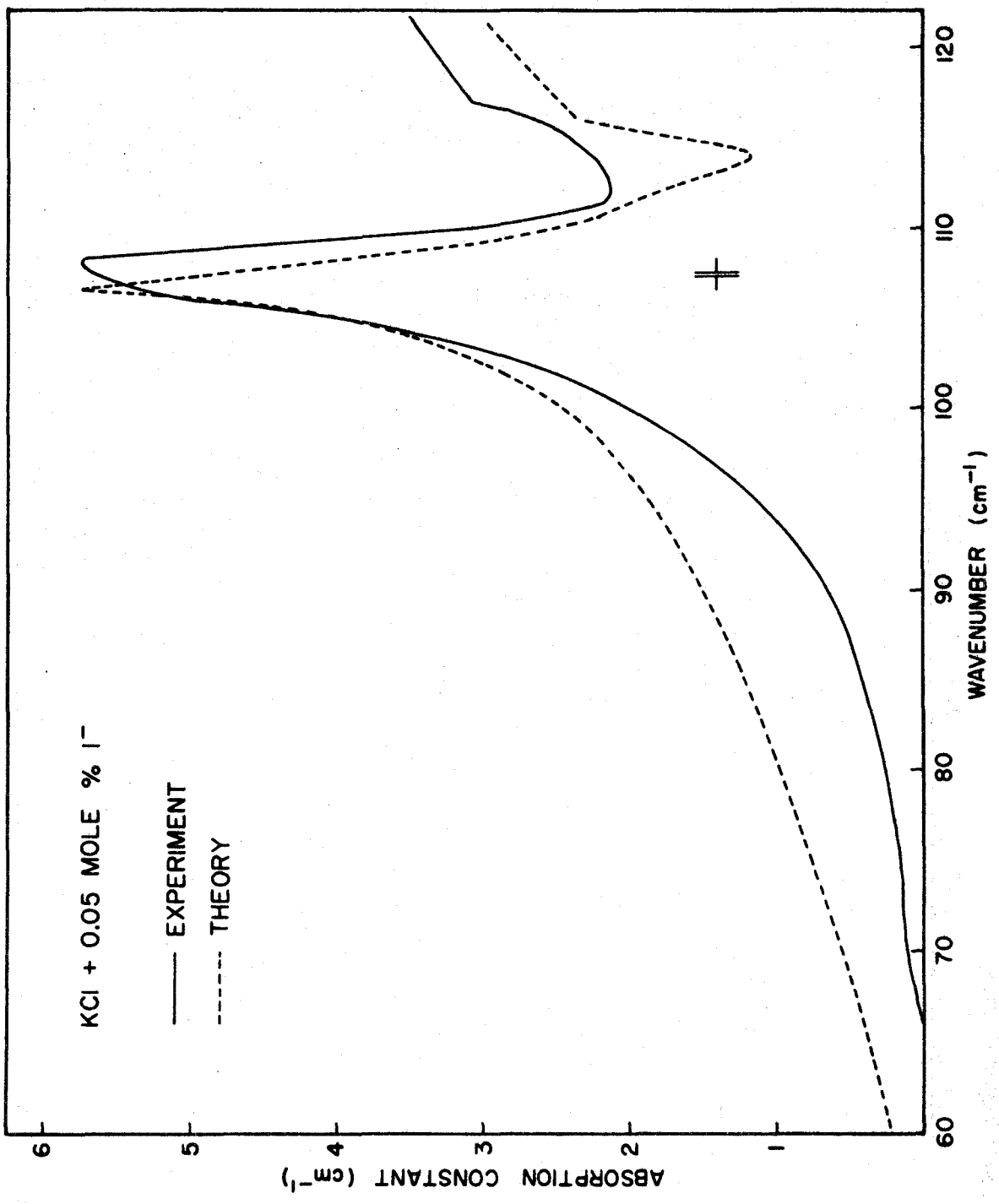
KCl + 0.05 MOLE % I⁻
EXPERIMENT
THEORY
ABSORPTION CONSTANT (cm⁻¹)
WAVENUMBER (cm⁻¹)
1
2
3
4
5
6
60
70
80
90
100
110
120

9. Oxygen

The experimentally measured far infrared absorption in KCl due to the addition of O_2^- molecules is compared with the calculated curve in Fig. (35). The experimental curve has a sharp peak at 108 cm^{-1} superimposed on the steeply sloping reststrahlen absorption. The usual shoulder is also observed, however there is an additional absorption in the region of 112 cm^{-1}. A distinct change of slope can be seen. The measurements were made down to 30 cm^{-1} but no additional absorption was found in this region.

Except for the addition of the absorption at 112 cm^{-1} the induced absorption is similar in all respects to all the other KCl defect spectra studied. In attempting to fit the absorption Δf and Δg were reduced until the main slope of the reststrahlen edge could be reproduced. This reduction in force constants is in agreement with the rigid ion picture of the defect site and is similar to the KBr:O_2^- system. However the calculated curve fails to reproduce the sharp peak at 108.6 cm^{-1}. The calculation shows a sharp drop in intensity at 106.3 cm^{-1} but the low frequency side of this absorption is too broad. Reducing the force constants further causes a strong resonance to move through the region to lower frequencies. This resonance could be placed at 112 cm^{-1} with a value of Δf of -5000 dynes/cm. However its strength was such

FIGURE 35

Induced far-infrared abscription due to O_2^- in KCl. A peak at 112 cm^{-1} can be seen in addition to the usual structure. The calculated absorption is from the shell model for the defect with force constant changes Δf =-1000 dyn/cm, Δg = -500 dyn/cm, Δk = 0.

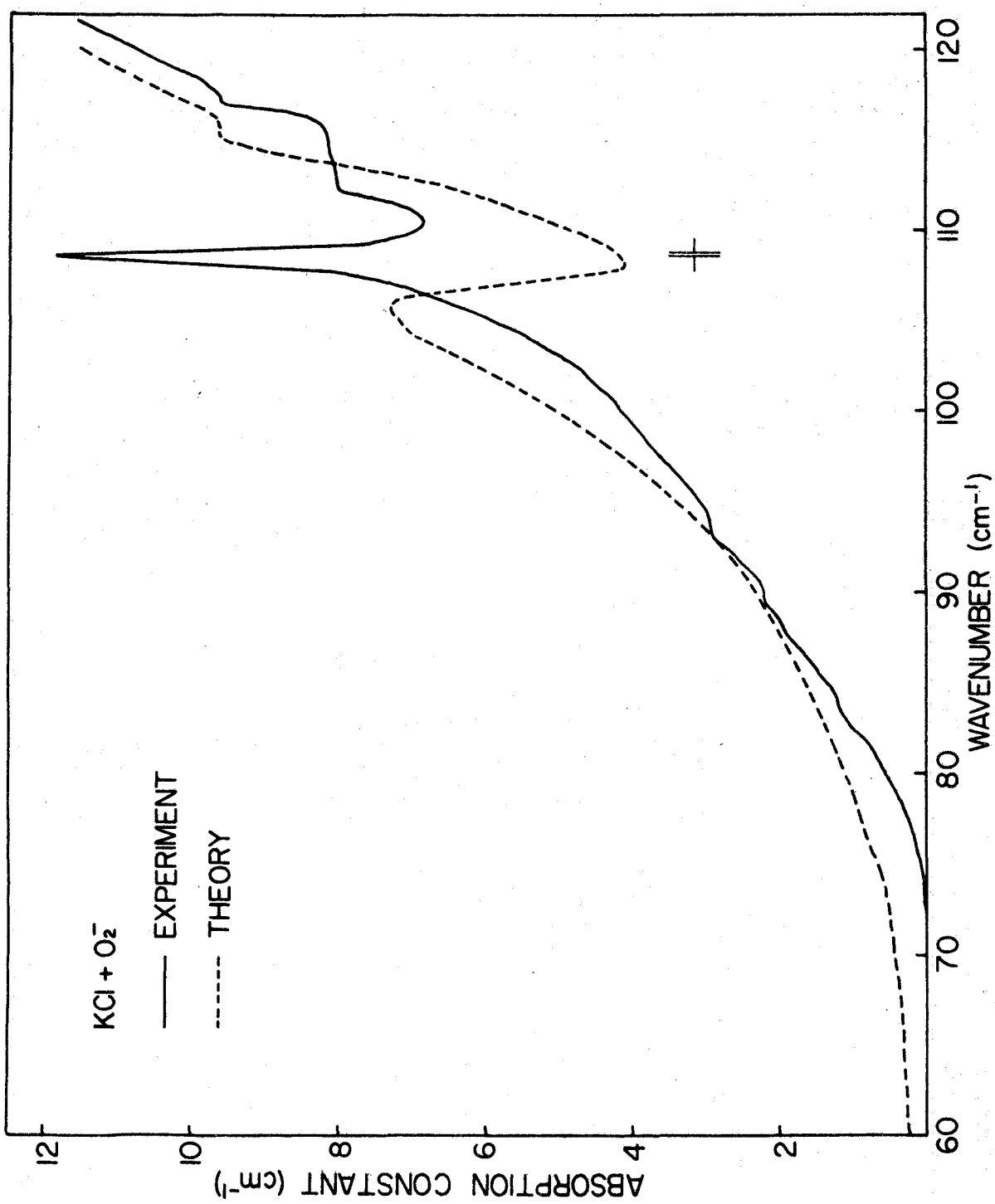
KCl + O_2^-
EXPERIMENT
THEORY
ABSORPTION CONSTANT (cm^{-1})
WAVENUMBER (cm^{-1})
12
10
8
6
4
2
60
70
80
90
100
110
120

that all other structure was obscured.

The calculated density of states between 106 and 115 cm^{-1} is low and shows little structure and consequently if the experimentally determined peak at 112 cm^{-1} is due to a band mode resonance of the O_2^- molecule one would expect a relatively strong sharp peak in this region. However the observed peak is weak and appears as a shoulder on the res-strahlen slope. A more thorough investigation of this absorption is required before any definite conclusions can be made.

The force constant changes used for each impurity in KCl are summarized in Table (4).

TABLE 4

Force constant changes used to fit the impurity induced far-infrared absorption in KCl. $\Delta k = 0$.

Impurity	Δf (dynes/cm)	Δg (dynes/cm)
Na^+	-500	0
Sm^{++}	14,500	-1,500
Eu^{++}	14,500	-1,500
Cl^- isotope	0	0
F^-	-10,900	-1,000
O_2^-	- 1,000	- 500
Br^-	- 3,000	1,500
I^-	- 3,000	1,500

Note: The accuracy of the force constant changes is of the order of ± 2000 dynes/cm.

CHAPTER VI

CONCLUSION

In this thesis we have demonstrated that high-resolution far-infrared Fourier spectroscopy can be a powerful tool in the study of lattice dynamics of crystalline solids. Measurements on single crystals of KBr and KCl containing a variety of different impurities have shown that the structure of the single phonon induced absorption is essentially independent of the impurity used, depending mainly on the lattice dynamics of the host crystal. Van Hove singularities characteristic of the density of states have been observed for nearly all the impurities used and found to agree very well with those predicted by the potassium halide shell model phonons.

Some singular points observed differ by as much as 6% from the shell model predictions. These differences may be accounted for by shell model errors, uncertainties in the neutron measurements or temperature differences between the infrared and neutron scattering measurements. The largest discrepancies are found to occur in off-symmetry directions in the Brillouin zone.

Shifts of Van Hove singularities with varying impurity concentration have been observed. Extrapolation to zero defect concentration has provided the highest resolution optical

measurements of certain phonon frequencies of the unperturbed lattice of insulating crystals at liquid helium temperatures. We have also presented a first direct experimental evidence on the metamorphosis of singularities previously predicted theoretically by Okazaki et al. (1967).

Detailed comparison of experimental spectra with impurity calculations based on the shell model of the alkali halides has shown that, with the absence of impurity resonances, the main features of the induced absorption can be understood in terms of a relatively simple model. In circumstances where force constant changes determined from other experiments have been used to calculate the infrared absorption, very good agreement between experiment and theory has been found.

The defect model however has been unable to predict the correct absorption intensity when low frequency impurity resonances are present in the system. Generally if the force constants between nearest neighbours are reduced to account for the resonant frequency, the intensity of the resonant absorption is overestimated with a subsequent loss of intensity toward higher frequencies. This situation might be improved if changes in the core and shell charges and changes in the ionic charge at the defect site are included. The present model also neglects changes in the force constants to second neighbours and anharmonic effects. No doubt the large-amplitude low-frequency resonances are very

anharmonic.

While there can be no doubt of the need for improvement of the present model to account for impurity resonances, it should not be overlooked that it has been adequate in describing the important features due to the majority of impurities studied.

BIBLIOGRAPHY

Alexander, R. W., Jr., Hughes, A.E. and Sievers, A.J. 1970. Phys. Rev. B 1, 1563.

Baumann, F. C., Harrison, J.P., Pohl, R.O. and Seward, W.D. 1967. Phys. Rev. 159, 691.

Baumann, F.C. and Pohl, R. O. 1967. Phys. Rev. 163, 843.

Benedek, G. and Nardelli, G. F. 1967. Phys. Rev. 155, 1004.

Benedek, G. and Nardelli, G.F. 1968. J. Chem. Phys. 48, 5242.

Bogardus, H. and Sack, H.S. 1966. Bull. Am. Phys. Soc. 11, 229.

Bosomworth, D.R. and Gush, H.P. 1965. Can. J. Phys. 43, 729.

Bosomworth, D.R. 1967. Solid State Commun. 5, 681.

Buchanan, M. and Woll, E.J. Jr., 1969. Can. J. Phys. 47, 1757.

Byer, N.E. and Sack, H.S. 1966. Phys. Rev. Letters 17, 72.

Byer, N.E. and Sack, H.S. 1967. J. Phys. Chem. Solids 29, 677.

Clayman, B.P., Kirby, R.D. and Sievers, A.J. 1971. Phys. Rev. B 3, 1351.

Connes, J. 1961. Rev. Opt. 40, 45, 116, 171 and 231.

Copley, J.R.D., MacPherson, R. W. and Timusk, T. 1969. Phys. Rev. 182, 965.

Cowley, R. A., Cochran, W., Brockhouse, B.N. and Woods, A.D.B. 1963. Phys. Rev. 131, 1030.

Dawber, P.G. and Elliott, R.J. 1963. Proc. Roy. Soc. (London) Ser. A, 273, 222.

Dawber, P. G. and Elliott, R.J. 1963. Proc. Phys. Soc. 81, 453.

Gethins, T., Timusk, T. and Woll, E.J., Jr. 1967. Phys. Rev. 157, 744.

Gilat, G. and Raubenheimer, L.J. 1966. Phys. Rev. 144, 390.

Gomez, M., Bowen, S.P. and Krumhansl, J.A. 1967. Phys. Rev. 153, 1009.

Grisar, R.G.J., Reiners, K.P., Renk, K.F. and Genzel, L. 1967. phys. stat. sol. 23, 613.

Hadni, A., Claudel, J., Chanal, D., Strimer, P. and Vergnat, P. 1967. Phys. Rev. 163, 836.

Harley, R. T., Page, J.B., Jr. and Walker, C. T. 1969. Phys. Rev. Letters 23, 922.

Harley, R. T., Page, J.B., Jr. and Walker, C.T. 1971. Phys. Rev. B 3, 1365.

Harley, R.T. and Walker, C.T. 1970. Phys. Rev. B 2, 2030.

Harrison, J.P., Peressini, P.P. and Pohl, R.O. 1968. Phys. Rev. 171, 1037.

Hurrell, J.P., Porto, S.P.S., Damen, T.C. and Mascarenhas, S. 1968. Physics Letters 26A, 194.

Jacquinot, P. 1960. Rept. Progr. Phys. 23, 267.

Känzig, W. and Cohen, M.H. 1959. Phys. Rev. Letters 3, 509.

Karlsson, A.V. 1970. Phys. Rev. 32, 3332.

Kellerman, E.W. 1940. Phil. Trans. Roy. Soc. (London) 238, 513.

Kirby, R.D. and Sievers, A.J. 1968. Solid State Commun. 6, 613.

Kirby, R.D., Nolt, I.G., Alexander, R.W., Jr. and Sievers, A.J. 1968. Phys. Rev. 168, 1057.

Kirby, R.D., Hughes, A.E. and Sievers, A.J. 1970. Phys. Rev. B 2, 481.

Klein, M.V. 1963. Phys. Rev. 131, 1500.

Klein, M.V. and Gould, J. 1967 in Physics of Colour Centres edited by W. Beall Fowler (Academic Press Inc., New York) Chap. 7.

Klein, M.V. and Macdonald, H.F. 1968. Phys. Rev. Letters 20, 1031.

Klein, M.V. 1968. Physics of Colour Centres edited by W. Beall Fowler (Academic Press Inc., New York) Chap. 7.

Klein, M. V., Wedding, B. and Levine, M.A. 1969. Phys. Rev. 180, 902.

Lax, M. and Burstein, E. 1955. Phys. Rev. 97, 39.

Levine, M.A. 1966. in Physics of Colour Centres edited by W. Beall Fowler (Academic Press Inc., New York)Chap. 7.

Lifschitz, I.M. 1943. J. Phys. U.S.S.R. 7, 211, 249.

Lifschitz, I.M. 1944. J. Phys. U.S.S.R. 8, 89.

Loewenstein, E.V. 1963. Applied Optics 2, 491.

Lombardo, G. and Pohl, R.O. 1965. Phys. Rev. Letters 15, 291.

Lombardo, G. and Pohl, R.O. 1966. Bull. Am. Phys. Soc. 11, 213.

Low, F.J. 1961. J. Opt. Soc. Am. 51, 1300.

Lüty, F. and Weinmann, K.F. 1967. Bull. Am. Phys. Soc. 12, 82.

Macdonald, H.F., Klein, M.V. and Martin, T.P. 1969. Phys. Rev. 177, 1292.

MacPherson, R.W. 1970. Ph.D. Thesis, McMaster University, unpublished.

MacPherson, R.W. and Timusk, T. 1970a. Can. J. Phys. 48, 2176.

MacPherson, R.W. and Timusk, T. 1970b. Can. J. Phys. 48, 2917.

Maradudin, A. A. 1964. Revs. Mod. Phys. 36, 417.

Maradudin, A.A. 1966. Solid State Physics, Vols. 18 and 19, edited by F. Seitz and D. Turnbull (Academic Press, New York).

Matthew, J.A.D. 1965. Solid State Commun. 3, 365.

Montroll, E.W. and Potts, R.B. 1955. Phys. Rev. 100, 525.

Nair, I. and Walker, C.T. 1971. Phys. Rev. B 3, 3446.

Nolt, I.G. and Sievers, A.J. 1966. Phys. Rev. Letters 16, 1103.

Nolt, I.G., Westwig, R.A., Alexander, R.W., Jr. and Sievers, A.J. 1967. Phys. Rev. 157, 730.

Nolt, I.G. and Sievers, A.J. 1968. Phys. Rev. 174, 1004.

Ohlmann, R. C., Richards, P.L. and Tinkham, M. 1958. J. Opt. Soc. Am. 48, 531.

Okazaki, M., Inoue, M., Tajozawa, Y., Hanamura, E. and Inui, T. 1968. Proceedings of the First International Conference on Localized Excitations in Solids, edited by R. F. Wallis (Plenum Press Inc., New York) p. 314.

Patnaik, K. and Mahanty, J. 1967. Phys. Rev. 155, 987.

Pohl, R.O. 1966 in Physics of Colour Centres edited by W. Beall Fowler (Academic PRess Inc., New York) Chap. 7.

Quigley, R. J. and Das, T.P. 1967. Phys. Rev. 164, 1185.

Quigley, R.J. and Das, T.P. 1969. Phys. Rev. 177, 340.

Raunio, G. and Almqvist, L. 1969. phys. stat. sol. 33, 209.

Richards, P. L. 1964. J. Opt. Soc. Am. 54, 1474.

Rolfe, J.,Lipsett, F.R. and King, W.J. 1961. Phys. Rev. 123, 447.

Rolfe, J. 1970. Private communication.

Rosenbaum, R.L., Chau, C-K. and Klein, M.V. 1969. Phys. Rev. 186, 852.

Rubens, H. and Wood, R.W. 1911. Phil. Mag. 21, 249.

Sack, H.S. and Moriarity, M.C. 1965. Solid State Commun. 3, 93.

Schäfer, G. 1960. J. Phys. Chem. Solids 12, 233.

Schwartz, J.W. and Walker, C.T. 1966. Phys. Rev. Letters 16, 97.

Schwartz, J.W. and Walker, C.T. 1967. Phys. Rev. 155, 959.

Sievers, A.J., Maradudin, A.A. and Jaswal, S.S. 1965. Phys. Rev. 138, A272.

Sievers, A.J. and Takeno, S. 1965. Phys. Rev. 140, A1030.

Strong, J. and Vanasse, G.A. 1959. J. Opt. Soc. Am. 49, 844.

Svensson, E.C., Brockhouse, B.N. and Rowe, J.M. 1965. Solid State Commun. 3, 245.

Takeno, S., 1967. Progr. Theor. Phys. 38, 995.

Templeton, T. and Clayman, B.P. 1970. Private communication.

Timusk, T. and Buchanan, M. 1967. Phys. Rev. 164, 345.

Timusk, T. and Ward, R.W. 1969. Phys. Rev. Letters 22, 396.

Tsvetov, V., Alfred, W. and Spitzer, W.G. 1968. Proc. First Intern. Conf. on Localized Excitations in Solids, edited by R. F. Wallis (Plenum Press Inc., New York).

Tumber, A.J. 1968. M.Sc. Thesis, McMaster University, unpublished.

Vanasse, G.A. 1962. J. Opt. Soc. Am. 52, 472.

Van Hove, L. 1953. Phys. Rev. 89, 1189.

Walton, D. 1967. Phys. Rev. LEtters 19, 305.

Weber, R. and Siebert, F. 1968. Z. Physik 213, 273.

Wedding, B. and Klein, M.V. 1969. Phys. Rev. 177, 1274.

Williamson, D.E. 1952. J. Opt. Soc. Am. 42, 712.

Wilson, W.D., Hatcher, R.D., Dienes, G.J. and Smoluchowski, R. 1967. Phys. Rev. 161, 888.

Woll, E.J., Jr., Gethins, T. and Timusk, T. 1968. Can. J. Phys. 46, 2263.

Woods, A.D.B., Brockhouse, B.N. and Cowley, R.A. 1963. Phys. Rev. 131, 1025.